

CHAPTER 8

Gravity and Isostasy

gravity (*grav' ə tē*) *n.*, [*< L. gravis, heavy*], 1. the force of attraction between masses 2. the force that tends to draw bodies in Earth's sphere toward Earth's center.

isostasy (*ī sō stā' sē*) *n.*, [*< Gr. isos, equal; < Gr. stasis, standing*], a state of balance whereby columns of material exert equal pressure at and below a compensating depth.

gravity and isostasy (*grav' ə tē ənd ī sō stā' sē*) *n.*, the study of spatial variations in Earth's gravitational field and their relationship to the distribution of mass within the Earth.

Earth's *gravity* and *magnetic forces* are potential fields that provide information on the nature of materials within the Earth. Potential fields are those in which the strength and direction of the field depend on the position of observation within the field; the strength of a potential field decreases with distance from the source. Compared to the magnetic field, Earth's gravity field is simple. Lines of force for the gravity field are directed toward the center of the Earth, while magnetic field strength and direction depend on Earth's positive and negative poles (Fig. 8.1).

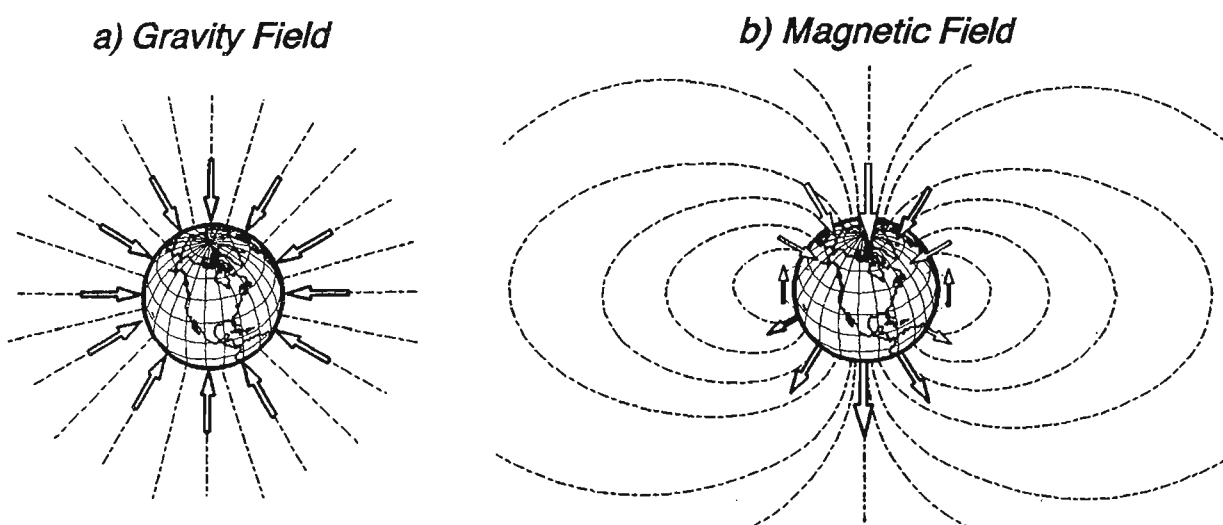


FIGURE 8.1 *Earth's potential fields.* a) The gravity field is symmetric. Force vectors (arrows) have approximately equal magnitude and point toward the center of the Earth. b) The magnitude and direction of the magnetic field is governed by positive (south) and negative (north) poles. Magnitude varies by a factor of two from equator to pole.

EARTH'S GRAVITY FIELD

Gravity is the attraction on one body due to the mass of another body. The force of one body acting on another is given by *Newton's Law of Gravitation* (Fig. 8.2a):

$$F = G \frac{m_1 m_2}{r^2}$$

where:

F = force of attraction between the two objects (N)

G = Universal Gravitational Constant ($6.67 \times 10^{-11} \text{ Nm}^2/\text{kg}^2$)

m_1, m_2 = mass of the two objects (kg)

r = distance between the centers of mass of the objects (m).

The force (F) exerted on the object with mass m_1 by the body with mass m_2 , is given by *Newton's Second Law of Motion* (Fig. 8.2b):

$$F = m_1 a$$

where:

a = acceleration of object of mass m_1 due to the gravitational attraction of the object with mass m_2 (m/s^2).

Solving for the acceleration, then combining the two equations (Fig. 8.2c):

$$a = \frac{F}{m_1} = \frac{1}{m_1} \frac{G m_1 m_2}{r^2}$$

$$a = \frac{G m_2}{r^2}$$

For Earth's gravity field (Fig. 8.3a), let:

$a = g$ = gravitational acceleration observed on or above Earth's surface;

$m_2 = M$ = mass of the Earth;

$r = R$ = distance from the observation point to Earth's center of mass;

so that:

$$g = \frac{GM}{R^2}$$

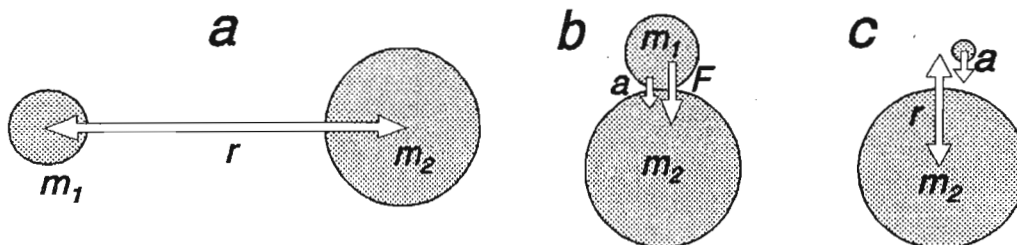


FIGURE 8.2 a) The gravitational force between two objects is directly proportional to their masses (m_1, m_2), and inversely proportional to the square of their distance (r). b) The mass (m_1), times the acceleration (a) due to mass (m_2), determines the gravitational force (F). c) The acceleration due to gravity (a) of a body depends only on the mass of the attracting body (m_2) and the distance to the center of that mass (r).

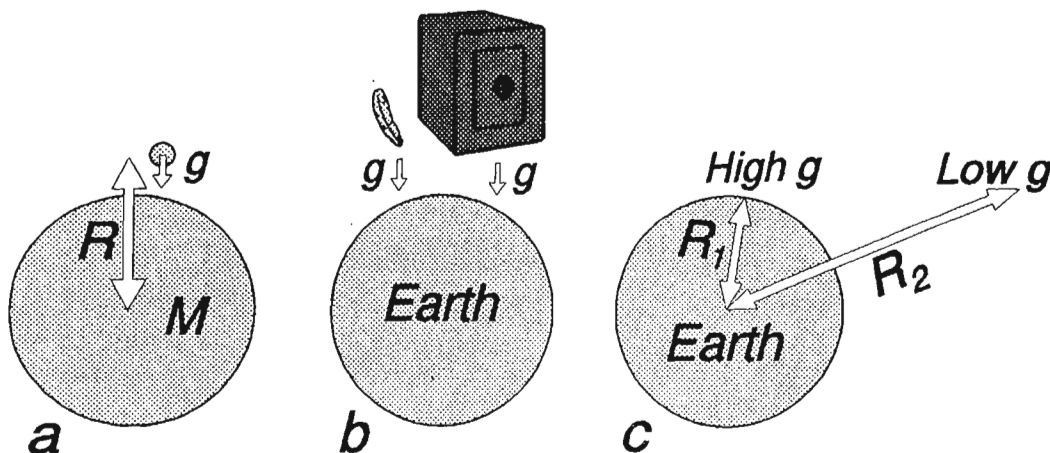


FIGURE 8.3 a) The mass (M) of the Earth and radius (R) to Earth's center determine the gravitational acceleration (g) of objects at and above Earth's surface. b) The acceleration is the same (g), regardless of the mass of the object. c) Objects at Earth's surface (radius R_1) have greater acceleration than objects some distance above the surface (radius R_2).

The above equation illustrates two fundamental properties of gravity. 1) Acceleration due to gravity (g) does *not* depend on the mass (m_1) attracted to the Earth (Fig. 8.3b); in the absence of air resistance, a small mass (feather) will accelerate toward Earth's surface at the same rate as a large mass (safe). 2) The farther from Earth's center of mass (that is, the greater the R), the smaller the gravitational acceleration (Fig. 8.3c); as a potential field, gravity thus obeys an *inverse square law*.

The value of the gravitational acceleration on Earth's surface varies from about 9.78 m/s^2 at the equator to about 9.83 m/s^2 at the poles (Fig. 8.4a). The smaller acceleration at the equator, compared to the poles, is because of the combination of three factors. 1) There is *less* inward acceleration because of *outward acceleration* caused by the spin of the Earth; the spin (rotation) is greatest at the equator but reduces to zero at the poles. 2) There is *less* acceleration at the equator because of the Earth's outward bulging, thereby increasing the radius (R) to the center of mass. 3) The added mass of the bulge creates *more* acceleration. Notice that the first two factors lessen the acceleration at the equator, while the third increases it. The net effect is the observed -0.05 m/s^2 difference.

Gravitational acceleration (*gravity*) is commonly expressed in units of *milligals* (mGal), where:

$$1 \text{ Gal} = 1 \text{ cm/s}^2 = 0.01 \text{ m/s}^2 \quad \begin{matrix} \text{mm.s}^{-2} \\ \equiv 10^2 \text{ mGal} \end{matrix} \quad \begin{matrix} \text{SI units} \\ \approx \end{matrix}$$

so that:

$$1 \text{ mGal} = 10^{-3} \text{ Gal} = 10^{-3} \text{ cm/s}^2 = 10^{-5} \text{ m/s}^2.$$

Gravity, therefore, varies by about 5000 mGal from equator to pole (Fig. 8.4b). $\frac{5000}{10000 \text{ mGal}} \approx \frac{1}{2}$

GRAVITY ANOMALIES

Gravity observations can be used to interpret changes in mass below different regions of the Earth. To see the mass differences, the broad changes in gravity from equator to pole must be subtracted from station observations. This is accomplished

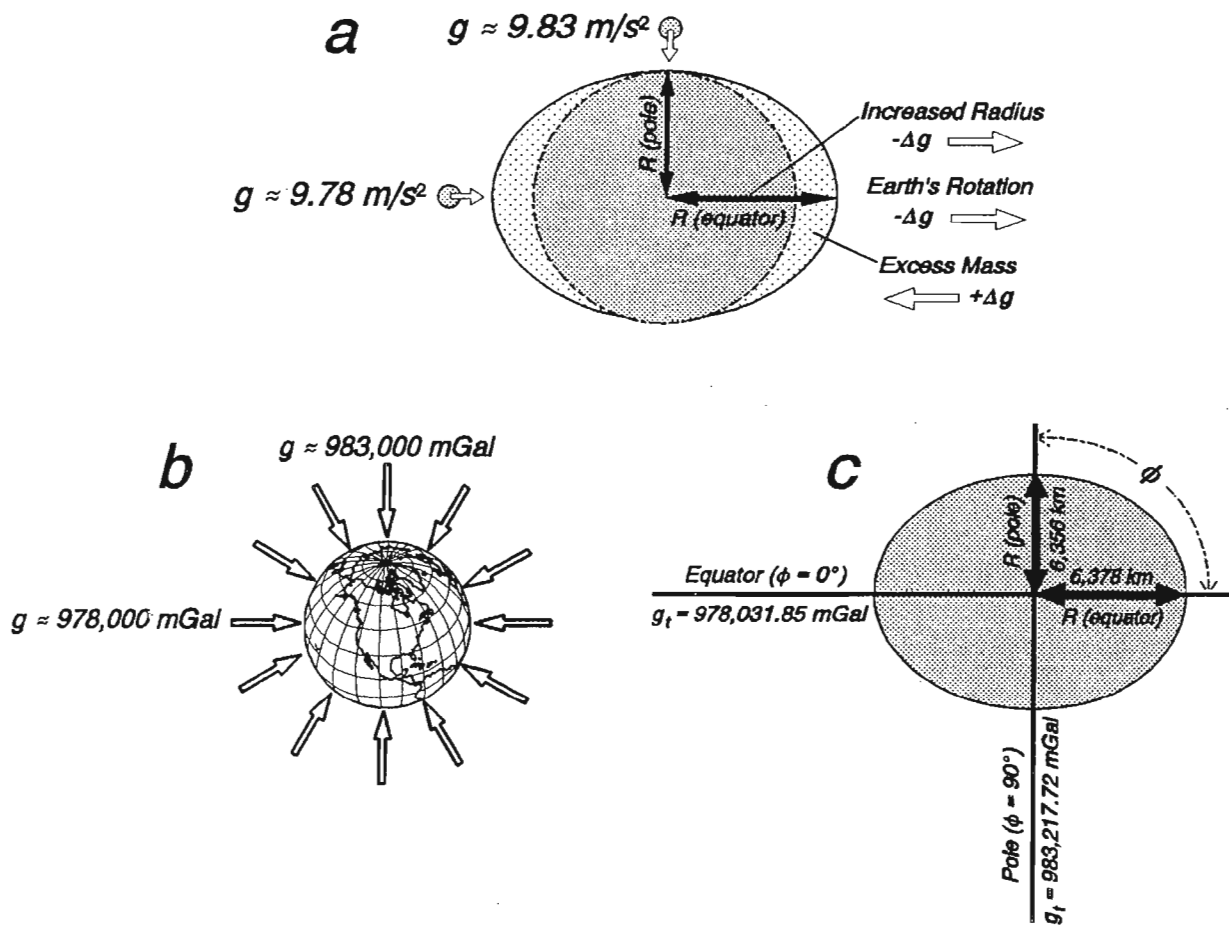


FIGURE 8.4 a) Three main factors responsible for the difference in gravitational acceleration at the equator compared to the poles. b) Gravity increases from about 978,000 mGal at the equator, to about 983,000 mGal at the poles. c) Variation in gravity from equator to pole, according to 1967 Reference Gravity Formula.

by predicting the gravity value for a station's latitude (*theoretical gravity*), then subtracting that value from the actual value at the station (*observed gravity*), yielding a *gravity anomaly*.

Theoretical Gravity

The average value of gravity for a given latitude is approximated by the *1967 Reference Gravity Formula*, adopted by the International Association of Geodesy:

$$g_t = g_e (1 + 0.005278895 \sin^2 \phi + 0.000023462 \sin^4 \phi)$$

where:

g_t = theoretical gravity for the latitude of the observation point (mGal)

g_e = theoretical gravity at the equator (978,031.85 mGal)

ϕ = latitude of the observation point (degrees).

The equation takes into account the fact that the Earth is an imperfect sphere, bulging out at the equator and rotating about an axis through the poles (Fig. 8.4a).

For such an *oblate spheroid* (Fig. 8.4c), it estimates that gravitational acceleration at the *equator* ($\phi = 0^\circ$) would be 978.031.85 mGal, gradually increasing with latitude to 983,217.72 mGal at the *poles* ($\phi = 90^\circ$).

Free Air Gravity Anomaly

Gravity observed at a specific location on Earth's surface can be viewed as a function of three main components (Fig. 8.5): 1) the *latitude* (ϕ) of the observation point, accounted for by the theoretical gravity formula; 2) the *elevation* (ΔR) of the station, which changes the radius (R) from the observation point to the center of the Earth; and 3) the *mass distribution* (M) in the subsurface, relative to the observation point.

The *free air correction* accounts for the second effect, the local change in gravity due to elevation. That deviation can be approximated by considering how gravity changes as a function of increasing distance of the observation point from the center of mass of the Earth (Fig. 8.6a). Consider the equation for the gravitational acceleration (g) as a function of radius (R):

$$g = \frac{GM}{R^2} \quad \int_0^R g(dR) = U = -\frac{GM}{R}$$

average potential

The first derivative of g , with respect to R , gives the change in gravity (Δg) with increasing distance from the center of the Earth (that is, increasing elevation, ΔR):

$$\lim_{\Delta R \rightarrow 0} \frac{\Delta g}{\Delta R} = \frac{dg}{dR} = -2\left(\frac{GM}{R^3}\right) = \frac{-2}{R}\left(\frac{GM}{R^2}\right) = \frac{-2}{R}(g)$$

$$\boxed{\frac{dg}{dR} = \frac{-2g}{R}}$$

Assuming average values of $g \approx 980,625$ mGal and $R \approx 6,367$ km = 6,367,000 m (Fig. 8.4c):

$$\boxed{dg/dR \approx -0.308 \text{ mGal/m}}$$

where:

dg/dR = average value for the change in gravity with increasing elevation.

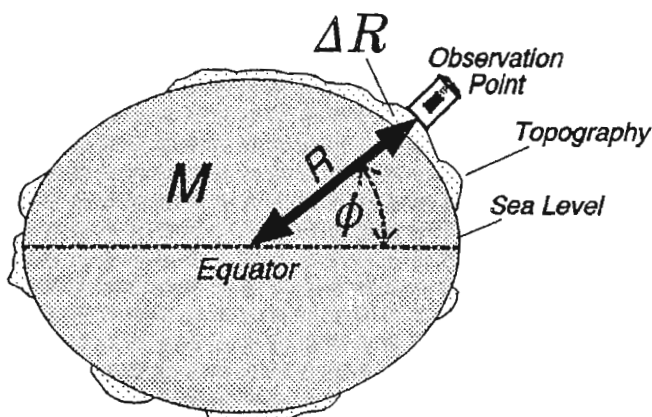


FIGURE 8.5 Three factors determining gravity at an observation point: a) latitude (ϕ); b) distance from sea-level datum to observation point (ΔR); c) Earth's mass distribution (M), relative to the station location (M includes material above as well as below sea level). ϕ is accounted for by subtracting the theoretical gravity from the observed gravity, and ΔR by the free air correction. The remaining value (free air anomaly) is thus a function of M .

$$\frac{M}{Z^2}$$

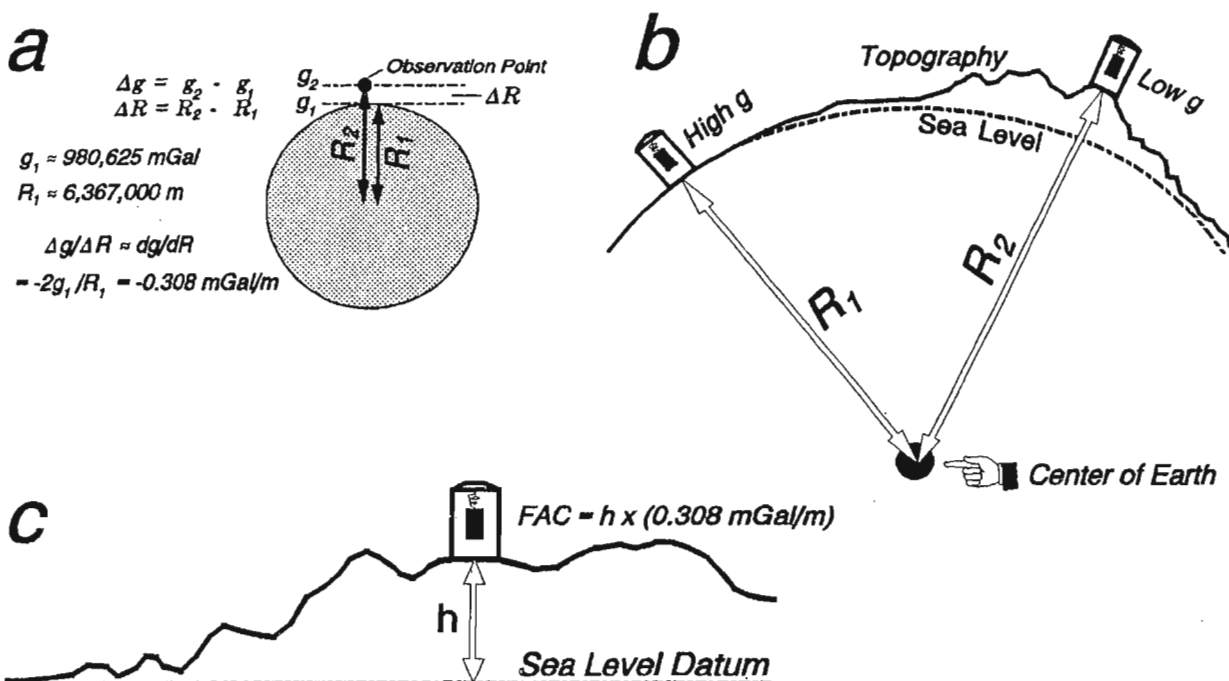


FIGURE 8.6 *Free air correction.* a) Rising upward from Earth's surface, gravitational acceleration decreases by about 0.308 mGal for every meter of height. b) A gravity station at high elevation tends to have a lower gravitational acceleration (g) than a station at lower elevation. c) The free air correction (FAC) accounts for the extended radius to an observation point, elevated h meters above a sea level datum.

The above equation illustrates that, for every 3 m (about 10 feet) upward from the surface of the Earth, the acceleration due to gravity decreases by about 1 mGal . Stations at elevations high above sea level therefore have lower gravity readings than those near sea level (Fig. 8.6b). To compare gravity observations for stations with different elevations, a *free air correction* must be added back to the observed values (Fig. 8.6c).

$$\text{FAC} = h \times (0.308 \text{ mGal/m})$$

where:

FAC = free air correction (mGal)

h = elevation of the station above a sea level datum (m).

The *free air gravity anomaly* is the observed gravity, corrected for the latitude and elevation of the station:

$$\boxed{\Delta g_{fa} = g - g_t + \text{FAC}}$$

where:

Δg_{fa} = free air gravity anomaly

g = gravitational acceleration observed at the station.

Notice in the above equation that: 1) subtracting the theoretical gravity (g_t) from the observed gravity (g) corrects for the *latitude*, thus accounting for the spin and

bulge of the Earth; and 2) adding the free air correction (FAC) puts back the gravity lost to *elevation*, thereby correcting for the increased radius (R) to Earth's center.

The free air gravity anomaly is a function of *lateral mass variations* (M in Fig. 8.5), because the latitude and elevation effects (ϕ and ΔR in Fig. 8.5) have been corrected. Fig. 8.7 shows what a profile of changing free air anomalies might look like across bodies of excess and deficient mass. Notice that the anomaly shows relatively high readings near the mass excess, low readings near the mass deficiency; there are also abrupt changes that mimic sharp topographic features.

Bouguer Gravity Anomaly

Even after elevation corrections, gravity can vary from station to station because of differences in mass between the observation points and the sea-level datum. Relative to areas near sea level, mountainous areas would have extra mass, tending to increase the gravity (Fig. 8.8a).

The *Bouguer correction* accounts for the gravitational attraction of the mass above the sea-level datum. This is done by approximating the mass as an *infinite slab*, with thickness (h) equal to the elevation of the station (Fig. 8.8b). The attraction of such a slab is:

$$BC = 2\pi\rho Gh$$

$$\text{N} \cdot \text{m}^2 / \text{kg}^2 \cdot \text{kg} \cdot \text{m}^2 \cdot \text{m}$$

where:

BC = Bouguer correction

ρ = density of the slab

G = Universal Gravitational Constant

h = thickness of the slab (station elevation).

$$2.67 \text{ g/cm}^3 \quad \text{N} \cdot \text{kg}^{-1} \quad \text{kg} \cdot \text{m}^{-2} \cdot \text{s}^{-2} \times 10^2 \text{ Gal}$$

Substituting the values of G and 2π yields:

$$BC = 0.0419\phi h$$

where BC is in $mGal$ (10^{-5} m/s^2); ρ in g/cm^3 (10^3 kg/m^3); h in m .

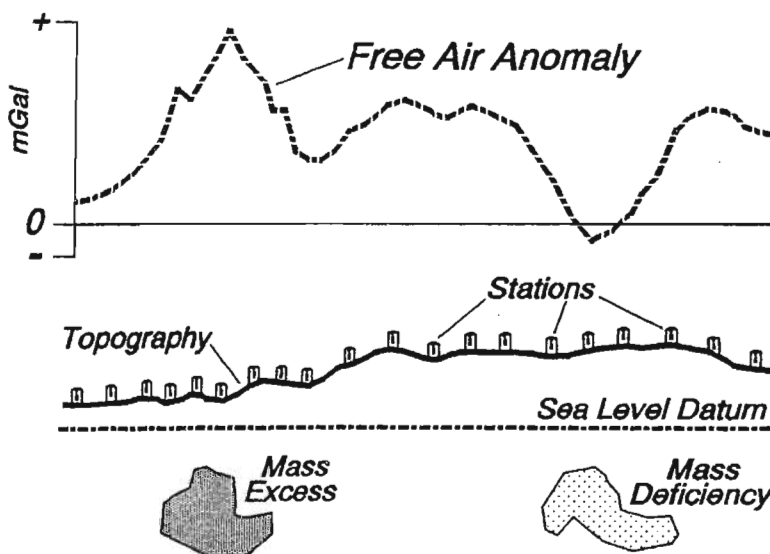


FIGURE 8.7 General form of free air gravity anomaly profile across areas of mass excess and mass deficiency.

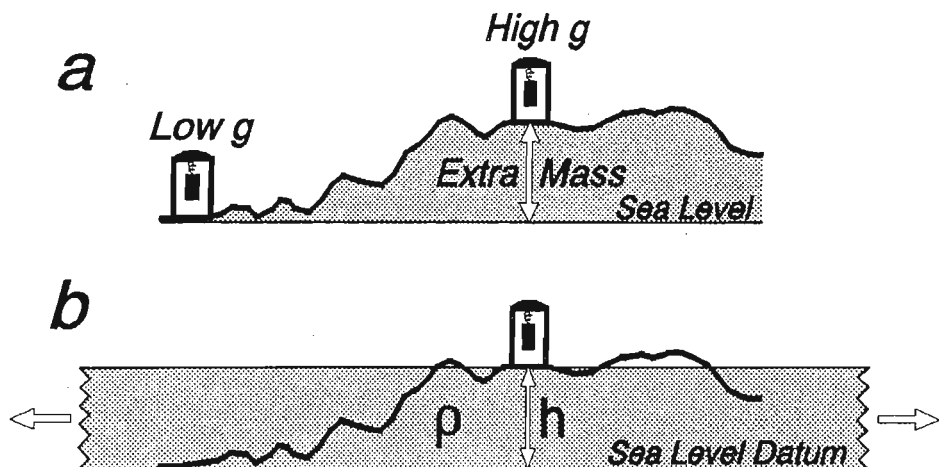
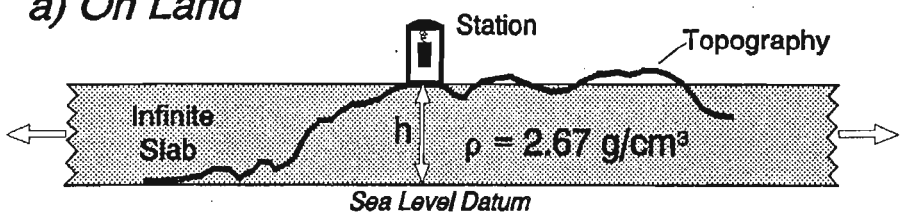


FIGURE 8.8 Bouguer correction. a) The extra mass of mountains results in higher gravity relative to areas near sea level. b) To account for the excess mass above a sea level datum, the Bouguer correction assumes an infinite slab of density (ρ), with thickness (h) equal to the station's elevation.

a) On Land



b) At Sea

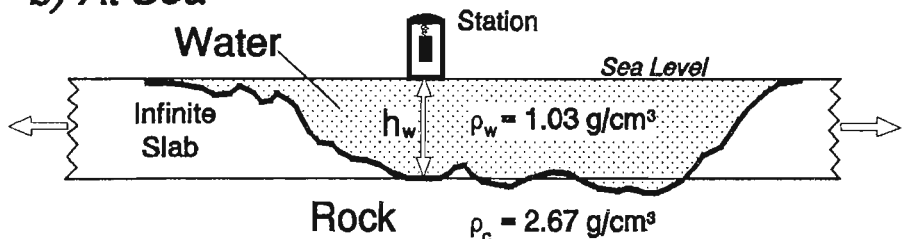


FIGURE 8.9 Standard Bouguer correction values. a) On land, the reduction density (ρ) is commonly taken as $+2.67 \text{ g/cm}^3$. The thickness of the infinite slab is equal to the station elevation (h). b) At sea, the reduction density (-1.64 g/cm^3) is the difference between that of sea water (1.03 g/cm^3) and underlying rock (2.67 g/cm^3). The thickness of the slab is equal to the water depth (h_w).

Bouguer Gravity Anomaly on Land For regions above sea level (Fig. 8.9a), the *simple Bouguer gravity anomaly* (Δg_B) results from subtracting the effect of the infinite slab (BC) from the free air gravity anomaly:

$$\Delta g_B = \Delta g_{fa} - BC$$

To determine the Bouguer correction, the density of the infinite slab (ρ) must be assumed (the *reduction density*). The reduction density is commonly taken as 2.67 g/cm^3 , a typical density of granite (Figs. 3.9, 3.10).

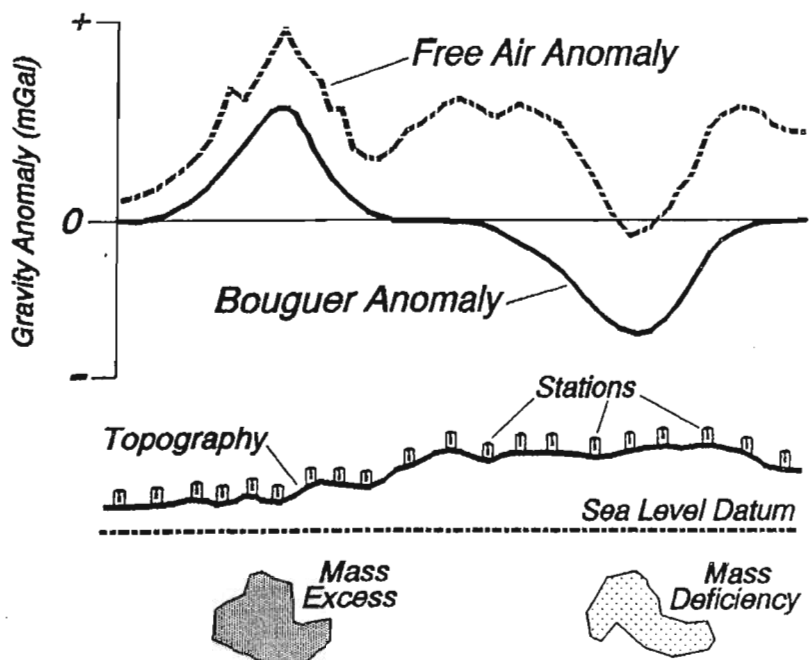


FIGURE 8.10 Bouguer correction applied to the free air gravity anomaly profile in Fig. 8.7.

The standard Bouguer correction for areas above sea level is thus:

$$\begin{aligned} BC &= 0.0419ph = (0.0419)(2.67g/cm^3)h \\ &= (0.112 \text{ mGal/m}) \times h \end{aligned}$$

where h is in m. The equation illustrates that, for about every 9 m of surface elevation, the increased mass below the observation point adds about 1 mGal to the observed gravity. Using the standard correction, the *simple Bouguer gravity anomaly on land* is computed from the free air gravity anomaly according to the formula:

$$\Delta g_B = \Delta g_{fa} - (0.112 \text{ mGal/m}) h \quad (\text{h in meters}).$$

Like the free air gravity anomaly, the Bouguer gravity anomaly reflects changes in mass distribution below the surface. The Bouguer anomaly, however, has had an additional correction, removing most of the effect of mass excess above a sea level datum (on land). Bouguer Corrections applied to the free air gravity profile (Fig. 8.7) would therefore yield a Bouguer gravity profile illustrated in Fig. 8.10. The two profiles illustrate three general properties of gravity anomalies. 1) For stations above sea level, the Bouguer anomaly is always less than the free air anomaly (the approximate attraction of the mass above sea level has been removed from the free air anomaly). 2) Short-wavelength changes in the free air anomaly, due to abrupt topographic changes, have been removed by the Bouguer correction; the Bouguer anomaly is therefore smoother than the free air anomaly. 3) Mass excesses result in positive changes in gravity anomalies; mass deficiencies cause negative changes.

Bouguer Gravity Anomaly at Sea In areas covered by the sea, gravity is generally measured on the surface of the water (Fig. 8.9b). In the strictest sense,

Bouguer anomalies at sea are exactly the same as free air anomalies, because station elevations (h) are zero:

$$\Delta g_B = \Delta g_{fa} - 0.0419ph; h = 0, \text{ so that: } \Delta g_B = \Delta g_{fa}$$

A type of Bouguer correction can be applied, however, because the density and depth of the water are well known. Instead of stripping the topographic mass away, as is done on land, the effect can be thought of as “pouring concrete” to fill the ocean. Thus, the Bouguer correction at sea can be envisioned as an infinite slab, equal to the depth of the water and with density equalling the difference between that of water and “concrete”:

$$BC_s = 0.0419ph = 0.0419(\rho_w - \rho_c)h_w$$

where:

BC_s = Bouguer correction at sea

ρ_w = density of sea water

ρ_c = density of “concrete”

h_w = water depth below the observation point.

Assuming $\rho_w = 1.03 \text{ g/cm}^3$ and $\rho_c = 2.67 \text{ g/cm}^3$:

$$BC_s = 0.0419 (-1.64 \text{ g/cm}^3) h_w = -0.0687 (\text{mGal/m}) \times h_w$$

where BC_s is in mGal and h_w in m.

Retaining the convention defined above, the Bouguer correction at sea is subtracted from the free air anomaly to yield the *Bouguer gravity anomaly at sea* (Δg_{Bs}):

$$\Delta g_{Bs} = \Delta g_{fa} - BC_s$$

Notice that the water is a mass deficit when compared to adjacent landmasses of rock; the negative Bouguer correction at sea thus means that some value must be added to the free air anomaly to compute the Bouguer anomaly at sea:

$$\Delta g_{Bs} = \Delta g_{fa} + (0.0687 \text{ mGal/m}) h_w \quad (h_w \text{ in meters}).$$

Complete Bouguer Gravity Anomaly The infinite slab correction described above yields a simple Bouguer anomaly. That correction is normally sufficient to approximate mass above the datum in the vicinity of the station (Fig. 8.11a). In rugged areas, however, there may be significant effects due to nearby mountains pulling upward on the station, or valleys that do not contain mass that was subtracted (Fig. 8.11b). For such stations, additional *terrain corrections* (TC; see Telford et al., 1976) are applied to the simple Bouguer anomaly (Δg_B), yielding the *complete Bouguer gravity anomaly* (Δg_{Bc}):

$$\Delta g_{Bc} = \Delta g_B + TC$$

Summary of Equations for Free Air and Bouguer Gravity Anomalies

Fig. 8.12 illustrates parameters used to determine free air and Bouguer gravity anomalies. The formulas below yield standard versions of the anomalies.

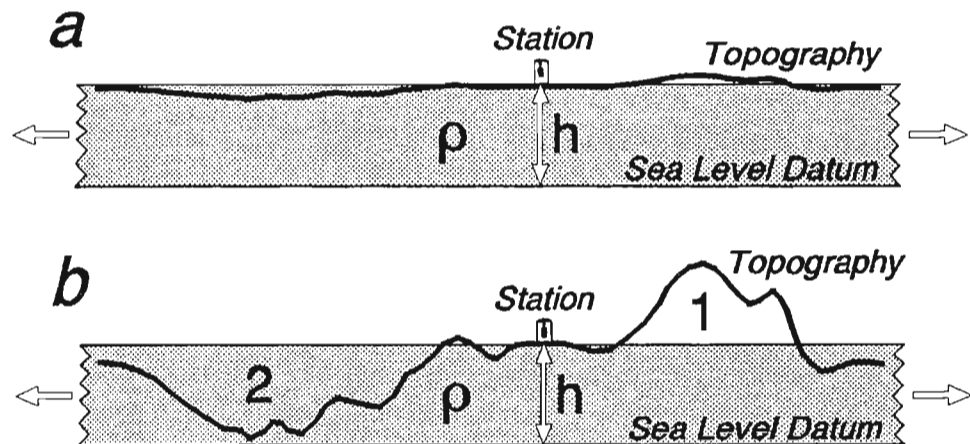


FIGURE 8.11 *Terrain correction.* a) In areas of low relief, the Bouguer slab approximation is adequate; terrain correction is unnecessary. b) High relief areas require terrain correction, to account for lessening of observed gravity due to mass of mountains above the slab (1), and overcorrection due to valleys (2). For both situations, the terrain correction is positive, making the complete Bouguer anomaly higher than the simple Bouguer anomaly.

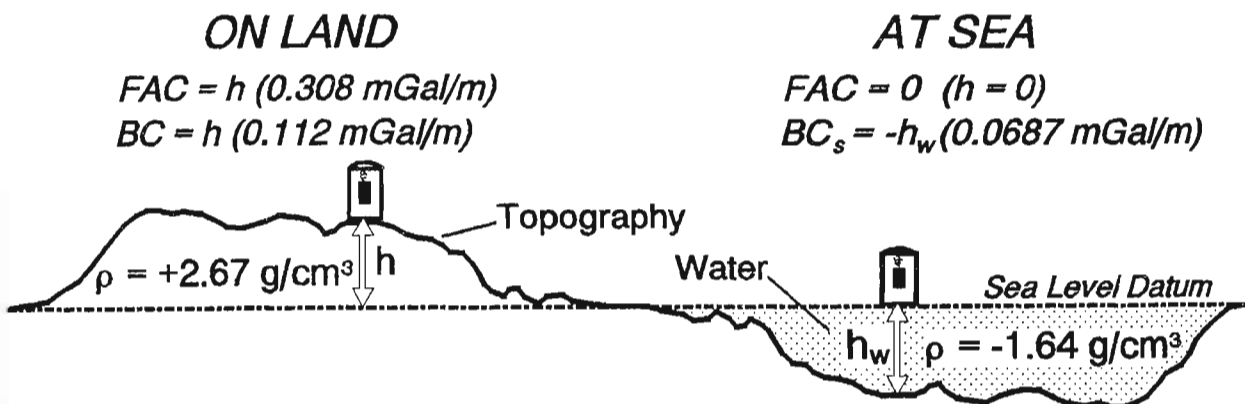


FIGURE 8.12 Standard parameters used to compute gravity anomalies on land and at sea. FAC = free air correction; BC = Bouguer correction; BC_s = Bouguer correction at sea; ρ = reduction density; h (elevation) and h_w (water depth) in meters.

Theoretical Gravity

$$g_t = g_e (1 + 0.005278895 \sin^2 \phi + 0.000023462 \sin^4 \phi)$$

g_t = theoretical gravity for the latitude of the observation point (*mGal*)
 g_e = theoretical gravity at the equator (978,031.85 *mGal*)
 ϕ = latitude of the observation point (degrees).

Free Air Gravity Anomaly

$$\Delta g_{fa} = (g - g_t) + h(0.308 \text{ mGal/m})$$

Δg_{fa} = free air gravity anomaly (*mGal*)

g = observed gravity (*mGal*) g_t = theoretical gravity (*mGal*) h = elevation above sea level datum (m).**Bouguer Gravity Anomaly**

$$\begin{aligned}\Delta g_B &= \Delta g_{fa} - BC \\ &= \Delta g_{fa} - 0.0419\rho h\end{aligned}$$

 BC = Bouguer correction (*mGal*) ρ = reduction density (g/cm^3)*a) On Land*

$$\Delta g_B = \Delta g_{fa} - (0.112 \text{ mGal/m}) h \quad (\text{for } \rho = +2.67)$$

 Δg_B = simple Bouguer gravity anomaly (*mGal*) h = elevation above sea-level datum (m).*b) At Sea*

$$\Delta g_{Bs} = \Delta g_{fa} + (0.0687 \text{ mGal/m}) h_w \quad (\text{for } \rho = -1.64)$$

 Δg_{Bs} = Bouguer gravity anomaly at sea (*mGal*) h_w = water depth below observation point (m).*c) In Rugged Terrain:*

$$\Delta g_{Bc} = \Delta g_B + TC$$

 Δg_{Bc} = complete Bouguer gravity anomaly (*mGal*)TC = terrain correction (*mGal*).**MEASUREMENT OF GRAVITY**

Gravitational acceleration on Earth's surface can be measured in absolute and relative senses (Fig. 8.13). *Absolute gravity* reflects the actual acceleration of an object as it falls toward Earth's surface, while *relative gravity* is the difference in gravitational acceleration at one station compared to another.

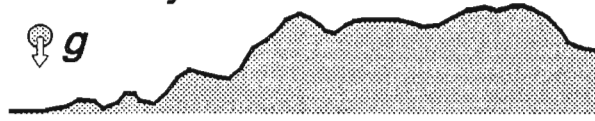
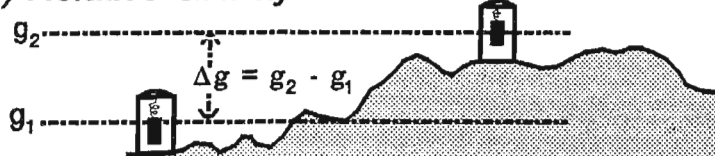
a) Absolute Gravity

FIGURE 8.13 a) Absolute gravity is the true gravitational acceleration (g). b) Relative gravity reflects the difference in gravitational acceleration (Δg) at one station (g_1) compared to another (g_2).

b) Relative Gravity

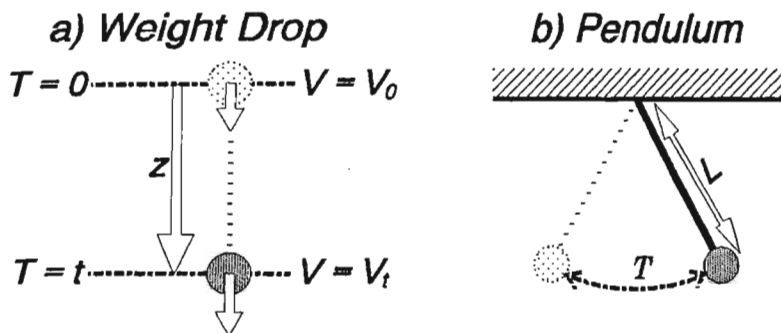


FIGURE 8.14 *Measurement of absolute gravity.* a) *Weight drop.* The object accelerates from an initial velocity of V_0 at time ($T = 0$), to a velocity of V_t , at time ($T = t$), as it falls a distance (z). b) *Pendulum.* Gravitational acceleration is a function of the pendulum's length (L) and period of oscillation (T).

Absolute Gravity

There are two basic ways to measure absolute gravity. In the *weight drop* method (Fig. 8.14a), the velocity and displacement are measured for an object in free fall. The absolute gravity is computed according to:

$$z = v_0 t + \frac{1}{2} g t^2$$

where:

- z = distance the object falls
- t = time to fall the distance z
- v_0 = initial velocity of the object
- g = absolute gravity.

The absolute gravity is thus:

$$g = 2(z - v_0 t) / t^2$$

Using the second method (Fig. 8.14b), a *pendulum* oscillates according to:

$$T = 2\pi\sqrt{L/g}$$

where:

- T = period of swing of the pendulum
- L = length of the pendulum.

The absolute gravity is computed according to:

$$g = L(4\pi^2/T^2)$$

Relative Gravity

The precision necessary to obtain reliable, absolute gravity observations makes those measurements expensive and time consuming. Relative gravity measurements, however, can be done easily, with an instrument (*gravimeter*) that essentially measures the length of a spring (L ; Fig. 8.15a). The *mass* of an object suspended from the spring remains constant. When the gravimeter is taken from one station location to another, however, the *force* (F) that the mass (m) exerts on the spring varies with the local gravitational acceleration (g):

$$F = mg$$

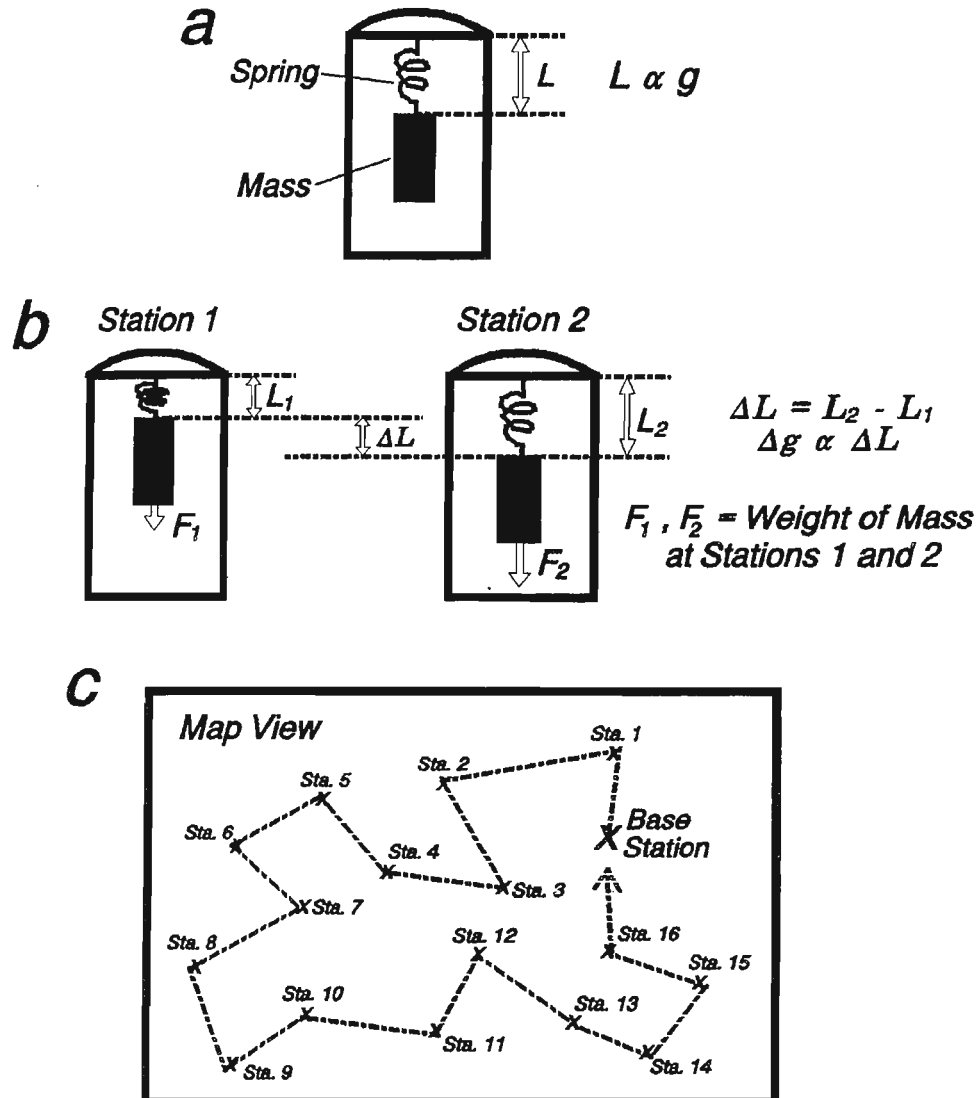


FIGURE 8.15 *Measurement of relative gravity.* a) A gravimeter measures the length of a spring (L), which is proportional to the gravitational acceleration (g). b) A force (F_1) at one station results in a spring length (L_1). The length may change to L_2 because of a different force (F_2) at another station. The force exerted by the mass is a function of g ; the change in length of the spring (ΔL) is thus proportional to the change in gravitational acceleration (Δg). c) Map of relative gravity survey. The traverse starts with a measurement at the base station, then each of the 16 stations, followed by a re-measurement at the base station.

so that:

$$g = F/m$$

In other words, the mass will *weigh* more or less (exert more or less force), depending on the pull of gravity (g) at the station. A gravimeter is simply weighing the mass at different stations; the spring stretches ($+\Delta L$) where there is more gravity and contracts ($-\Delta L$) when gravity is less (Fig. 8.15b).

If we know the absolute gravity at a starting point (*base station*), we can use a gravimeter to measure points relative to that station (Fig. 8.15c). The initial reading

(that is, the initial length of the spring) measured at the base station represents the absolute gravity at that point. Measurements are then taken at other stations, with the changes in length of the spring recorded. The gravimeter is calibrated so that a given change in spring length (ΔL) represents a change in gravity (Δg) by a certain amount (in *mGal*). The acceleration (g) can then be computed by adding the value of Δg to the absolute gravity of the base station.

At sea, gravity surveying is complicated by the fact that the measurement platform is unstable. Waves move the ship up and down, causing accelerations that add or subtract from the gravity. Also, like Earth's rotation, the speed of the ship over the water results in an outward acceleration; in other words, the ship's velocity adds to the velocity of Earth's rotation. An additional correction, known as the *Eötvös correction*, is therefore added to marine gravity measurements (Telford et al., 1976):

$$\text{EC} = 7.503 V \cos\phi \sin\alpha + 0.004154 V^2$$

where:

EC = Eötvös correction (*mGal*)

V = speed of ship (knots; 1 knot = 1.852 km/hr = 0.5144 m/s)

ϕ = latitude of the observation point (degrees)

α = course direction of ship (azimuth, in degrees).

ISOSTASY

Until quite recently, surveyors leveled their instruments by suspending a lead weight (plumb bob) on a string. In the vicinity of large mountains, it was recognized that a correction must be made because the *mass excess* of the mountains standing high above the surveyor's location made the plumb bob deviate slightly from the vertical (Fig. 8.16a).

In the mid-1800's a large-scale survey of India was undertaken. Approaching the Himalaya Mountains from the plains to the south, the correction was calculated and applied. A systematic error was later recognized, however, as the plumb bob was not deviated toward the mountains as much as it should have been (Fig. 8.16b). This difference was attributed to *mass deficiency* within the Earth, beneath the excess mass of the mountains.

Pratt and Airy Models (Local Isostasy)

Scientists proposed two models to explain how the mass deficiency relates to the topography of the Himalayas. *Pratt* assumed that the crust of the Earth comprised blocks of different density; blocks of lower density need to extend farther into the air in order to exert the same pressure as thinner blocks of higher density (Fig. 8.17a). The situation is analogous to blocks of wood, each of different density, floating on water. By the Pratt model, the base of the crust is flat, so that the surface of equal pressure (depth of compensation) is essentially a flat crust/mantle boundary.

In the model of *Airy* (Fig. 8.17b), crustal blocks have equal density, but they float on higher-density material (Earth's mantle), similar to (low-density) icebergs floating on (higher-density) water. The base of the crust is thus an exaggerated, mirror image of the topography. Areas of high elevation have low-density "crustal roots" supporting their weight, much like a beach ball lifting part of a swimmer's body out of the water.

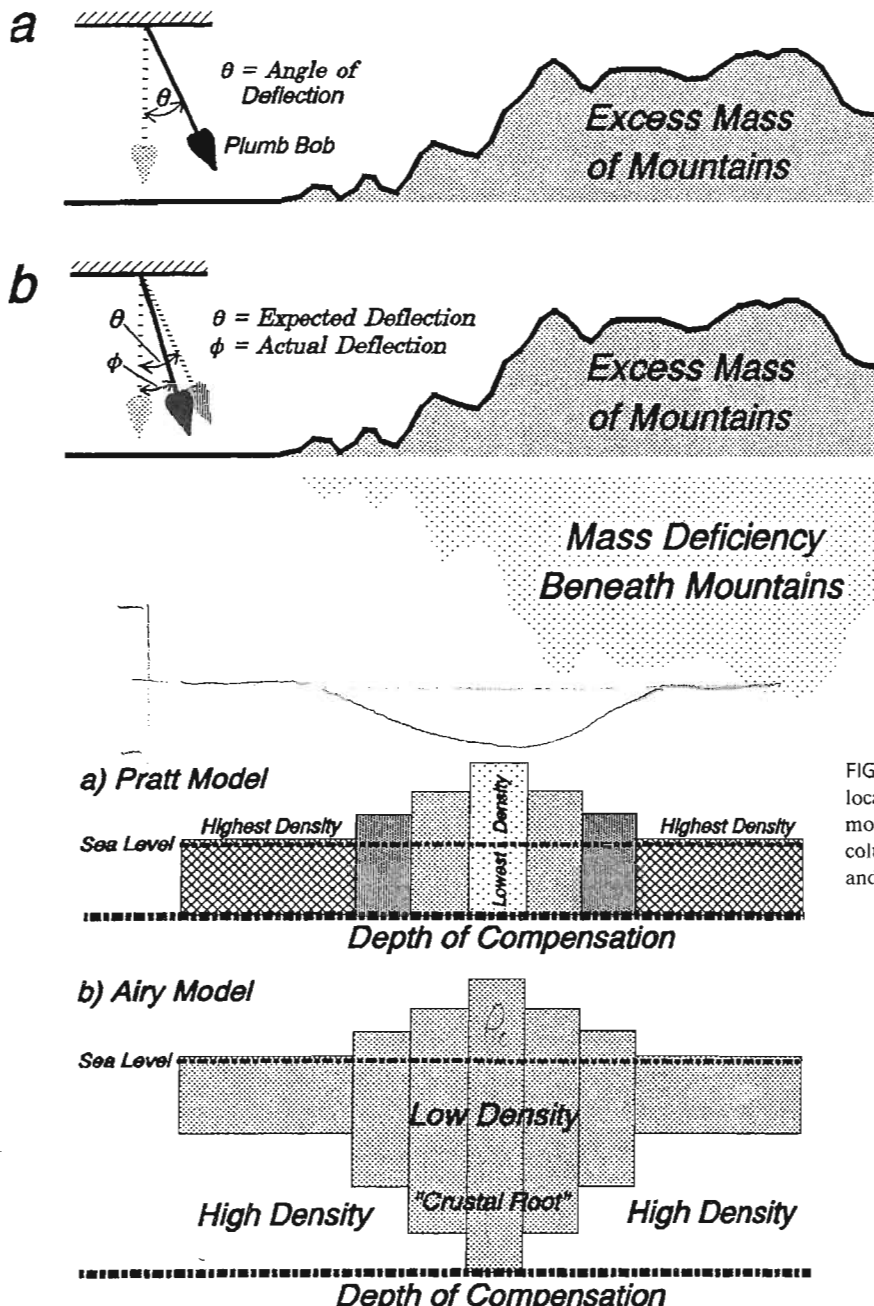


FIGURE 8.16 a) Expected deflection of a plumb bob (highly exaggerated), due to the attraction of the mass of a mountain range. b) The actual deflection for the Himalayas was less than expected, due to a deficiency of mass beneath the mountains:

FIGURE 8.17 Pratt and Airy models of local isostatic compensation. In both models, pressure exerted by crustal columns is equal on horizontal planes at and below the depth of compensation.

Hydrostatic pressure is the pressure exerted on a point within a body of water. Similarly, pressure at a given depth within the Earth (Fig. 8.18a) can be viewed as lithostatic pressure, according to:

$$P = \rho g z$$

where:

P = pressure at the point within the Earth

ρ = average density of the material above the point

on of
due to
taint
he
due to

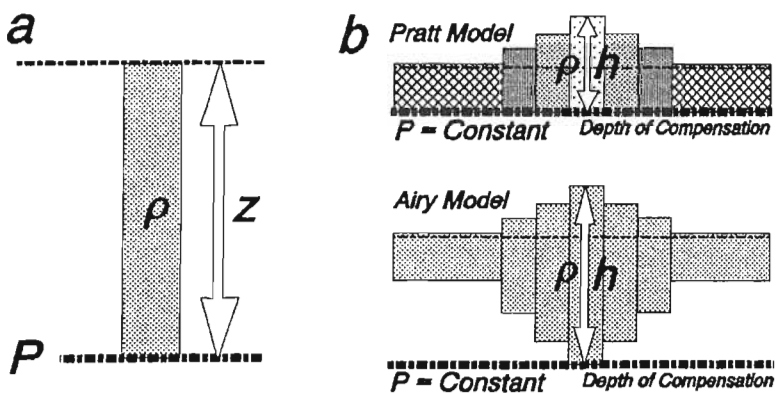


FIGURE 8.18 a) Pressure (P) at depth (z) is a function of the density (ρ) of the material above a point within the Earth. b) For the Pratt and Airy models, the pressure depends on the density and thickness (h) of crustal blocks. In both models, pressure equalizes at the depth of compensation.

$$g = \text{acceleration due to gravity} (\approx 9.8 \text{ m/s}^2)$$

$$z = \text{depth to the point.}$$

For the Pratt and Airy models (Fig. 8.18b), the pressure exerted by a crustal block can be expressed as:

$$P = \rho gh$$

where:

- P = pressure exerted by the crustal block
- ρ = density of the crustal block
- h = thickness of the crustal block.

In both the Pratt and Airy models, the pressure must be the same everywhere at the *depth of compensation*. For the Pratt model, the base of each block is at the exact depth of compensation, so that:

$$P = \rho_2 gh_2 = \rho_3 gh_3 = \rho_4 gh_4 = \rho_5 gh_5$$

where:

- $\rho_2, \rho_3, \rho_4, \rho_5$ = density of each block
- h_2, h_3, h_4, h_5 = thickness of each block.

Dividing out a constant gravitational acceleration (g):

$$\boxed{P/g = \rho_2 h_2 = \rho_3 h_3 = \rho_4 h_4 = \rho_5 h_5}$$

In the particular Pratt model shown in Fig. 8.19a, $\rho_5 < \rho_4 < \rho_3 < \rho_2 < \rho_1$, where ρ_1 is the density of the substratum (Earth's mantle).

In an Airy model the crustal density (ρ_2) is constant and less than the mantle density (ρ_1). Only the thickest crustal block extends to the depth of compensation. For the Airy isostatic model in Fig. 8.19b, the pressure exerted at the depth of compensation (divided by g) is:

$$\boxed{P/g = \rho_2 h_5 = (\rho_2 h_4 + \rho_1 h'_4) = (\rho_2 h_3 + \rho_1 h'_3) = (\rho_2 h_2 + \rho_1 h'_2)}$$

where:

- h'_2, h'_3, h'_4 = thickness of mantle column from the base of each crustal block to the depth of compensation.

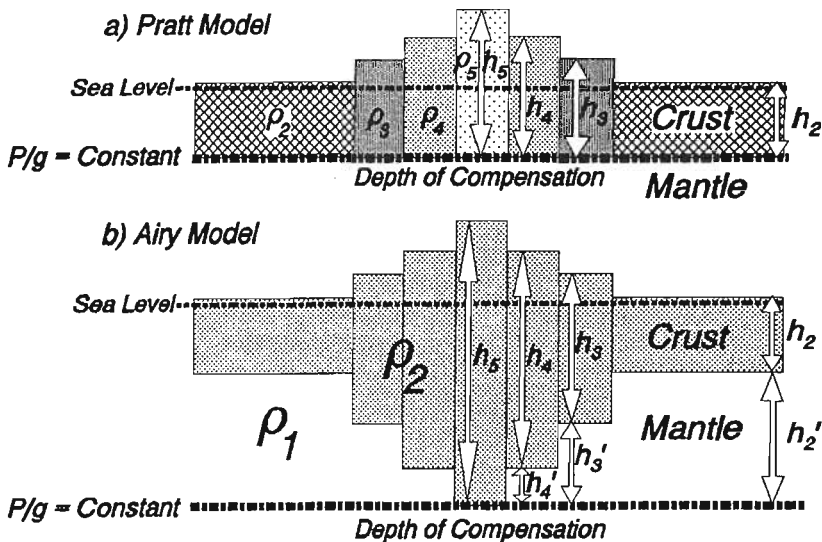


FIGURE 8.19 Density (ρ) and thickness (h, h') relationships for Pratt and Airy isostatic models. P = pressure; g = gravitational acceleration.

Airy Isostatic Model

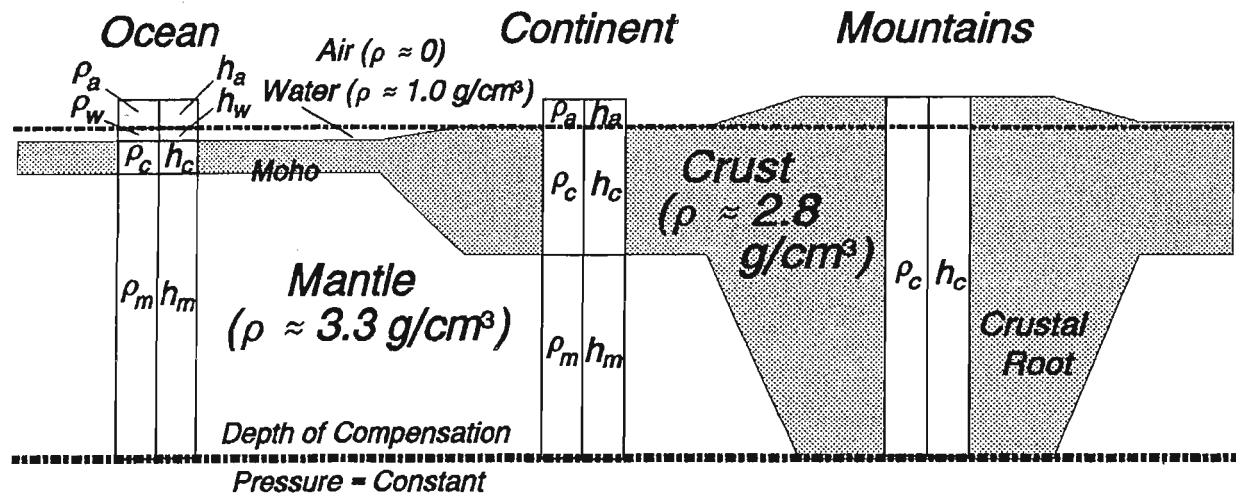


FIGURE 8.20 Airy isostatic model. Oceanic regions have thin crust, relative to continental regions. The weight of extra mantle material beneath the thin oceanic crust pulls downward until just enough depth of water fills the basin to achieve isostatic equilibrium. Mountainous regions have thick crust, relative to normal continental regions. The crustal root exerts an upward force until it is balanced by the appropriate weight of mountains.

While regions often exhibit components of both hypotheses, isostatic compensation is generally closer to the Airy than the Pratt model. Pure Airy isostatic compensation for regions with oceanic and continental crust, as well as thickened crust weighted down by mountains, might exhibit the form illustrated in Fig. 8.20. Notice that the crustal root beneath elevated regions is typically 5 to 8 times the height of the topographic relief. At the *depth of compensation* beneath each region, two equations hold true. 1) The total *pressure* (P) exerted by each vertical column, divided by the gravitational acceleration (g), is constant:

$$\frac{P}{g} = \rho_a h_a + \rho_w h_w + \rho_c h_c + \rho_m h_m = \text{Constant}$$

where:

- ρ_a = density of the air ($\rho_a \approx 0$)
- h_a = thickness of the air column, up to the level of the highest topography
- ρ_w = density of the water
- h_w = thickness of the water column
- ρ_c = density of the crust
- h_c = thickness of the crust
- ρ_m = density of the mantle
- h_m = thickness of the mantle column, down to the depth of compensation.

2) The total *thickness* (T) of each vertical column is constant:

$$T = h_a + h_w + h_c + h_m = \text{Constant}$$

If the isostatic column (P/g) can be determined or assumed for one area, then solving the two equations simultaneously can be used to estimate thicknesses (h) and/or densities (ρ) for vertical columns beneath other areas.

Lithospheric Flexure (Regional Isostasy)

Both the Pratt and Airy models assume *local isostasy*, whereby compensation occurs directly below a load (Fig. 8.21a); supporting materials behave like liquids, flowing to accommodate the load. In other words, the materials are assumed to have *no rigidity*. Most Earth materials, however, are somewhat rigid; the effect of a load is distributed over a broad area, depending on the *flexural rigidity* of the supporting material. Models of *regional isostasy* therefore take lithospheric strength into account (Fig. 8.21b).

A common model of regional isostatic compensation is that of an *elastic plate* that is bent by topographic and subsurface loads. The *flexural rigidity* (D) of the plate determines the degree to which the plate supports the load. The elastic plate model is analogous to a diving board, the *load* being the *diver* standing near the end of the board (Fig. 8.22). A thin, weak board (small D) bends greatly, especially near the diver. A thicker board of the same material behaves more rigidly; the diver causes a smaller deflection. The flexural rigidity (resistance to bending) thus depends on the *elastic thickness* of each board.

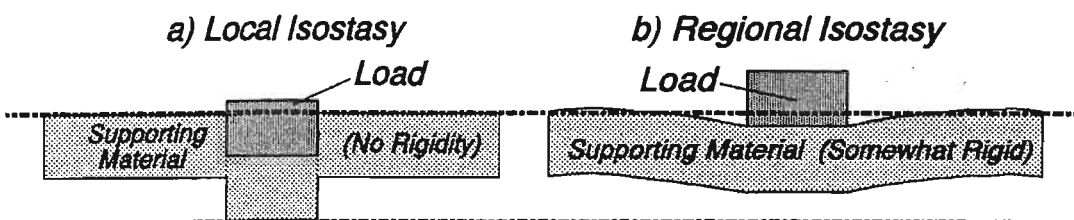


FIGURE 8.21 The type of isostatic compensation depends on the flexural rigidity of the supporting material. a) *Local isostasy*. Where there is no rigidity, compensation is directly below the load. b) *Regional isostasy*. Materials with rigidity are flexed, distributing the load over a broader region.

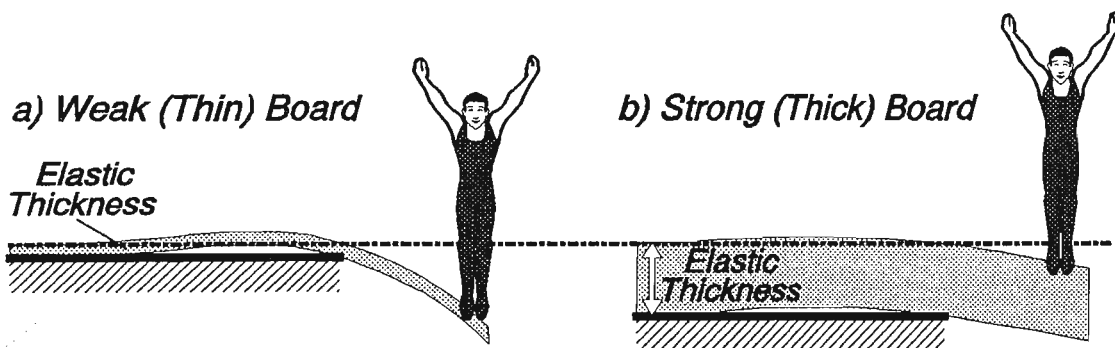


FIGURE 8.22 *Flexural rigidity.* a) A thin diving board (small elastic thickness) has low flexural rigidity. b) A thick board (large elastic thickness) has high flexural rigidity.

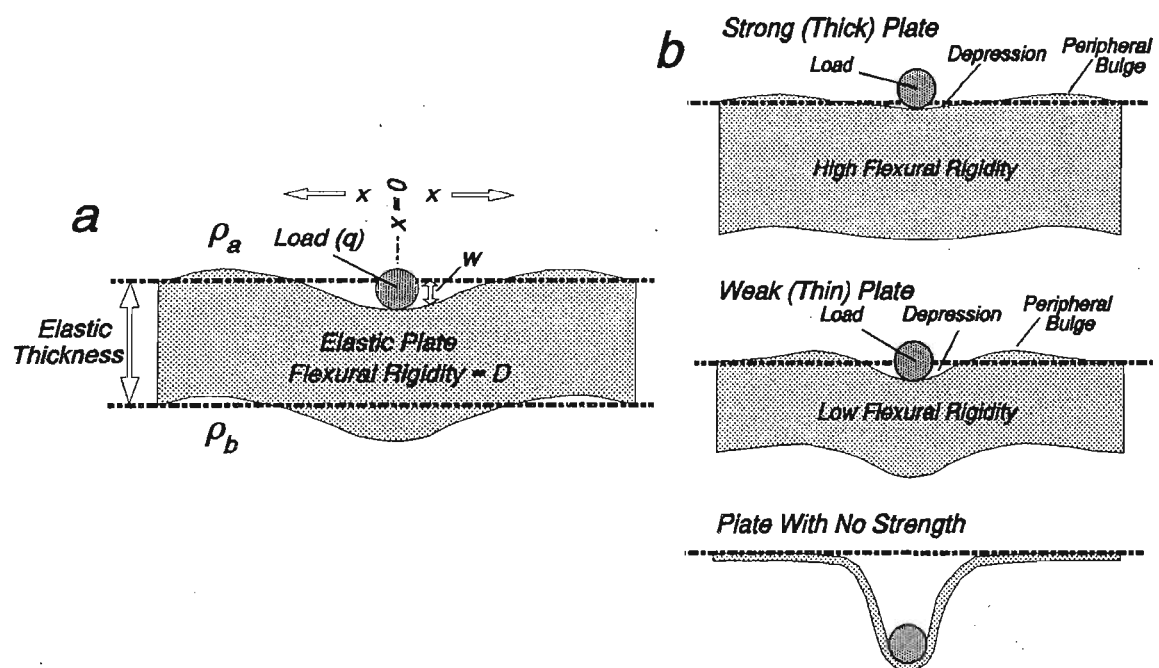


FIGURE 8.23 a) Parameters for two-dimensional model of a plate flexed by a linear load. Both the plate and load extend infinitely in and out of the page. See text for definition of variables. b) Positions of depressions and bulges formed on the surface of a flexed plate. A strong plate has shallow but wide depressions. The depressions and peripheral bulges have larger amplitudes on a weak plate, but are closer to the load. A very weak plate collapses into local isostatic equilibrium.

The deflection of a two-dimensional plate, due to a linear load depressing the plate's surface, is developed by Turcotte and Schubert (1982). The model (Fig. 8.23a) assumes that material below the plate is fluid. The vertical deflection of points along the surface of the plate can be computed according to:

$$D(\frac{d^4w}{dx^4}) + (\rho_b - \rho_a)gw = q(x)$$

where:

D = flexural rigidity of the plate

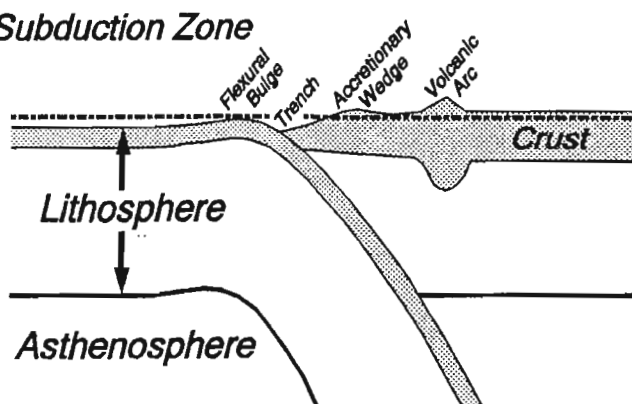
w = vertical deflection of the plate at x

x = horizontal distance from the load to a point on the surface of the plate
 ρ_a = density of the material above the plate
 ρ_b = density of the material below the plate
 g = gravitational acceleration
 $q(x)$ = load applied to the top of the plate at x .

Four important concepts are illustrated by solutions to the above equation (Fig. 8.23b): 1) a strong lithospheric plate (large D) will have a small amplitude deflection (small w), spread over a long wavelength; 2) a weak lithospheric plate (small D) has large deflection (large w), but over a smaller wavelength; 3) where plates have significant strength, an upward deflection ("peripheral" or "flexural" bulge) develops some distance from the load, separated by a depression; 4) plates with no strength collapse into local isostatic equilibrium.

Two simplified examples of lithospheric flexure are shown in Fig. 8.24. At a subduction zone (Fig. 8.24a), flexure is analogous to the bending at the edge of a diving board (Fig. 8.22). The load is primarily the topography of the accretionary wedge and volcanic arc on the overriding plate. Flexure of the downgoing plate results in a depression (trench) and, farther out to sea, a bulge on the oceanic crust. The mass of high mountains puts a load on a plate that can be expressed in both directions (Fig. 8.24b). Depressions between the mountains and flexural bulges ("foreland basins") can fill with sediment to considerable thickness.

a) Subduction Zone



b) Mountain Range

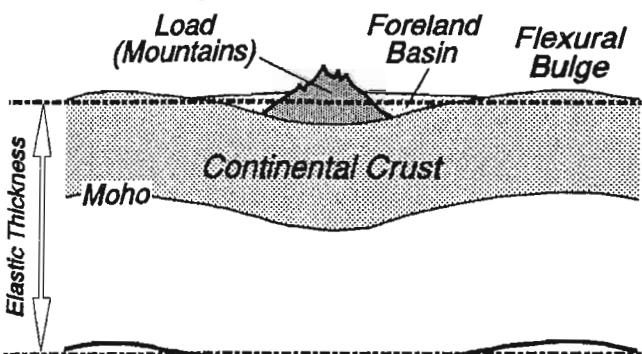


FIGURE 8.24 Examples of lithospheric flexure. a) A flexural bulge and depression (trench) develop as the downgoing plate is flexed at a subduction zone. b) The weight of a mountain range causes adjacent depressions that fill with sediment (foreland basins).

GRAVITY MODELING

Forward modelling of mass distributions is a powerful tool to visualize free air and Bouguer gravity anomalies that result from different geologic situations. For large tectonic features, gravity modeling can be even more insightful if considerations of the isostatic state of the region are incorporated.

A common method used to model gravity data is the two-dimensional approach developed by Talwani et al. (1959). The gravity anomaly resulting from a model is computed as the sum of the contributions of individual bodies, each with a given density (ρ) and volume (V) (that is, a mass, m , proportional to $\rho \times V$). The two-dimensional bodies are approximated, in cross section, as polygons (Fig. 8.25).

Gravity Anomalies from Bodies with Simple Geometries

To appreciate contributions from complex-shaped polygons, it is helpful to understand, first, the gravity expression of two simple geometric shapes: 1) a *sphere* and 2) a *semi-infinite slab*.

Sphere The attraction of a sphere buried below Earth's surface can be viewed in much the same way as the attraction of the entire Earth from some distance in space (Figs. 8.3; 8.26). The equation for both cases follows an inverse square law of the form:

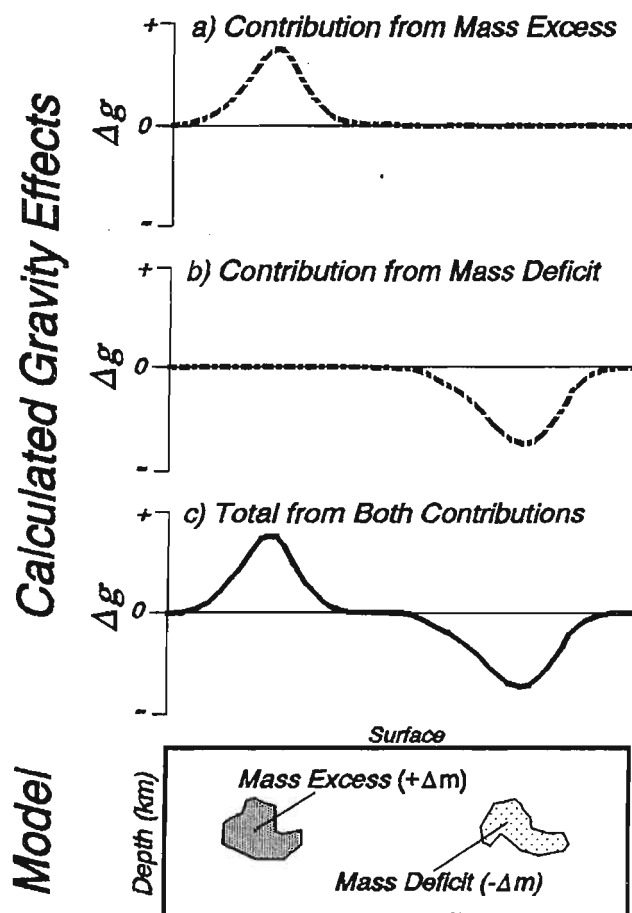


FIGURE 8.25 Two-dimensional gravity modeling of subsurface mass distributions. Bodies of anomalous mass are polygonal in cross section, maintaining their shapes to infinity in directions in and out of the page. a) Relative to surrounding material, a body with excess mass results in a positive contribution to the gravity anomaly profile (Δg). b) A negative contribution results from a body with a deficiency of mass. c) The gravity anomaly for the simple model is the sum of the contributions shown in (a) and (b).

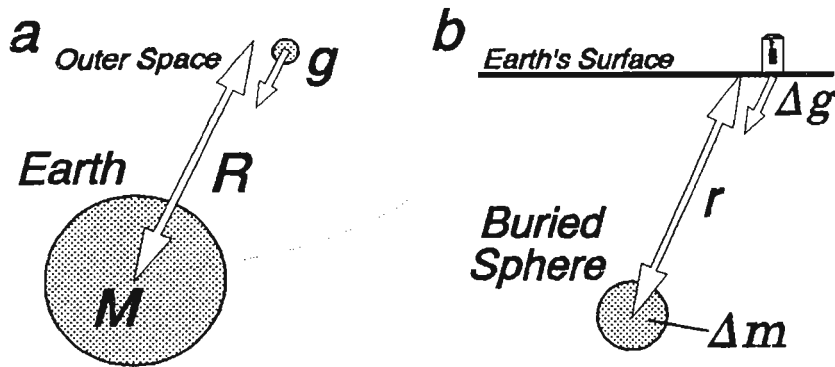


FIGURE 8.26 Analogy between the gravitational attraction of the Earth from space and a sphere of anomalous mass buried beneath Earth's surface. a) Earth's gravitational acceleration (g) at a distant observation point depends on the mass of the Earth (M) and the distance (R) from the center of mass to the observation point. b) The change in gravity (Δg) due to a buried sphere depends on the difference in mass (Δm , relative to the surrounding material), and the distance (r) from the sphere to an observation point on Earth's surface.

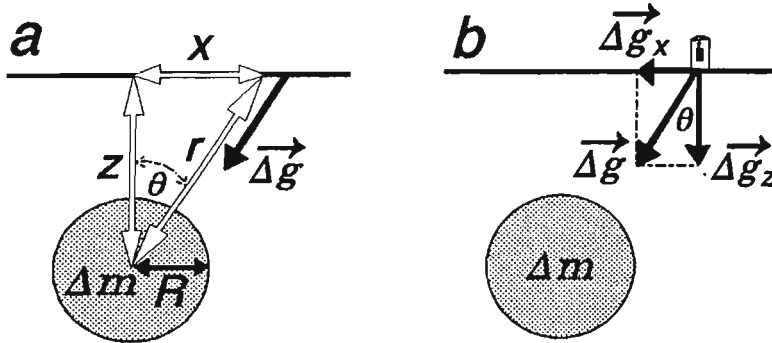


FIGURE 8.27 Gravitational effect ($\vec{\Delta g}$) of a buried sphere of radius (R) and anomalous mass (Δm). a) The distance (r) to the center of the sphere can be broken into horizontal (x) and vertical (z) components. b) The magnitude (Δg) of the gravitational attraction vector can be broken into horizontal (Δg_x) and vertical (Δg_z) components. For a perfect sphere with uniform Δm , the angle θ is the same as in (a).

$$g = \frac{GM}{R^2}$$

A buried sphere may have excess or deficient mass (Δm) relative to the surrounding material; its center lies a distance (r) from the observation point (Fig. 8.27a). The change in gravitational attraction (Δg) due to the sphere is:

$$\Delta g = \frac{G(\Delta m)}{r^2}$$

The density (ρ) of the material is defined as mass (m) per unit volume (V):

$$\rho = m/V$$

so that:

$$m = \rho V$$

The excess (or deficient) mass of the sphere, in terms of the density difference ($\Delta\rho$) between the sphere and the surrounding material, is therefore:

$$\Delta m = (\Delta\rho)V$$

the change in gravity is thus:

$$\Delta g = \frac{G(\Delta\rho)(V)}{r^2}$$

The volume (V) of a sphere of radius R is:

$$V = 4/3 \pi R^3$$

so that:

$$\begin{aligned}\Delta g &= \frac{G(\Delta\rho)}{r^2} (4/3 \pi R^3) \\ &= \frac{4\pi R^3 G(\Delta\rho)}{3} \frac{1}{r^2}\end{aligned}$$

Since $r^2 = x^2 + z^2$:

$$\boxed{\Delta g = \frac{4\pi R^3 G(\Delta\rho)}{3} \frac{1}{(x^2 + z^2)}}$$

Δg is the magnitude of the *total attraction*, at the observation point, due to Δm (Fig. 8.27a). The total attraction is a vector sum of horizontal and vertical components (Fig. 8.27b):

$$\vec{\Delta g} = \vec{\Delta g}_x + \vec{\Delta g}_z$$

where:

$\vec{\Delta g}$ = vector expressing magnitude (Δg) and direction of total attraction due to the anomalous mass of the sphere

$\vec{\Delta g}_x$ = horizontal component of $\vec{\Delta g}$

$\vec{\Delta g}_z$ = vertical component of $\vec{\Delta g}$

$\Delta g_x = \Delta g(\sin\theta)$ = horizontal component of Δg

$\Delta g_z = \Delta g(\cos\theta)$ = vertical component of Δg

θ = angle between a vertical line and the $\vec{\Delta g}$ direction.

The magnitude can be expressed as the vector sum of horizontal and vertical components:

$$\Delta g = \sqrt{(\Delta g_x)^2 + (\Delta g_z)^2}$$

A gravimeter measures only the vertical component of the gravitational attraction (Fig. 8.27b):

$$\boxed{\Delta g_z = \Delta g (\cos\theta)}$$

From Fig. 8.27a:

$$\cos\theta = z/r$$

so that:

$$\Delta g_z = \Delta g(z/r) = \frac{4\pi R^3 G(\Delta\rho)}{3} \frac{1}{(x^2 + z^2)} \frac{z}{r}$$

Again, using:

$$r^2 = x^2 + z^2, \text{ meaning } r = (x^2 + z^2)^{1/2}$$

$$\Delta g_z = \frac{4\pi R^3 G(\Delta\rho)}{3} \frac{1}{(x^2 + z^2)} \frac{z}{(x^2 + z^2)^{1/2}}$$

Substituting the value for $4\pi/3$:

$$\Delta g_z = 4.1888 R^3 G(\Delta\rho) \frac{z}{(x^2 + z^2)^{3/2}}$$

Using $G = 6.67 \times 10^{-11} \text{ Nm}^2/\text{kg}^2$:

$$\Delta g_z = 0.02794 (\Delta\rho) R^3 \frac{z}{(x^2 + z^2)^{3/2}}$$

where the variables and units are:

Δg_z = vertical component of gravitational attraction measured by a gravimeter ($mGal$)

$\Delta\rho$ = difference in density between the sphere and the surrounding material (g/cm^3)

R = radius of the sphere (m)

x = horizontal distance from the observation point to a point directly above the center of the sphere (m)

z = vertical distance from the surface to the center of the sphere (m).

Fig. 8.28a shows the variables in the above equation. The buried sphere model illustrates some fundamental properties of gravity anomalies (Fig. 8.28b): 1) mass

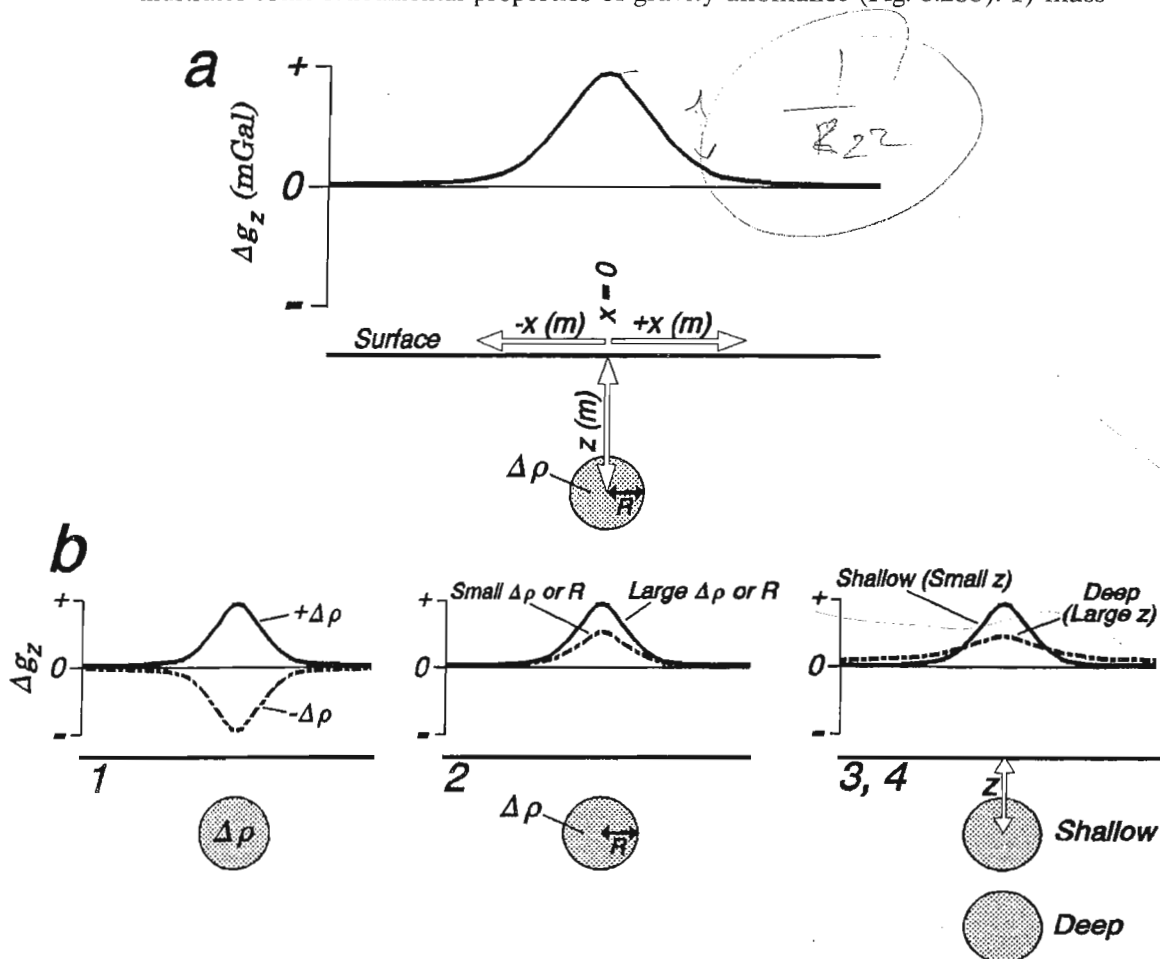


FIGURE 8.28 a) Gravity anomaly profile (Δg_z) attributable to a buried sphere of radius (R_1 in m), depth (z), and anomalous density ($\Delta\rho_1$ in g/cm^3). The horizontal distance (x) is measured in negative ($-x$) and positive ($+x$) directions from a point on the surface directly above the sphere. b) Form of gravity anomaly profiles due to (1) positive vs. negative density contrasts; (2) changing mass anomaly; and (3,4) changing depth.

excess ($+\Delta m$, implying $+\Delta\rho$) causes an increase in gravity ($+\Delta g_z$), while mass deficit ($-\Delta m$, implying $-\Delta\rho$) results in a gravity decrease ($-\Delta g_z$); 2) the more massive the sphere (larger $\Delta\rho$ and/or larger R), the greater the amplitude ($|\Delta g_z|$) of the gravity anomaly; 3) the anomaly is attenuated (smaller $|\Delta g_z|$) as the sphere is buried more deeply within the Earth; 4) the width of the gravity anomaly increases as the sphere is buried more deeply.

Semi-Infinite Slab Where there are density changes that can be approximated by horizontal layering, it is convenient to model lateral changes in gravity as the effects of abrupt truncations of infinite slabs. An infinite slab (Fig. 8.29a) that has excess mass ($+\Delta m$) will increase the gravity ($+\Delta g_z$), while mass deficit ($-\Delta m$) will cause the gravity to decline ($-\Delta g_z$). Truncating the slab (Fig. 8.29b) results in: 1) essentially no gravity effect in regions far from the slab; 2) an increase (or decrease) in gravity crossing the edge of the slab; and 3) the full (positive or negative) gravity effect in regions over the slab but far from the edge.

An infinite slab represents a mass anomaly (Δm) that is a function of the thickness of the slab (Δh) and its density ($\Delta\rho$) relative to surrounding materials (Fig. 8.29c). The amount the slab adds or subtracts to gravitational attraction (Δg_z) is exactly the same as that of the infinite slab used in the Bouguer correction (Fig. 8.9):

$$\Delta g_z = 0.0419(\Delta\rho)(\Delta h)$$

The gravity effect of a *semi-infinite slab*, however, changes according to position relative to the slab's edge (Fig. 8.29d): 1) far away from the slab, the contribution (Δg_z)

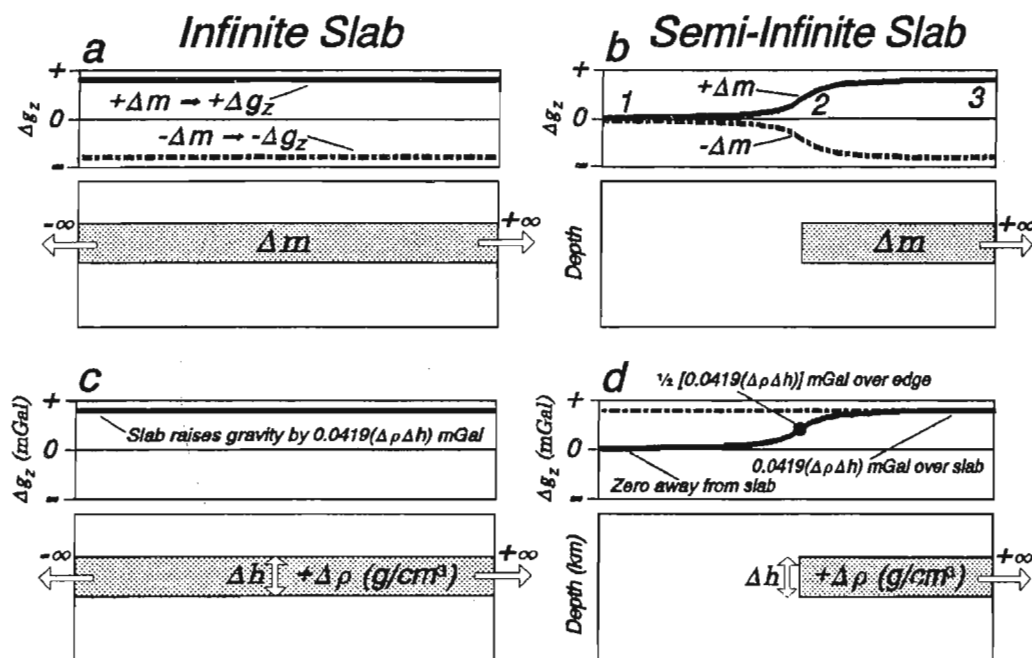


FIGURE 8.29 a) An *infinite slab* adds or subtracts a constant amount to the gravity field, depending on whether the slab represents a positive ($+\Delta m$) or negative ($-\Delta m$) mass anomaly. b) The gravity effect of a *semi-infinite slab* changes gradually as the edge of the slab is crossed. c) An infinite slab produces exactly the same gravity effect as the slab used for the Bouguer correction. d) The gravity effect of a semi-infinite slab is equal to the Bouguer slab approximation far out over the slab (right), $\frac{1}{2}$ of that value directly over the slab's edge, and zero far away from the edge (left).

is zero; 2) above the edge of the slab, the contribution is exactly 1/2 the maximum value ($\Delta g_z = \frac{1}{2}[0.0419\Delta\rho\Delta h]$); 3) over the slab, but far from the slab's edge, Δg_z is the same as for an infinite slab ($\Delta g_z = 0.0419\Delta\rho\Delta h$); 4) the rate of change in gravity (the gradient of Δg_z) depends on the depth of the slab.

Griffiths and King (1981) develop an equation for the anomaly caused by a semi-infinite slab (Fig. 8.30a,b):

$$\Delta g_z = G(\Delta\rho)(\Delta h)(2\phi)$$

where:

ϕ = angle (in radians) from the observation point, between the horizontal surface and a line drawn to the central plane at the slab's edge

G = Universal Gravitational Constant ($6.67 \times 10^{-11} \text{ Nm}^2/\text{kg}^2$).

The angle ϕ can be expressed as:

$$\phi = \pi/2 + \tan^{-1}(x/z)$$

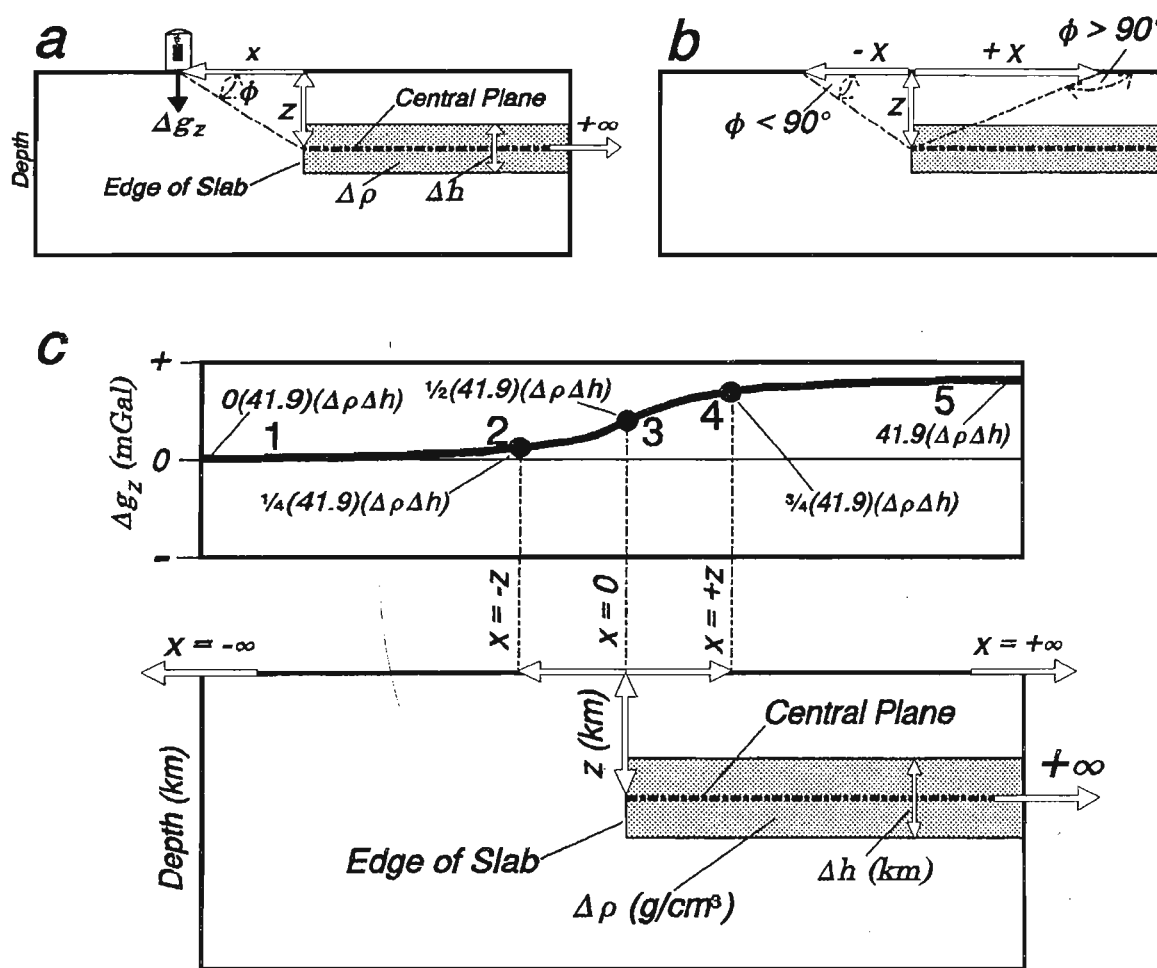


FIGURE 8.30 a) For a semi-infinite slab, the gravity anomaly measured at the surface is $\Delta g_z = G(\Delta\rho)(\Delta h)(2\phi)$, where ϕ is measured in radians. b) Away from the slab, $\phi < \pi/2$ (that is, $\phi < 90^\circ$). Over the slab, $\phi > \pi/2$. c) Method to estimate the change in gravity anomaly (Δg_z) at five horizontal distances (x , in km) from the edge of a semi-infinite slab.

where:

- x = horizontal distance from a point on the surface above the slab's edge
 z = depth of a horizontal surface bisecting the slab (central plane).

The equation is thus:

$$\Delta g_z = 2G(\Delta\rho)(\Delta h)(\pi/2 + \tan^{-1}[x/z])$$

or:

$$\boxed{\Delta g_z = 13.34 (\Delta\rho) (\Delta h) (\pi/2 + \tan^{-1}[x/z])}$$

when the units are: Δg_z in $mGal$; $\Delta\rho$ in g/cm^3 ; Δh , x , z in km. Note five important points from the above equation, illustrated in Fig. 8.30c:

1. $x = -\infty \Rightarrow \Delta g_z = \text{zero} \quad \Rightarrow \Delta g_z = 0(41.9\Delta\rho\Delta h).$
2. $x = -z \Rightarrow \Delta g_z = \frac{1}{2} \text{ its full value} \quad \Rightarrow \Delta g_z = \frac{1}{2}(41.9\Delta\rho\Delta h).$
3. $x = 0 \Rightarrow \Delta g_z = \frac{1}{2} \text{ its full value} \quad \Rightarrow \Delta g_z = \frac{1}{2}(41.9\Delta\rho\Delta h).$
4. $x = +z \Rightarrow \Delta g_z = \frac{1}{2} \text{ its full value} \quad \Rightarrow \Delta g_z = \frac{1}{2}(41.9\Delta\rho\Delta h).$
5. $x = +\infty \Rightarrow \Delta g_z = \text{its full value} \quad \Rightarrow \Delta g_z = 1(41.9\Delta\rho\Delta h).$

For layered cases, a quick estimate of the gravity change across the edge of an anomalous mass can be made by calculating and plotting those five points.

The semi-infinite slab approximation illustrates two fundamental properties of gravity anomalies (Fig. 8.31).

1. The *amplitude* (full value) of the anomaly reflects the *mass excess or deficit* (Δm). The mass excess or deficit depends on the product of density contrast ($\Delta\rho$) and thickness (Δh) of the anomalous body.
2. The *gradient* (rate of change) of the anomaly reflects the *depth of the excess or deficient mass below the surface* (z). The depth thus determines how abruptly the gravity anomaly changes from near zero to near its full value, according to the term $(\pi/2 + \tan^{-1}[x/z])$. A body near the surface results in a gravity

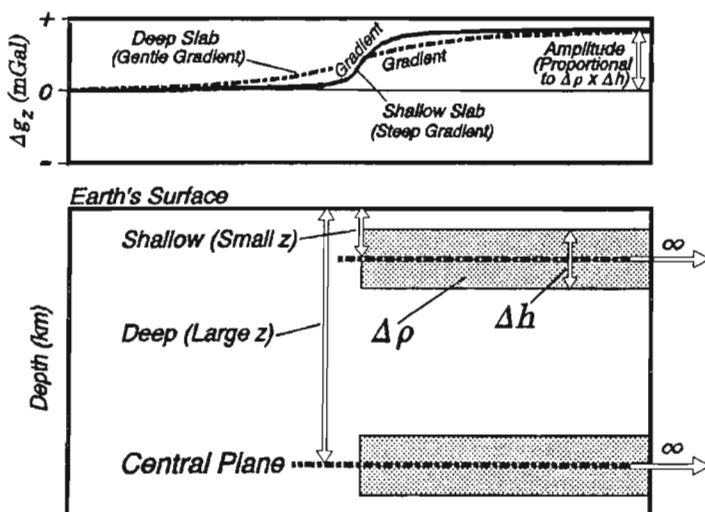


FIGURE 8.31 Lateral change in gravity due to a semi-infinite slab of density contrast ($\Delta\rho$) and thickness (Δh). The amount of change (amplitude) depends on the mass anomaly ($\Delta\rho \times \Delta h$), while the rate of change (gradient) depends on the depth (z) to the central plane of the slab. The greater the mass anomaly, the greater the amplitude; the more deeply buried the slab, the more gentle the gradient.

change with a steep gradient, while the same body deep within the Earth would produce a more gentle gradient.

Models Using Semi-Infinite Slab Approximations

Semi-infinite slab models can be used to approximate contributions to the free-air gravity anomaly at regions in isostatic equilibrium. Two insightful examples are the transition from continental to oceanic crust along a passive continental margin and the thickening of crust at a mountain range.

Passive Continental Margin Thin oceanic crust at passive margins is underlain by mantle at the same depth as the mid-to-lower crust of the adjacent continent. The *mass excess* ($+\Delta m$) of the mantle exerts a force that pulls the oceanic crust downward. By the Airy model, the resulting ocean basin subsides until it has exactly enough water ($-\Delta m$) so that the region is in isostatic equilibrium.

The model in Fig. 8.32 is in Airy isostatic equilibrium, according to parameters modified from Fig. 8.20:

Densities:

$$\rho_w = \text{density of the water} = 1.03 \text{ g/cm}^3$$

$$\rho_c = \text{density of the crust} = 2.67 \text{ g/cm}^3$$

$$\rho_m = \text{density of the mantle} = 3.1 \text{ g/cm}^3.$$

Thicknesses for the ocean side:

$$h_w = \text{thickness of the water column} = 5 \text{ km}$$

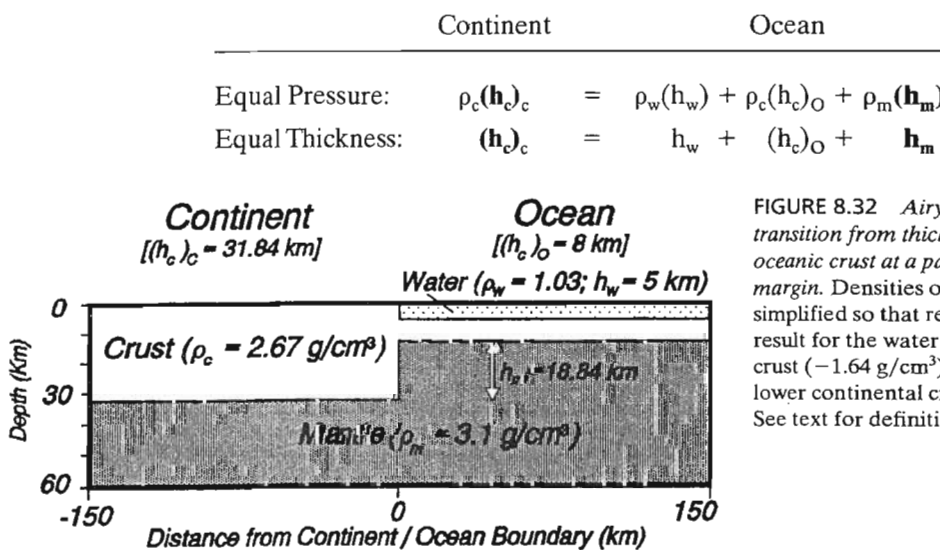
$$(h_o)_o = \text{thickness of the oceanic crust} = 8 \text{ km}$$

$$h_m = \text{thickness of the extra mantle column} = ?$$

Thickness for the continent side:

$$(h_c)_c = \text{thickness of the continental crust} = ?$$

The two unknowns (h_m) and $(h_c)_c$ can be determined from equations expressing the two conditions for local isostatic equilibrium:



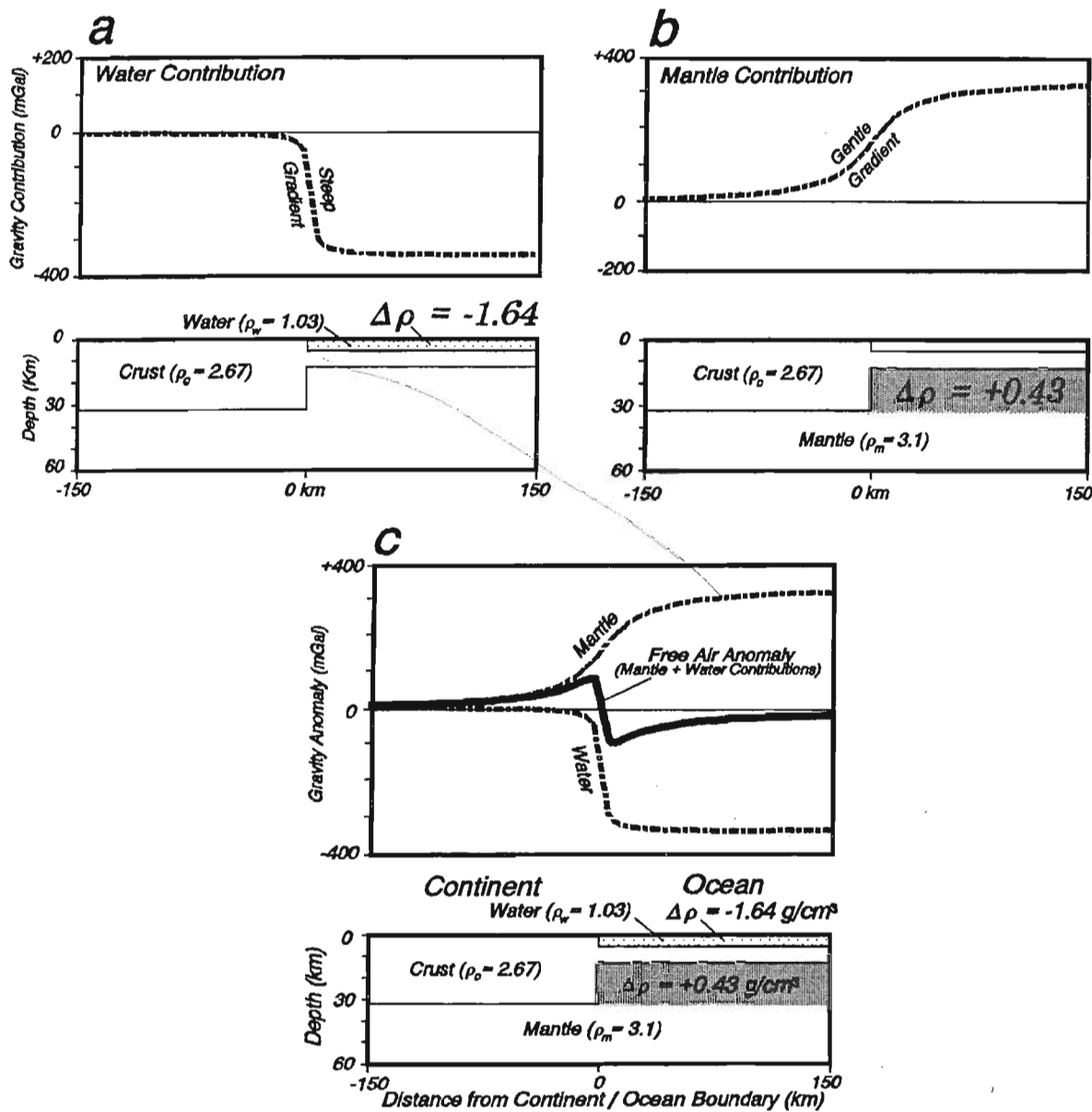


FIGURE 8.33 The main gravity contributions at a passive continental margin have equal amplitude but different gradient. a) The water effect is shallow, causing an abrupt change (steep gradient). b) The extra mantle beneath the oceanic crust is a deeper effect, giving a less abrupt change in gravity (gentle gradient). c) The free air gravity anomaly at a passive continental margin is a positive/negative “edge effect,” due to the summing of contributions that have equal amplitudes but different gradients.

Solving the two equations for the two unknowns yields:

$$(h_c)_c = 31.84 \text{ km} \quad \text{and} \quad h_m = 18.84 \text{ km}$$

The water deepening seaward represents a mass deficit ($-\Delta m$), a function of the product of the water depth (h_w) times the density difference at upper crustal levels ($\Delta \rho = \rho_w - \rho_c = -1.64 \text{ g/cm}^3$). Fig. 8.33a shows that this negative contribution to

the gravity anomaly is an abrupt change, along a steep gradient where the water deepens.

The mass excess ($+\Delta m$) that compensates the shallow water relates to the amount of shallowing of the mantle (h_m) times the difference between mantle and crustal densities ($\Delta\rho = \rho_m - \rho_c = +0.43 \text{ g/cm}^3$; Fig. 8.33b). At great distance from the continental margin, the positive contribution to gravity (due to the mantle shallowing) has the same *amplitude* as the negative contribution (due to the water deepening), because the two effects represent compensatory mass excess and deficit, respectively. The *gradient* for the mantle contribution is more gentle, however, because the anomalous mass causing it is deeper.

The *free air gravity anomaly* (Δg_{fa}) for the simple, passive margin model is the sum of the contributions from the shallow (water) and deep (mantle) effects (Fig. 8.33c). Note that the anomaly is near zero over the interiors of the continent and ocean, but shows a *maximum* over the continental edge and a *minimum* over the edge of the ocean. This positive/negative couple, known as an *edge effect*, results because the contributions due to the shallow and deep sources have different gradients.

The passive margin model shows two important attributes of the *free air gravity anomaly* for a region in *isostatic equilibrium* (Fig. 8.34a): 1) values are *near zero* (except for edge effects), because the mass excess ($+\Delta m$) equals the mass deficit ($-\Delta m$); 2) at edge effects, the *area under the curve* of the gravity anomaly *equals zero*, because the integral of the anomaly, with respect to x , is equal to zero.

The second point is worth further discussion, because it provides a quick test for local isostatic equilibrium. The free air anomaly curve for the passive margin model is the sum of two contributions (Fig. 8.33):

$$\begin{aligned}\Delta g_z &= \Delta g_z(\text{bath}) + \Delta g_z(\text{moho}) \\ &= 2G(\Delta\rho)_b(\Delta h)_b(\pi/2 + \tan^{-1}[x/z_b]) \\ &\quad + 2G(\Delta\rho)_m(\Delta h)_m(\pi/2 + \tan^{-1}[x/z_m])\end{aligned}$$

where:

Δg_z = free air anomaly

$\Delta g_z(\text{bath})$ = contribution to the free air anomaly due to the mass deficiency of the water deepening seaward (bathymetry)

$\Delta g_z(\text{moho})$ = contribution to the free air anomaly due to the mass excess of the mantle shallowing seaward

$(\Delta\rho)_b$ = density contrast of the water compared to upper continental crust

$(\Delta\rho)_m$ = density contrast of the shallow mantle compared to lower continental crust

$(\Delta h)_b$ = thickness of semi-infinite slab of water

$(\Delta h)_m$ = thickness of semi-infinite slab of elevated mantle

x = horizontal distance from the continent/ocean boundary

z_b = vertical distance from sea level to the central plane of the semi-infinite slab of water

z_m = vertical distance from sea level to the central plane of the semi-infinite slab of elevated mantle.

The equation can be simplified:

$$\Delta g_z = 2G \left\{ (\Delta\rho)_b(\Delta h)_b(\pi/2 + \tan^{-1}[x/z_b]) + (\Delta\rho)_m(\Delta h)_m(\pi/2 + \tan^{-1}[x/z_m]) \right\}$$

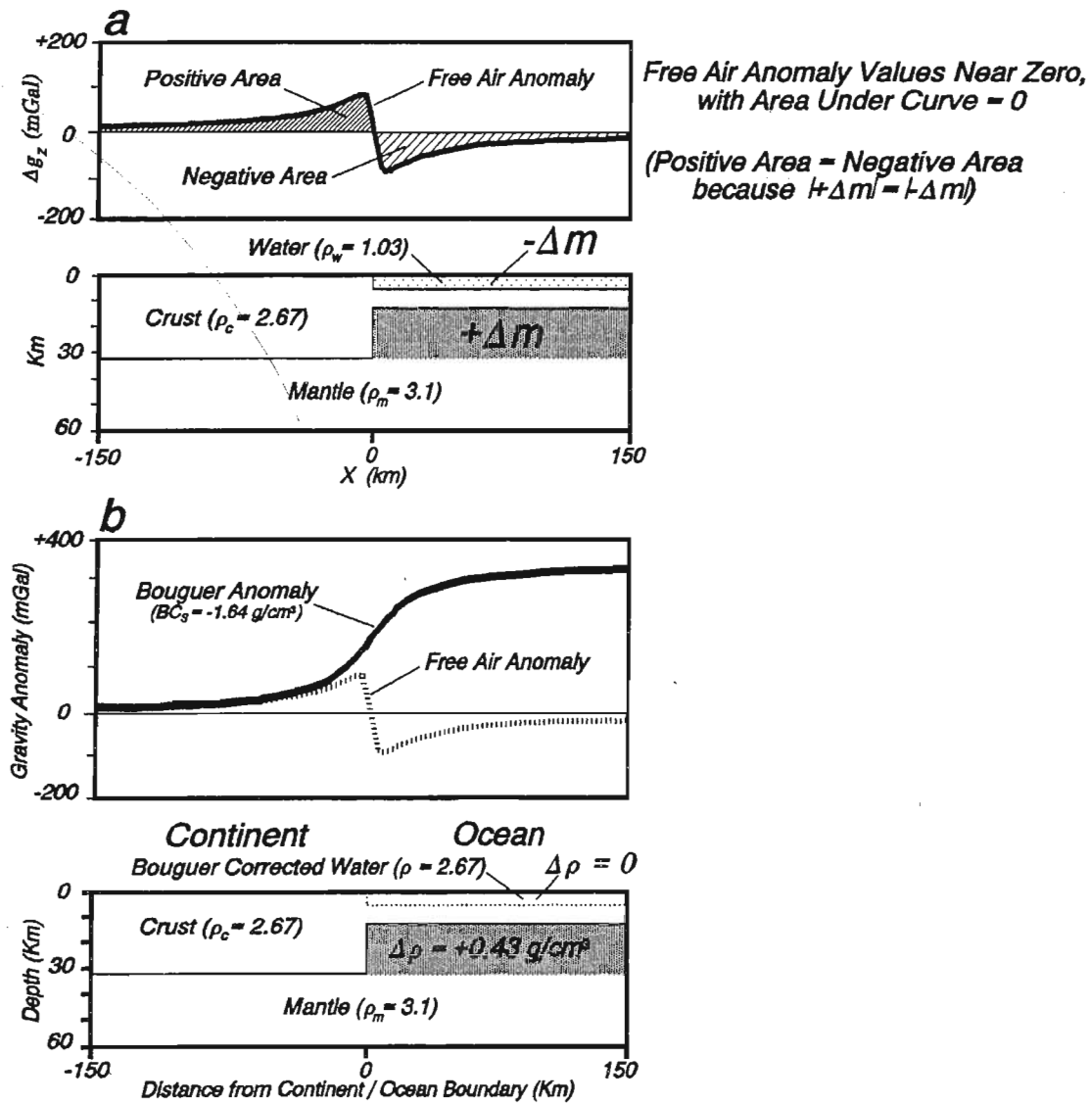


FIGURE 8.34 Free air and Bouguer gravity anomalies for passive continental margin in local isostatic equilibrium.
a) Isostatic equilibrium means the absolute value of excess mass ($|+\Delta m|$) equals the absolute value of deficient mass ($|-\Delta m|$). With this equality, the integral of the change in gravity with respect to x ($\int \Delta g_z dx$) = 0. The zero integral means that the positive and negative areas under the free air anomaly curve sum to zero. b) The Bouguer correction at sea (Fig. 8.9b), applied to the free air anomaly in (a), yields the general form of the Bouguer anomaly at a passive continental margin.

Let:

A = horizontal surface area of a slab (same for each slab).

The density of a slab is:

$$\rho = m/V$$

where:

m = mass of a slab

V = volume of a slab = $A(\Delta h)$.

therefore:

$$m = \rho V = \rho A(\Delta h)$$

For each slab:

$$\Delta m = (\Delta \rho)A(\Delta h)$$

$$(\Delta \rho)(\Delta h) = \Delta m/A$$

so that:

$$\Delta g_z = 2G \left\{ \begin{array}{l} ([\Delta m]_b/A)(\pi/2 + \tan^{-1}[x/z_b]) \\ + ([\Delta m]_m/A)(\pi/2 + \tan^{-1}[x/z_m]) \end{array} \right\}$$

where:

$[\Delta m]_b$ = mass deficit of the water slab

$[\Delta m]_m$ = mass excess of the mantle slab.

Airy isostatic equilibrium implies that:

$$[\Delta m]_b = -[\Delta m]_m$$

so that:

$$\Delta g_z = 2G([\Delta m]_b/A) \{(\pi/2 + \tan^{-1}[x/z_b]) - (\pi/2 + \tan^{-1}[x/z_m])\}$$

$$\Delta g_z = 2G([\Delta m]_b/A) (\tan^{-1}[x/z_b] - \tan^{-1}[x/z_m])$$

The area under the free air anomaly curve is the integral of Δg_z , with respect to x :

$$\int_{-\infty}^{+\infty} \Delta g_z dx = 2G([\Delta m]_b/A) \int_{-\infty}^{+\infty} (\tan^{-1}[x/z_b] - \tan^{-1}[x/z_m]) dx$$

Standard integral tables show that, regardless of the depths of the slabs (z_b and z_m), the integral from $-\infty$ to $+\infty$ is zero:

$$\int_{-\infty}^{+\infty} (\tan^{-1}[x/z_b] - \tan^{-1}[x/z_m]) dx = 0$$

therefore:

$$\boxed{\int_{-\infty}^{+\infty} \Delta g_z dx = 0}$$

The last expression demonstrates that the area under the curve for the free air anomaly equals zero (Fig. 8.34a). This relationship is seen in each of the models below that are in a state of local isostatic equilibrium.

Fig. 8.35 shows an observed free air gravity anomaly profile, and a density model, for the passive continental margin on the east coast of the United States. The free air anomaly shows clearly the edge effect due to the water deepening as the mantle shallows (Fig. 8.33). Some isostatic imbalance is also evident, because the negative area (under the curve) is greater than the positive area.

The *Bouguer gravity anomaly* (Δg_B) for the simple, passive margin model results from correcting the mass deficit of the water to approximate that of the upper part of the crust (Fig. 8.34b). The passive margin model thus illustrates the general form of the Bouguer anomaly for a region in local isostatic equilibrium: 1) values are near zero over normal continental crust; 2) the Bouguer anomaly mimics

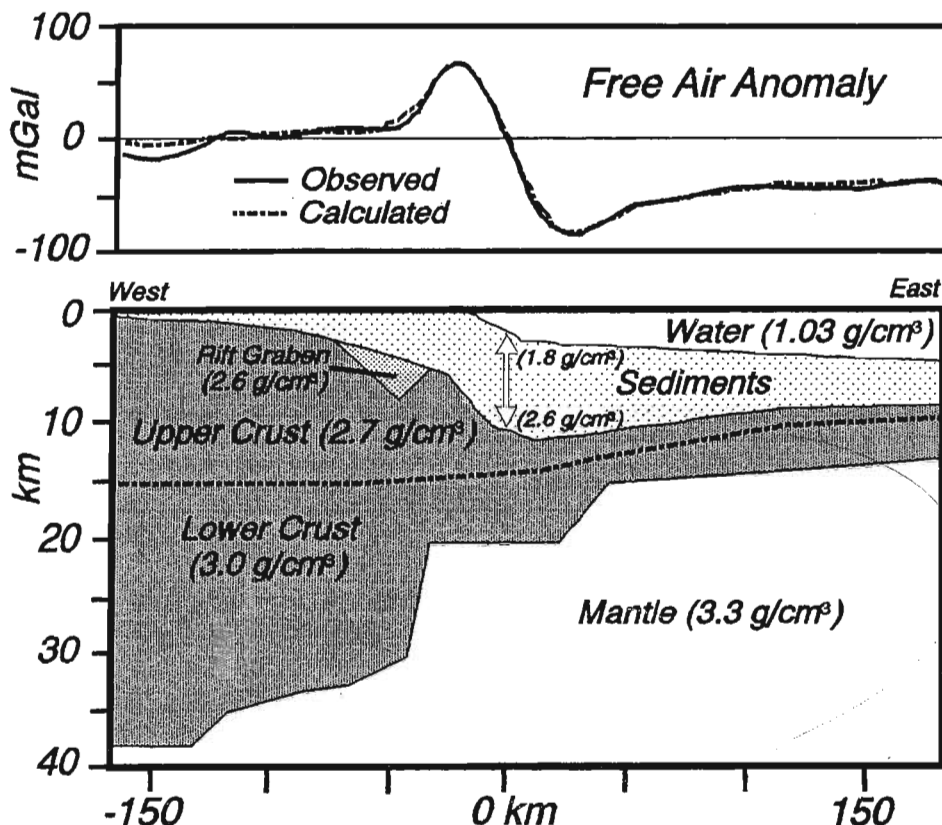


FIGURE 8.35 Observed free air gravity anomaly from the passive continental margin off the Atlantic coast of the United States. The dashed line is the anomaly calculated from the two-dimensional density model. Note the edge effect, with the high toward the continent, the low over the ocean. The zero crossing is near the edge of the continental shelf, where the water column deepens abruptly. Line IPOD off Cape Hatteras, North Carolina. From “Deep structure and evolution of the Carolina Trough,” by D. Hutchinson, J. Grow, K. Klitgord, and B. Swift, AAPG Memoir, no. 34, pp. 129–152, © 1983. Redrawn with permission of the American Association of Petroleum Geologists, Tulsa, Oklahoma, USA.

the Moho, increasing to large positive values as the mantle shallows beneath the ocean; 3) the form of the Bouguer anomaly is somewhat a mirror image of the topography (or bathymetry); the increase in the anomaly thus correlates with deepening of the water.

Mountain Range As continental crust thickens during orogenesis (Figs. 2.18, 6.35), the crustal root exerts upward force, due to its buoyancy relative to surrounding mantle. By the Airy model, the topography ($+\Delta m$) grows until its weight exactly balances the effect of the low-density root ($-\Delta m$). The mountain range model (Fig. 8.36) is in Airy isostatic equilibrium, according to parameters modified from Fig. 8.20:

Densities:

$$\rho_a = \text{density of the air} = 0$$

$$\rho_c = \text{density of the crust} = 2.67 \text{ g/cm}^3$$

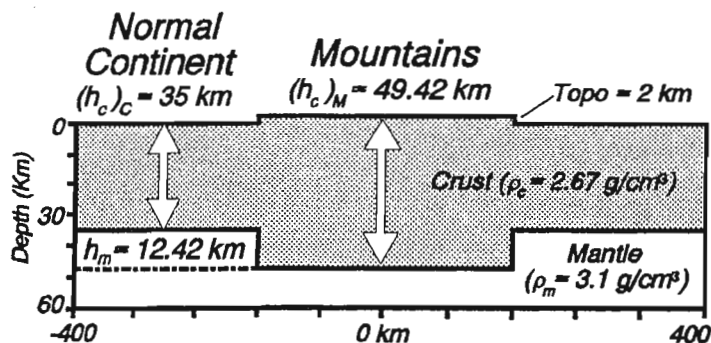


FIGURE 8.36 Airy isostatic model of 2 km high mountain range. Densities of crust and mantle are simplified so that reasonable contrasts result for the topography vs. air ($+2.67 \text{ g/cm}^3$) and the crustal root vs. mantle (-0.43 g/cm^3).

$$\rho_m = \text{density of the mantle} = 3.1 \text{ g/cm}^3.$$

Thicknesses at the Normal Continental Crust:

$$h_a = \text{thickness of the air column} = 2 \text{ km}$$

$$(h_c)_C = \text{thickness of crust outside mountains} = 35 \text{ km}$$

$$h_m = \text{thickness of the extra mantle column} = ?$$

Thickness at the Mountains:

$$(h_c)_M = \text{thickness of total crust at mountains} = ?$$

As with the passive margin model, the two unknowns can be determined from the two conditions for local isostatic equilibrium:

	Normal Continent	Mountains
Equal Pressure:	$\rho_a(h_a) + \rho_c(h_c)_C + \rho_m(h_m) =$	$\rho_c(h_c)_M$
Equal Thickness:	$h_a + (h_c)_C + h_m = (h_c)_M$	

Solving the two equations for the two unknowns yields:

$$h_m = 12.42 \text{ km}$$

and

$$(h_c)_M = 49.42 \text{ km}$$

(Moho depth = 47.42 km)

The contribution to the free-air anomaly due to *topography* of the mountains (Fig. 8.37a) results from the *mass excess* of the material above sea level ($+\Delta m$). This excess is a function of the product of the mountain height (equal to h_a) times the density difference at upper crustal levels ($\Delta\rho = \rho_c - \rho_a = +2.67 \text{ g/cm}^3$). Note that, as with the water effect for the passive margin, the contribution is abrupt, resulting in a steep gradient.

The *crustal root* provides a *mass deficit* ($-\Delta m$) that compensates the extra weight of the topography (Fig. 8.37b). The deficit relates to the product of the amount of deepening of the crust (equal to h_m) times the difference between crustal and mantle densities ($\Delta\rho = \rho_c - \rho_m = -0.43 \text{ g/cm}^3$). If the mountain range is wide (several hundred km), the negative contribution due to the crustal root has the same *amplitude* as the positive contribution due to topography. The *gradient* for the crustal root contribution is more gentle, however, because that anomalous mass is deeper.

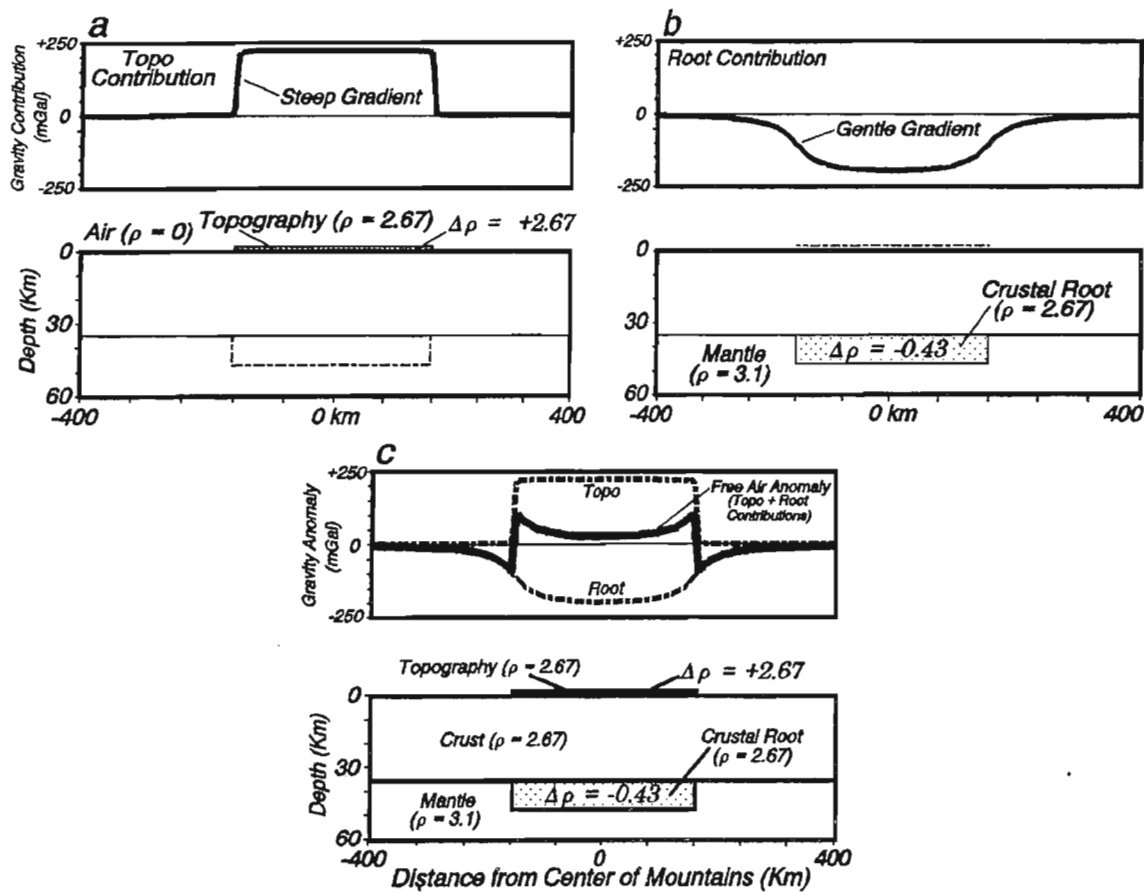


FIGURE 8.37 Contributions to gravity for mountain range in Airy isostatic equilibrium (Fig. 8.36). a) A sharp increase, with nearly full amplitude, results from mass excess of topography. b) Mass deficit of crustal root gives a more gradual decrease. c) The free air gravity anomaly profile for a mountain range in local isostatic equilibrium has edge effects due to the differing gradients of the shallow (a) and deep (b) contributions. Unless the range is very broad, so that the deep effect of the root approaches full amplitude, the free air anomaly has significant positive values over the range.

As in the passive margin model, the free air gravity anomaly (Δg_{fa}) for the mountain range is the sum of the contributions from the shallow and deep sources (Fig. 8.37c). The anomaly is zero over the normal thickness continent and approaches zero over the central part of the mountains. It shows edge effects, however, along the flanks of the range.

The free air gravity anomaly for a mountain range often illustrates some of the fundamental properties of a region in *local isostatic equilibrium* (Fig. 8.38a): 1) values are near zero because the mass excess ($+\Delta m$) of the topography equals the mass deficit ($-\Delta m$) of the crustal root; 2) significant edge effects occur because shallow and deep contributions have different gradients; 3) the area under the curve of the anomaly sums to zero.

Fig. 8.39 shows observed and modeled free gravity anomalies across western South America. Note that the observed free air gravity anomaly profile shows classic edge effects, suggesting that the region is close to local isostatic equilibrium (Fig. 8.38a). The model shows that the crust is very thick (≈ 60 km), beneath the high topography of the Andes Mountains. Thinner crust flanks the mountains, as normal thickness

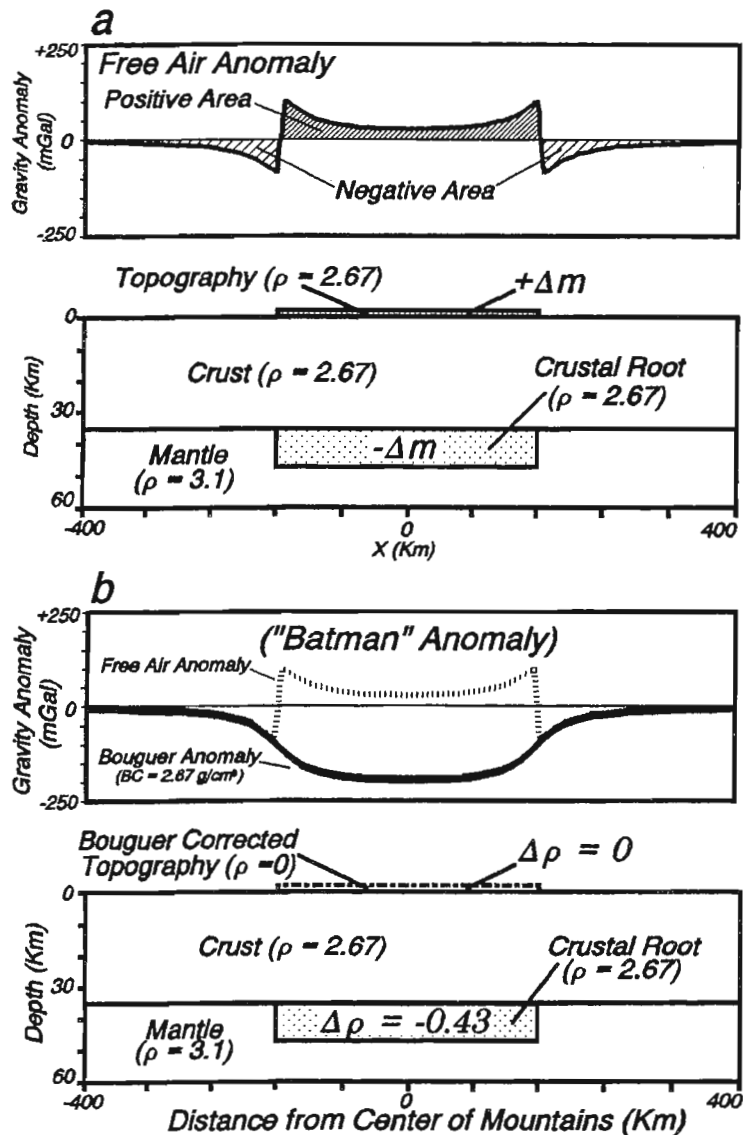


FIGURE 8.38 *Free air and Bouguer gravity anomalies for mountain range in local isostatic equilibrium. a)* Compensatory positive ($+Δm$) and negative ($-Δm$) mass anomalies mean that the integral, with respect to x , of the free air gravity anomaly is zero ($\int Δg_z dx = 0$). In other words, the “area under the curve” sums to zero. b) The Bouguer correction (BC) removes most of the contribution of the mass above sea level (Fig. 8.37a). Bouguer anomaly profiles of mountain ranges thus commonly show low values reflecting the contribution of the crustal root (Fig. 8.37b). Taken together, the free air and Bouguer gravity anomalies form the “Batman anomaly” characteristic of a mountain range in local isostatic equilibrium.

continental craton to the east and oceanic crust to the west. The broad region is thus a mountain range close to a state of Airy isostasy (Fig. 8.36). Deviations from local isostasy (discussed below) occur at the subduction zone on the west side, where the edge effect low is exaggerated at the trench and a flexural bulge high occurs over the adjacent oceanic crust.

The Bouguer gravity anomaly ($Δg_B$) for the mountain range results from subtracting the effect of the mass excess of the topography from the free air anomaly (Fig. 8.9a). Attributes of the Bouguer gravity anomaly that result from isostatic equilibrium are illustrated in Fig. 8.38b: 1) values are near zero over continental crust of normal thickness; 2) the form of the Bouguer anomaly mimics the root contribution; the anomaly decreases as the Moho deepens beneath the mountains; 3) the form of the Bouguer anomaly is almost a mirror image of the topography; the anomaly decreases where the topography of the mountains rises.

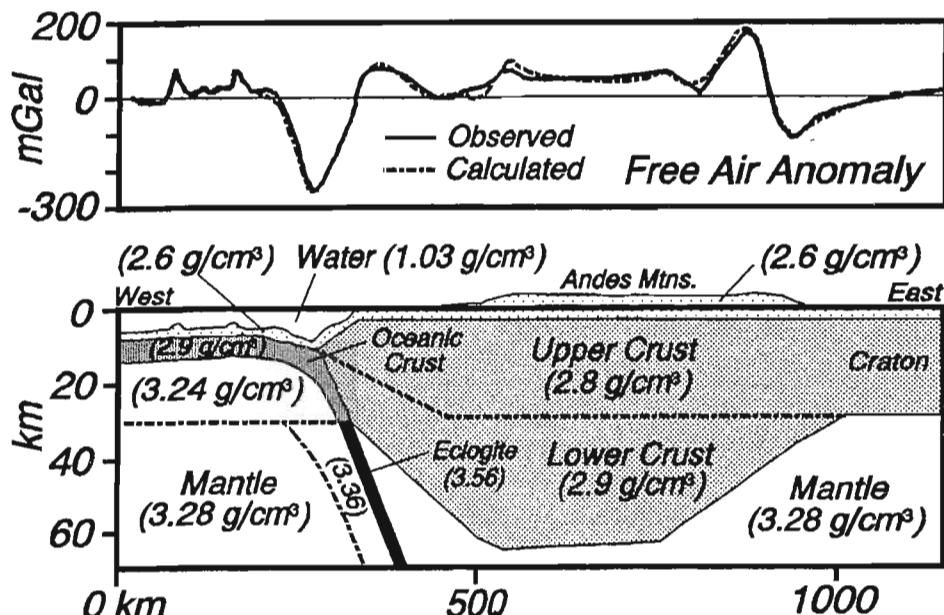


FIGURE 8.39 Observed and modeled free air gravity anomaly of the Andes Mountains and adjacent regions, showing the east portion of the classic "Batman anomaly." The model shown results in a calculated anomaly in close agreement with the observed. Densities in g/cm^3 ($= 10^3 \text{ kg}/\text{m}^3$). From J. Grow and C. Bowin, *Journal of Geophysical Research*, vol. 80, pp. 1449–1458, © 1975. Redrawn with permission of the American Geophysical Union, Washington, D.C.

TECTONIC SETTINGS AND THEIR GRAVITY EXPRESSIONS

The gross forms of free air and Bouguer gravity anomalies reflect: 1) the *density distribution* of Earth materials in a region; and 2) the *flexural strength* of the materials. The Airy isostatic model is an end-member case where supporting materials have no flexural strength. While an oversimplification, the Airy model is nonetheless useful in understanding the general form of gravity anomalies. Once those simple forms are appreciated, modeling of other parameters can be attempted (flexural strength, complex density distributions).

The Airy model suggests isostatic balance involving two boundaries: 1) the *topography* and/or *bathymetry*; and 2) the crust/mantle boundary (*Moho*). Those boundaries are important because they are universal and represent large density contrasts. In some regions, a third boundary is a significant element in isostatic balance: 3) the *lithosphere/asthenosphere boundary*.

The Airy isostatic model in Fig. 8.20 can be modified to incorporate all three boundaries, as summarized below and illustrated in Fig. 8.40. At the *depth of compensation* beneath each region, two equations hold true. 1) The total *pressure* (*P*) exerted by any vertical column (divided by *g*) is equal to that of any other vertical column:

$$P/g = \rho_a h_a + \rho_w h_w + \rho_c h_c + \rho_m h_m + \rho_A h_A = \text{Constant}$$

where:

$$\rho_a = \text{density of the air } (\rho_a \approx 0)$$

CHAPTER 9

Magnetic Interpretation

magnet (*mag'nit*) **n.**, [*< OFr. < magnes < Gr. Magnētis, stone of Magnesia*], a piece of iron, steel, or lodestone that has the property of attracting iron, steel, etc.

force (*fôrs*) **n.**, [*< OFr. < LL., L. fortis, strong*], the cause, or agent, that puts an object at rest into motion or alters the motion of a moving object.

magnetic force (*mag net'ik fôrs*) **n.**, the attracting or repelling force between a magnet and a ferromagnetic material.

field (*feld*) **n.**, [*O.E. feld*], a space in which lines of force are active.

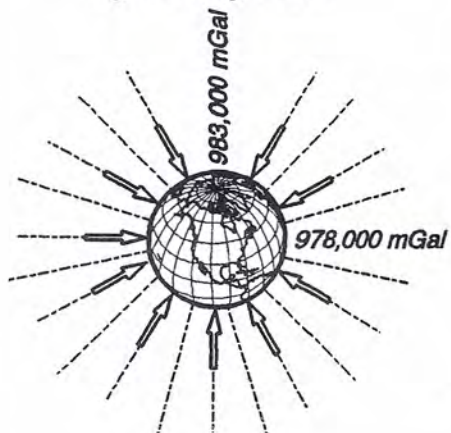
magnetic field (*mag net'ik feld*) **n.**, a region of space in which there is an appreciable magnetic force.

interpret (*in tur'prit*) **vt.**, [*< Mfr. < L. interpretari < interpres, negotiator*], to explain the meaning of; to give one's own understanding of.

magnetic interpretation (*mag net'ik in tur'prä tā'shən*) **n.**, an explanation of the distribution of magnetic materials within the Earth that causes observed changes in Earth's magnetic field.

The magnetic field observed at Earth's surface varies considerably in both strength and direction. Unlike gravitational acceleration, which is directed nearly perpendicular to Earth's surface, magnetic field directions change from nearly horizontal at the equator, to nearly vertical at the poles (Fig. 9.1). The variation in strength of the gravity field is only about 0.5% ($\approx 978,000 \text{ mGal}$ at the equator, $983,000 \text{ mGal}$ at the poles), compared to doubling of the magnetic field ($\approx 30,000 \text{ nT}$ at the equator, $60,000 \text{ nT}$ at the poles).

a) Gravity Field



b) Magnetic Field

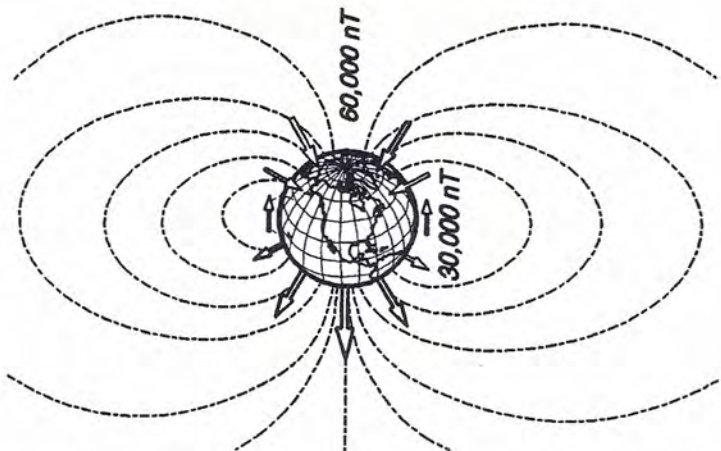


FIGURE 9.1 *Magnitudes and directions of Earth's gravity and magnetic fields.* a) The gravity field is approximately vertical, with only slight variation in magnitude from equator to pole. b) The magnetic field shows strong variations in both magnitude and direction.

The magnetic method has many important applications. Anomalies induced by Earth's natural field give clues to the geometry of magnetized bodies in the crust, and the depth to sources of the anomalies. The depth to the deepest sources of anomalies (Curie Depth) illustrates the depth below which rocks are too hot to retain strong magnetization (Curie Temperature). Studies of rocks that have been permanently magnetized (paleomagnetism) give clues to the ages of the rocks, the latitudes at which they formed, and to the relative positions of continents in the past.

EARTH'S MAGNETIC FIELD

About 98% of Earth's magnetic field is of internal origin, thought to be caused by motions of liquid metal in the core; the remaining 2% is external, of solar origin. Unlike the gravitational field, which is essentially fixed, the magnetic field has secular variations. Measurements in Europe since the 1600's show that the direction of the magnetic field has gradually drifted westward at rates up to 0.2° per year. The overall strength of the field has also decreased by about 8% in the last 150 years. In addition, several factors result in daily, monthly, seasonal, yearly, and longer period variations in the magnetic field. There are also sporadic variations ("magnetic storms") which momentarily disrupt the field.

Axial Dipolar Model

A *magnetic dipole*, inclined about 10.9° from Earth's rotational axis, can be used to describe about 90% of Earth's internal field. With such a model Earth's magnetic field is analogous to that of a bar magnet (Fig. 9.2). A homogeneous Earth with such a dipole would have north and south magnetic poles ("geomagnetic poles") exactly 180° apart (Fig. 9.3a).

The complex source of Earth's magnetism, however, produces lines of force that vary considerably from that of a simple dipole. The actual north and south magnetic poles (that is, positions where the field is vertical) are not 180° apart; they deviate considerably from both the geomagnetic and the geographic poles (Fig. 9.3b).

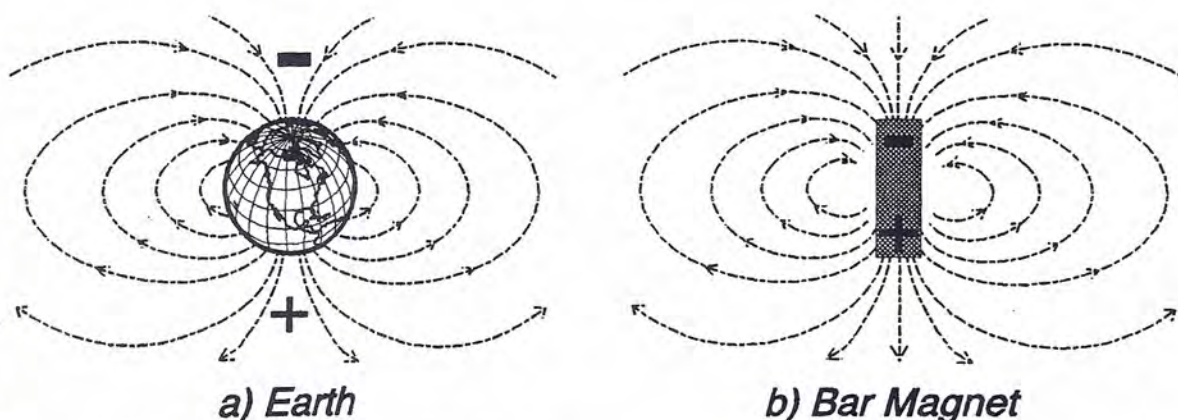


FIGURE 9.2 Earth's magnetic field is similar to that of a bar magnet, with the negative magnetic pole in the northern hemisphere and the positive magnetic pole in the southern hemisphere. The positive end of a compass needle (defined originally as "north-seeking") thus points roughly toward the geographic north pole.

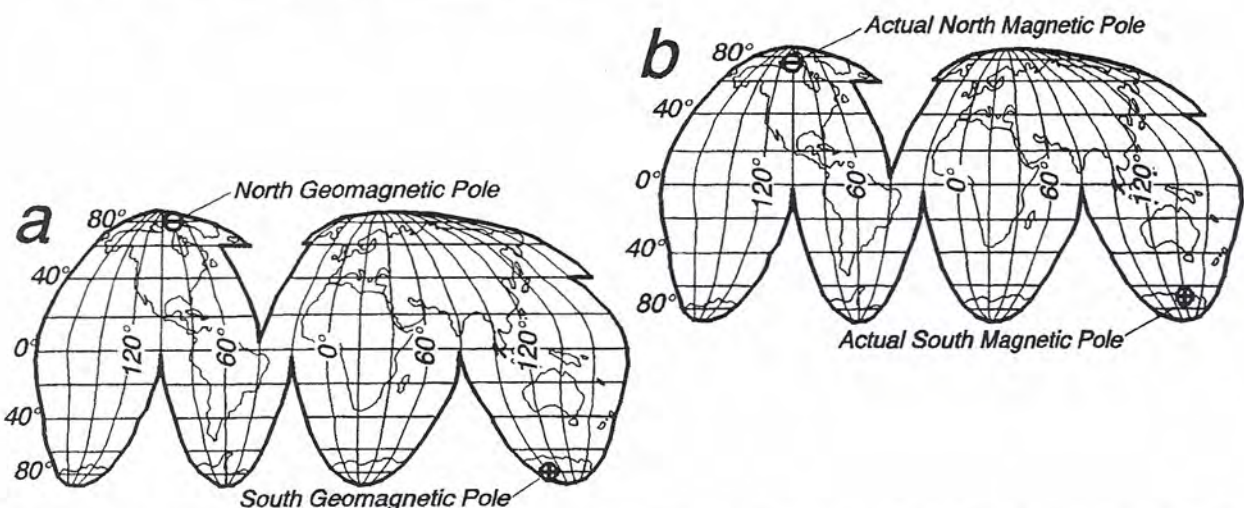


FIGURE 9.3 Earth's magnetic poles. a) Geomagnetic poles, according to a best-fit dipolar model. These poles are exactly 180° apart, deviating 10.9° from the geographic poles (North Geomagnetic Pole = 79.1° N, 71.1° W; South Geomagnetic Pole = 79.1° S, 108.9° E). b) Actual magnetic poles, where the magnetic field is vertical, are not 180° apart (North Magnetic Pole = 75° N, 101° W, on Bathurst Island, Canada; South Magnetic Pole = 67° S, 143° E, in northeast Antarctica).

Strength and Direction of Magnetic Field

A magnetic field is composed of vectors, having both magnitude and direction. The orientation of a compass needle illustrates the direction of Earth's magnetic field (Fig. 9.4).

The *magnetic inclination* (i) is the angle that a compass needle makes with a horizontal ground surface (Fig. 9.4a). A compass needle points vertically toward the ground at the north magnetic pole ($+90^\circ$ inclination), straight upward at the south magnetic pole (-90° inclination). At the magnetic equator, a horizontal compass needle indicates an inclination of 0° .

The angle between a compass needle and true (geographic) north indicates the *magnetic declination* (δ). The north magnetic pole lies approximately along a line (roughly the arc of a great circle) running through the central United States to the geographic north pole; a compass needle would point close to true north along that line. In the northwest United States, a compass needle deviates about 20° eastward from geographic north (Fig. 9.4b).

Unlike gravity, where slight deviations from vertical are commonly not significant, knowledge of the direction of Earth's magnetic field is critical. A vector that describes the magnetic field strength and direction from a given position can be broken into its components as follows (Fig. 9.5):

\vec{F} = total magnetic field vector

\vec{F}_H = horizontal component of total field vector

\vec{F}_N = north component of horizontal vector

\vec{F}_E = east component of horizontal vector

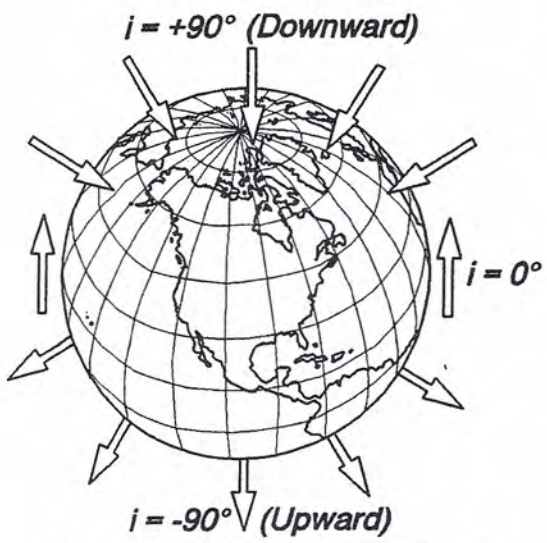
\vec{F}_V = vertical component of total field vector

i = angle of magnetic inclination

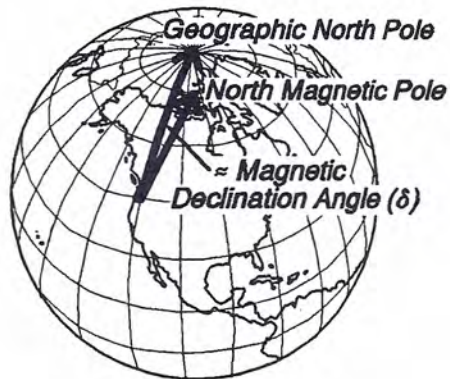
δ = angle of magnetic declination.

The magnitude (F) of the total magnetic field vector (or total field *intensity*) is:

$$F = \sqrt{F_H^2 + F_V^2} = \sqrt{F_N^2 + F_E^2 + F_V^2}$$



a) Magnetic Inclination



b) Magnetic Declination

FIGURE 9.4 *Magnetic inclination and declination.* a) The angle between magnetic lines of force (Fig. 9.1b) and horizontal ground surface is the magnetic inclination (i). b) The magnetic declination (δ) is the angle a compass needle deviates from geographic north.

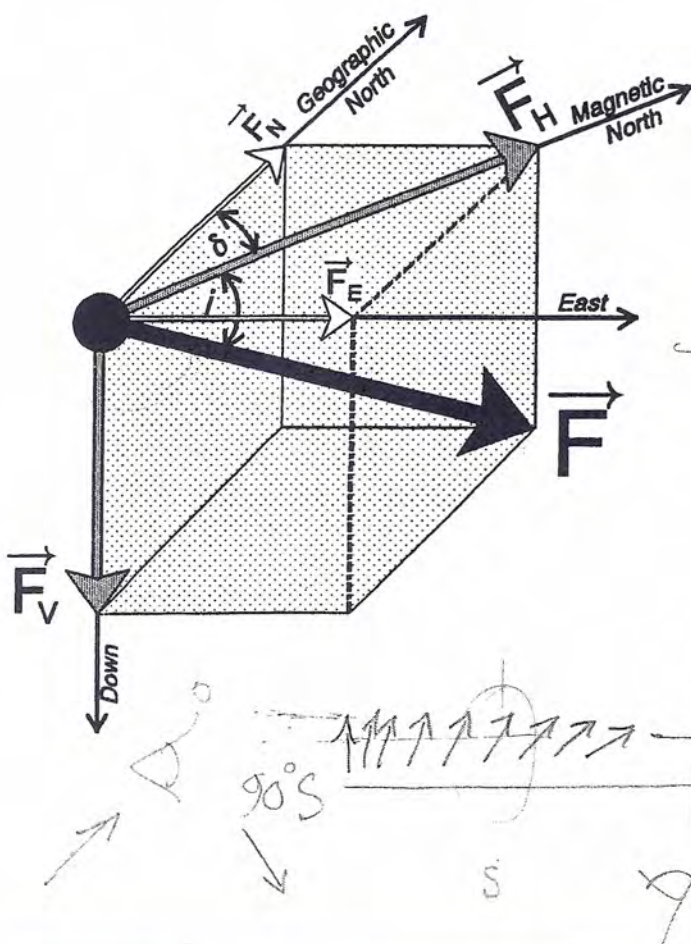
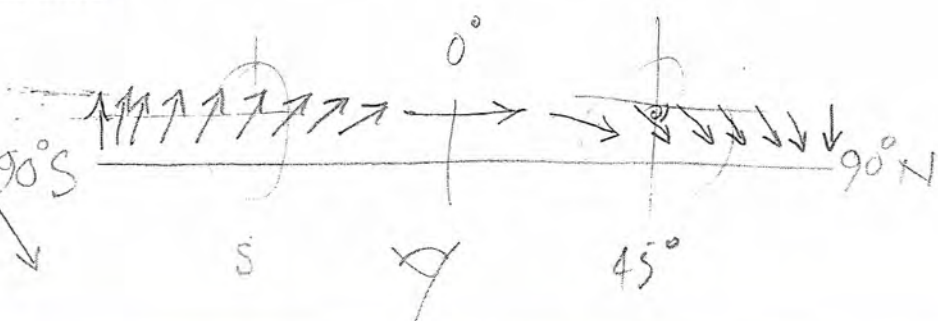
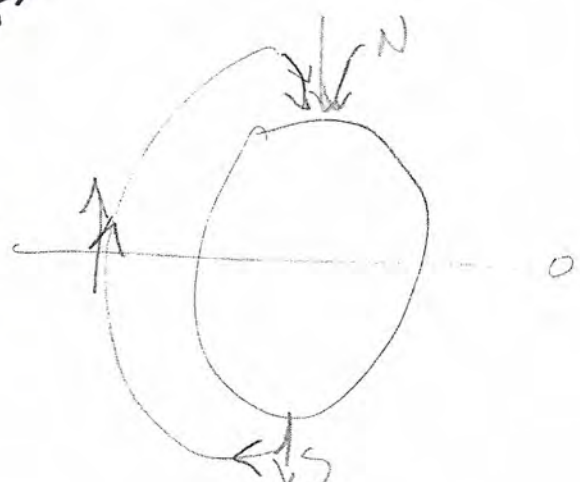


FIGURE 9.5 Components of total magnetic field vector defined in text.



where:

- F_H = magnitude of horizontal component of total field vector
- F_V = magnitude of vertical component of total field vector
- F_N = magnitude of north component of total field vector
- F_E = magnitude of east component of total field vector

The magnetic inclination and declination are:

$$i = \tan^{-1}(F_V/F_H)$$

$$\delta = \tan^{-1}(F_E/F_N)$$

The axial dipole model simplifies discussion of Earth's overall field because equations can be developed to describe the strength and direction of the field. With such a model the magnitudes of the horizontal, vertical, and total field vectors are (Butler, 1992):

$$F_H = \frac{M \cos \phi}{R^3}$$

$$F_V = \frac{2M \sin \phi}{R^3}$$

$$F = \frac{M\sqrt{1 + 3 \sin^2 \phi}}{R^3}$$

where:

- R = radius of the Earth
- M/R^3 = total field intensity at the magnetic equator
- ϕ = magnetic latitude (for axis inclined 10.9° from the true rotational axis; Fig. 9.3a)

The magnetic inclination for an axial dipole also varies systematically with magnetic latitude as:

$$\tan i = 2 \tan \phi$$

The equation expressing the total field intensity (F) illustrates that unlike the gravity field, which decreases by $1/R^2$, the magnetic intensity falls off by $1/R^3$. The same equation is analogous to the theoretical gravity formula discussed in Chapter 8. It thus illustrates that, for a value of $F = M/R^3 \approx 30,000$ nT at the magnetic equator ($\phi = 0^\circ$), the total field intensity doubles to about 60,000 nT at the magnetic pole ($\phi = 90^\circ$). Earth's field, though complex, approximates the axial dipolar model (Fig. 9.6a). Observed inclinations and declinations (Fig. 9.6b, c) also show general agreement with that idealized model.

MAGNETIZATION OF EARTH MATERIALS

Earth's magnetic field is perturbed locally by materials that are capable of being magnetized. Perturbations in the direction of the field can be illustrated by moving a magnet around a compass; the inclination and declination of the compass needle change in response to the position of the magnet (Fig. 9.7). Likewise, when magnetized rocks occur at or below Earth's surface, the direction and magnitude of Earth's overall magnetic field change slightly. It is thus important to understand the

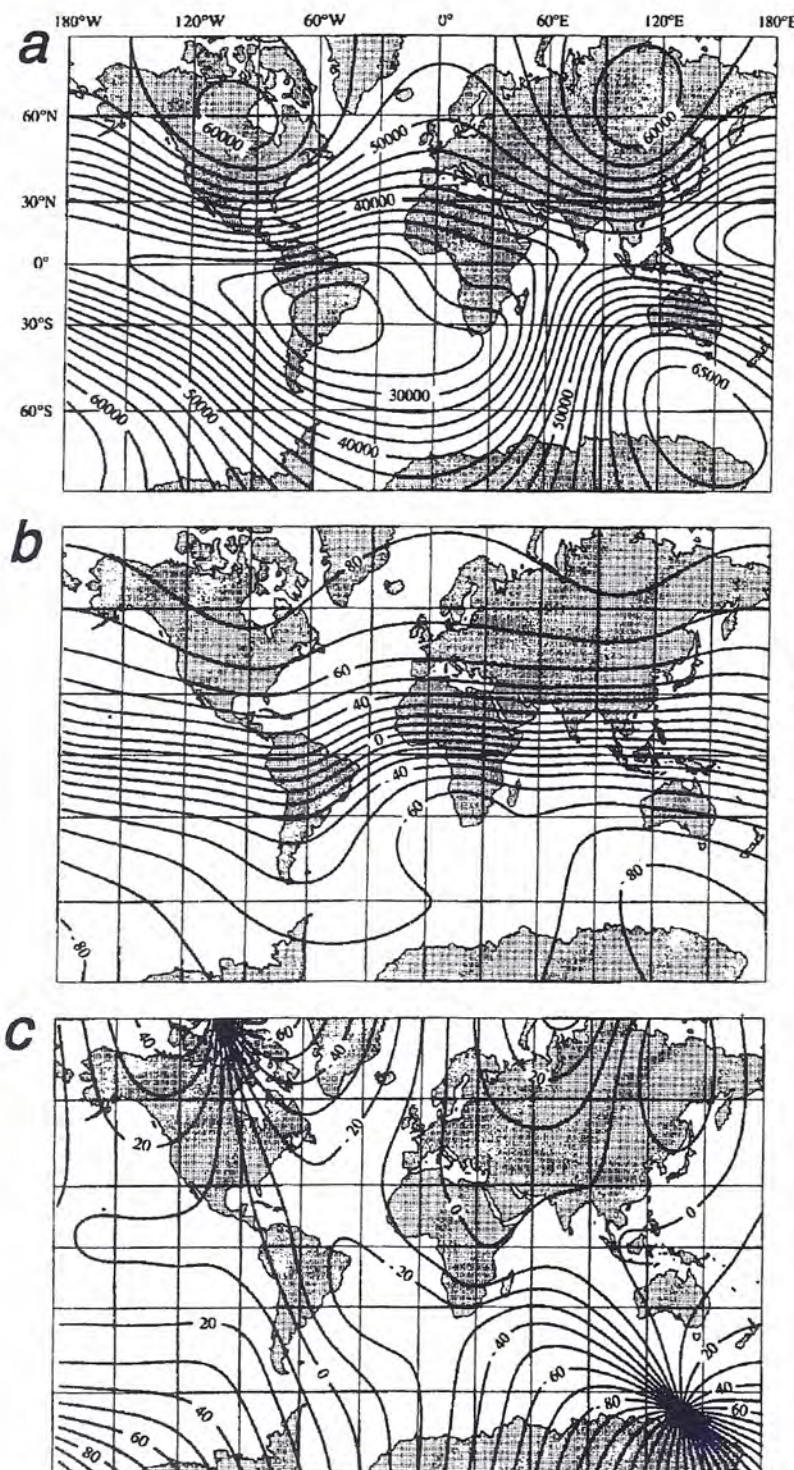


FIGURE 9.6 *Earth's magnetic field.*
From *Potential Theory in Gravity and Magnetic Applications*, by R. Blakely,
©1995 Cambridge University Press.
Reprinted with the permission of
Cambridge University Press, New York.
a) Intensity varies from about 30,000 nT
near the magnetic equator, to about
60,000 nT at the poles. b) Inclination is
roughly 0° near the magnetic equator,
90° near the poles. c) Declination, in
degrees, is most pronounced near the
magnetic poles.

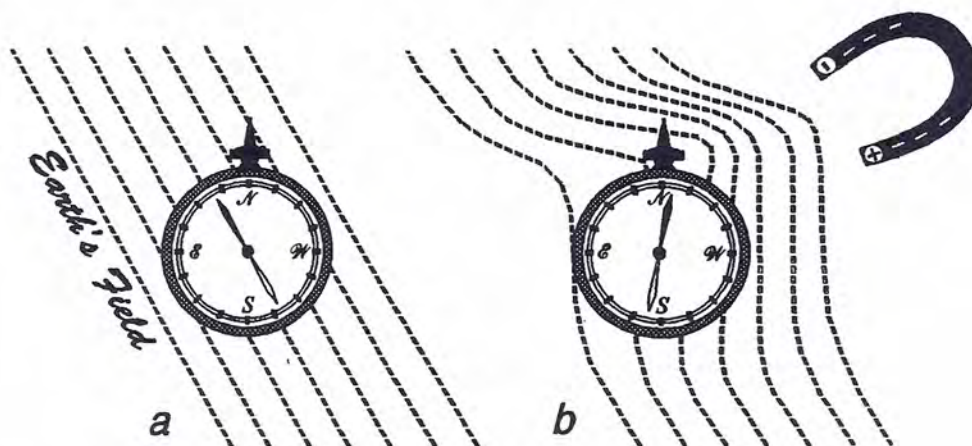


FIGURE 9.7 a) Compass responding to Earth's ambient magnetic field. b) Magnet causes a local deviation of Earth's field.

propensity of various types of materials toward magnetization, and how the magnetization locally affects Earth's field.

Units of measurement employed in magnetic field studies can be confusing to nonspecialists (see pp. 15–18 of Butler, 1992). For applications discussed here, it is sufficient to appreciate the relationship between the magnitude of Earth's total magnetic field (\bar{F}) and the magnetization (\bar{J}), induced within a body of magnetic susceptibility (χ). A typical magnetic survey employs a proton precession magnetometer, which measures the magnitude (intensity) of the total field vector, but not the direction. The International Standard (SI) unit for both magnetic field intensity and magnetization is the ampere/meter ($1 \text{ Am}^{-1} = 1 \text{ Cs}^{-1}\text{m}^{-1}$), while magnetic susceptibility is dimensionless. The unit of magnetic induction, the tesla (T) is also equivalent to 1 Am^{-1} . For convenience and to avoid confusion, the nanotesla ($1 \text{ nT} = 10^{-9} \text{ T}$) is used in this text to express both magnetic field intensity and magnetization. In the older literature intensity is sometimes expressed in gammas ($1 \gamma = 1 \text{ nT}$); intensity may appear in oersted ($1 \text{ Oe} = 10^3 \text{ T}/4\pi$), magnetization in gauss ($1 \text{ G} = 10^3 \text{ T}$).

The magnitude and direction of magnetization induced within a material depends on the magnitude and direction of the external (ambient) field, and the ability of the material to be magnetized:

$$\bar{J} = \chi \bar{F}_{\text{amb}}$$

where:

\bar{J} = induced magnetization of the material

χ = magnetic susceptibility of the material

\bar{F}_{amb} = magnitude and direction of the ambient field.

The *magnetic susceptibility* (χ , a dimensionless quantity) is a measure of the degree to which a substance may be magnetized. The overall susceptibility of a rock is roughly equivalent to the susceptibility of the magnetic mineral (or minerals) present, times the percentage of that mineral (or minerals), divided by 100. Table 9.1 illustrates that the amount of iron in a material, particularly in the form of the mineral magnetite (Fe_3O_4), strongly influences magnetic susceptibility. Ultramafic and mafic rocks (peridotite, basalt, gabbro), which are rich in magnetite, have high susceptibilities compared to felsic rocks (diorite, sandstone, granite).

TABLE 9.1 Typical magnetic susceptibilities of some common Earth materials.

Material	Magnetic Susceptibility
Magnetite	10000×10^{-5}
Peridotite	500×10^{-5}
Basalt/Gabbro	200×10^{-5}
Diorite	20×10^{-5}
Sandstone	10×10^{-5}
Granite	1×10^{-5}
Salt	-1×10^{-5}

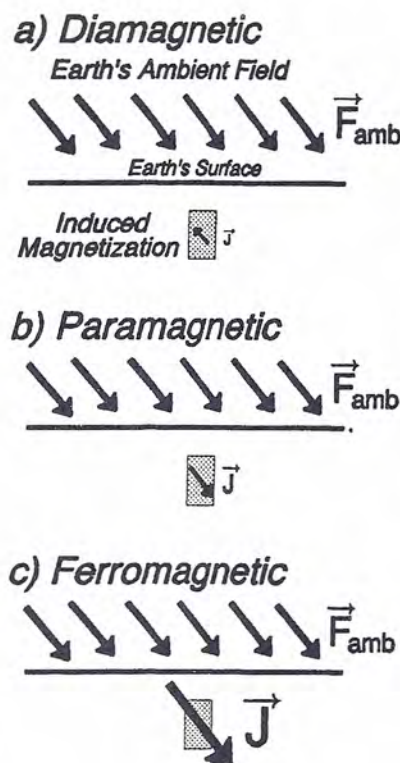


FIGURE 9.8 Types of magnetic behavior.
a) Diamagnetic minerals acquire a weak magnetization (\vec{J}) opposite to the external field (\vec{F}_{amb}). b) The magnetization in paramagnetic minerals is weak but in the same direction as the external field.
c) A strong magnetization, in the same direction as the external field, occurs in ferromagnetic minerals. [Note: In a strict sense, solids with coupling of atomic magnetic moments may be ferromagnetic (parallel magnetic moments), antiferromagnetic (antiparallel magnetic moments), or ferrimagnetic (antiparallel magnetic moments that do not cancel). As in Butler (1992) and Blakeley (1995) the term "ferromagnetic" is used here in a general sense for all three cases.]

Types of Magnetic Behavior

The type of magnetism exhibited by a mineral, in the presence of an external magnetic field, depends on the mineral's magnetic susceptibility. If a body containing the mineral is placed within an external (ambient) magnetic field (\vec{F}_{amb}), the body acquires a magnetization (\vec{J}) with intensity proportional to the overall magnetic susceptibility of the body.

Diamagnetism ($\chi \approx -10^{-5}$) A diamagnetic mineral, such as halite (rock salt), has negative magnetic susceptibility, acquiring an induced magnetization opposite in direction to an applied external field (Fig. 9.8a). The weak magnetization results from alteration of electron orbitals as force from the external field is

applied to the material. Susceptibilities of only about -10^{-5} mean that magnetization is on the order of 1/100,000th the strength of the external field.

Paramagnetism ($\chi \approx +10^{-4}$) The magnetic susceptibility of paramagnetic minerals is positive; they acquire a magnetism parallel to an external field (Fig. 9.8b). The magnetism occurs as magnetic moments of atoms are partially aligned in the presence of the external field. Most magnetic minerals exhibit this type of weak magnetic behavior.

Ferromagnetism ($\chi \approx +10^{-1}$) In some metallic minerals rich in iron, cobalt, manganese, or nickel, atomic magnetic moments align strongly with an external field (Fig. 9.8c). Susceptibilities on the order of 10^{-1} indicate that the magnetization is in the same direction as, and about 1/10 the magnitude of, the external field. Under some circumstances induced magnetization may remain in ferromagnetic materials, even after the external field is removed (remanent magnetization).

Types of Magnetization

Magnetization of a rock occurs in two ways: it can be induced by Earth's present magnetic field, or it could have formed some time in the past, as the rock lithified.

Induced Magnetization Earth's overall (or ambient) magnetic field is an external field that can cause rocks to be temporarily magnetized (Fig. 9.9a). When taken out of the ambient field, this *induced magnetization* may be lost. The magnitude and direction of the induced field depends on the magnitude and direction of the ambient field and the magnetic susceptibility of the rock.

Remanent Magnetization When rocks form, the magnetic domains of some minerals (particularly magnetite) behave as compass needles, orienting themselves

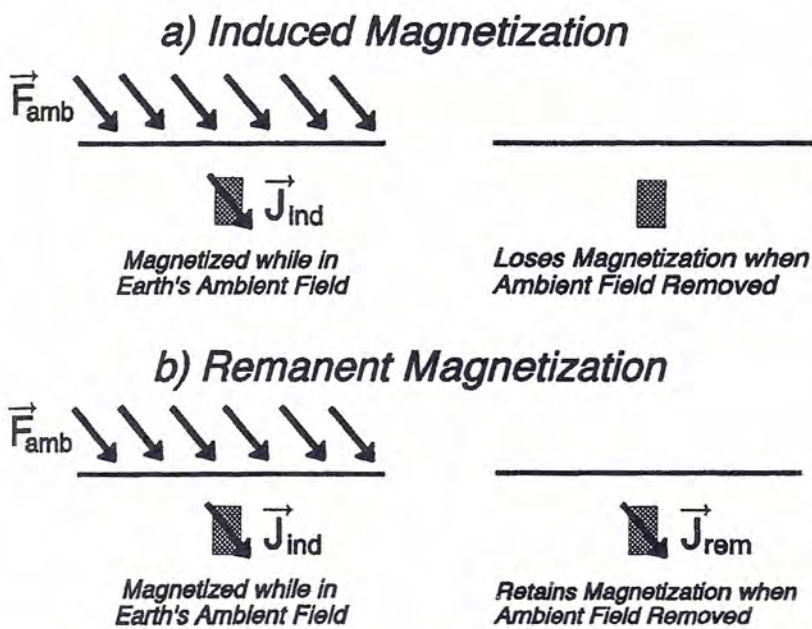


FIGURE 9.9 Types of magnetization.
a) In the presence of an external magnetic field, magnetization may be *induced* in a material. Materials commonly lose their induced magnetization when the external field is removed. b) Some materials remain magnetized after the external field is removed, retaining a *remanent* magnetization.

in the direction of the ambient magnetic field. As the rock lithifies, the orientation of the magnetic domains may be frozen into the rock. This *remanent magnetization* remains even after the ambient field changes (Fig. 9.9b); it is commonly 5 times as great as the magnetization induced by the present field.

INTERPRETATION OF INDUCED MAGNETIC ANOMALIES

Induced magnetization results from application of an external magnetic field; the magnetization in turn leads to a local field about the magnetized body. In the absence of remanent magnetization, the total magnetic field observed in the vicinity of a magnetic body is the sum of Earth's ambient field at that location and the field induced within the magnetic body (Fig. 9.10):

$$\vec{F} = \vec{F}_{\text{amb}} + \vec{F}_{\text{ind}}$$

where:

- \vec{F} = total magnetic field
- \vec{F}_{amb} = Earth's ambient magnetic field in region
- \vec{F}_{ind} = induced magnetic field.

Local perturbations in Earth's field thus provide clues to the presence of magnetically susceptible materials in the subsurface. Such materials can be studied by subtracting the average value of the ambient field in the region from the total field, yielding the induced field surrounding the material:

$$\vec{F}_{\text{ind}} = \vec{F} - \vec{F}_{\text{amb}}$$

Even though the total magnetic field is a vector (\vec{F}), with both magnitude and direction, studies of subsurface susceptibility can be accomplished by taking simple measurements of only the magnitude of the total field (F). The *total field anomaly* (ΔF) is computed by subtracting the magnitude (intensity) of the ambient field (F_{amb}) from F (Fig. 9.10c):

$$\Delta F = F - F_{\text{amb}}$$

ΔF is analogous to the gravity anomaly obtained by subtracting the observed gravity (g) from the theoretical gravity (g_i), according to the latitude of a station (see Chapter 8). A notable difference is that, while the overall gravity field ($\approx g_i$) has simple changes that correspond closely to latitude, the overall magnetic field ($\approx F_{\text{amb}}$) has changes that are complex; the values for F_{amb} must therefore be estimated empirically (for example, from a map, as in Fig. 9.6a).

Geometry of Magnetic Bodies in the Subsurface

Magnetization is induced in a material according to the direction and magnitude of Earth's ambient field, and the magnetic susceptibility (χ) of the material. Fig. 9.11 illustrates that, because the ambient field lies at varying angles (inclinations) with respect to Earth's surface, the forms of induced magnetic anomalies depend on latitude. The induced magnetization (\vec{J}) within the body is parallel to the ambient field (\vec{F}_{amb}), according to $\vec{J} = \chi \vec{F}_{\text{amb}}$. \vec{J} in turn leads to an induced field (\vec{F}_{ind}). Where (\vec{F}_{ind}) crosses the surface with a component in the same direction as \vec{F}_{amb} , the total field

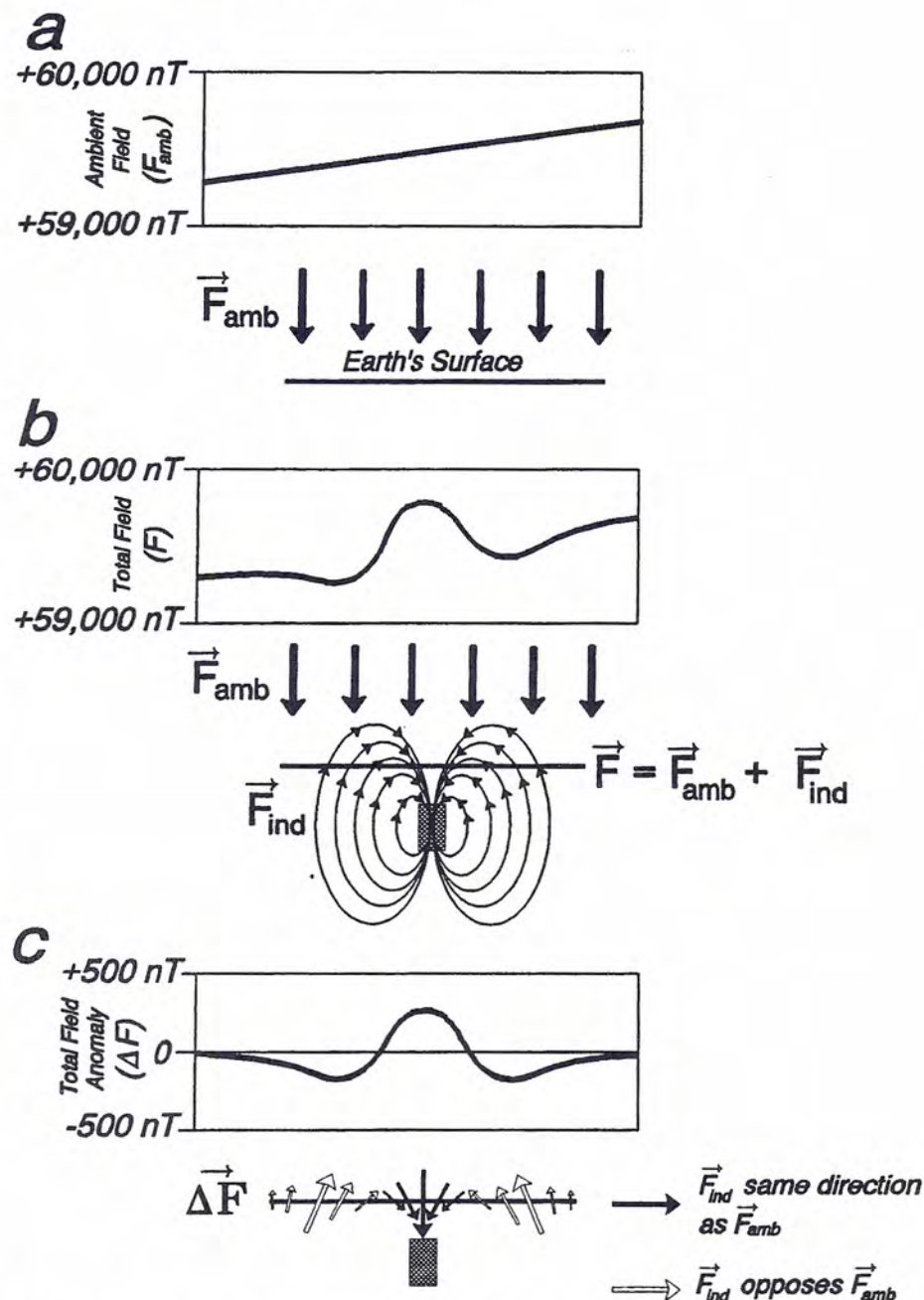


FIGURE 9.10 Total field magnetic anomaly produced by local magnetic body. a) Earth's ambient field (\vec{F}_{amb}) has magnitude of several thousand nT, with very long wavelength changes. b) A body of magnetization (\mathbf{J}) is surrounded by an induced magnetic field (\vec{F}_{ind}), with amplitudes of perhaps a few hundred nT occurring over much shorter wavelengths. The total magnetic field (\vec{F}) that results is the sum of the ambient and induced fields. c) Subtracting the magnitude of the ambient field (F_{amb}) from that of the total field (F) yields the total field anomaly (ΔF). A profile of ΔF thus reflects the effect of the induced field.

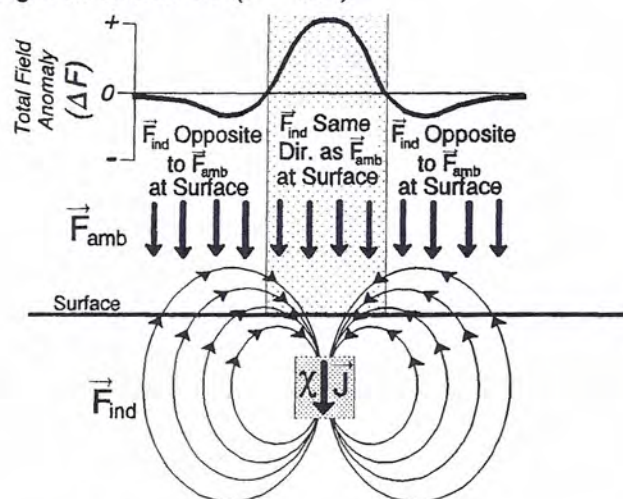
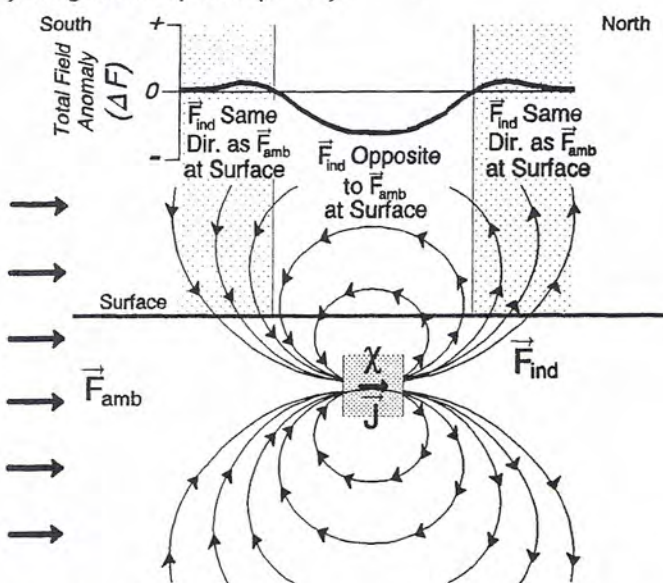
a) Magnetic North Pole ($i = +90^\circ$)b) Magnetic Equator ($i = 0^\circ$)

FIGURE 9.11 At different magnetic latitudes, magnetic anomalies from the same magnetic body (that is, a body of exactly the same shape, size, depth, and magnetic susceptibility, χ) are quite different. a) At the magnetic north pole, Earth's ambient field (\vec{F}_{amb}) is strong ($\approx 60,000$ nT) and points downward (magnetic inclination $i = 90^\circ$). Where the induced field (\vec{F}_{ind}) points in the same direction as \vec{F}_{amb} (gray shading), the total field anomaly (ΔF) is positive. Negative total field anomalies occur where the two fields oppose one another. b) At the magnetic equator, \vec{F}_{amb} is horizontal ($i = 0^\circ$) and weaker ($\approx 30,000$ nT). The magnetization (\vec{J}) is smaller, leading to a weaker induced field. The total field anomaly is thus lower amplitude than in (a). \vec{F}_{ind} opposes \vec{F}_{amb} over the body, leading to negative ΔF values. (Modified from R. F. Butler, personal communication, 1996).

anomaly (ΔF) is positive. In areas where \bar{F}_{ind} has a component opposite to \bar{F}_{amb} , ΔF is negative. For the same body, magnetic anomalies observed at the magnetic north pole (Fig. 9.11a) and the magnetic equator (Fig. 9.11b) are thus quite different. (The problem is even more complicated, because the *direction* of the *magnetic profile* is also important. Fig. 9.11b assumes a profile running in a south-north direction, cutting across induced field lines. East-west profiles would parallel induced field lines, resulting in a different total field anomaly profile).

Although some magnetic surveys are undertaken on the surface, an airplane is an effective means to cover large areas and to record large amounts of data. Unlike gravity surveys, which require a platform with no (or relatively small, predictable) motions, a standard proton precession magnetometer can be towed behind an airplane. Such *aeromagnetic surveys* measure the magnitude (F), but not the direction, of the total magnetic field. That measurement, along with knowledge of the local magnitude of Earth's ambient field (F_{amb}), is sufficient to determine the total field magnetic anomaly (ΔF). Thus, while magnetic anomalies are commonly more complex to interpret due to their latitude and direction dependence, adequate coverage of an area is generally easier to attain compared to gravity surveying.

Forward modeling of magnetic anomalies can be used to interpret the distribution of magnetic susceptibility contrasts ($\Delta\chi$) in the subsurface, analogous to estimating density contrasts ($\Delta\rho$) from gravity data. Changes in the magnitude and direction of Earth's ambient field, however, make the forms of magnetic anomalies far less intuitive than gravity anomalies. The same mass anomaly, buried at a given depth, will produce essentially the same gravity anomaly anywhere on the Earth; magnetic anomalies from the same body, however, vary in form and amplitude according to magnetic latitude (Fig. 9.12). It should be noted, too, that remanent magnetization is often much stronger than that induced by the ambient field. If the remanent and induced magnetizations are in the same direction, their net effect may be incorporated by choosing an equivalent susceptibility for modeling purposes.

Mapping of Magnetic Bodies Magnetics is a useful tool for mapping materials that have susceptibilities or remanent magnetizations that contrast with those of surrounding rocks, and for distinguishing between types of intrusive bodies. Igneous rocks often have large amounts of magnetite, inducing high magnetization (Table 9.1). Salt exhibits diamagnetic behavior, inducing a weak field opposite in direction to the ambient field (Fig. 9.8a). Like igneous intrusions, salt domes are recognized from seismic refraction experiments as high velocity material. Potential field studies can differentiate the two features (Fig. 9.13); the high density and high magnetic susceptibility of an igneous intrusion will produce pronounced gravity and magnetic anomalies, compared to a gravity minimum and subdued magnetic anomalies resulting from a low-density, low-susceptibility salt dome.

Depth to Magnetic Basement High ferromagnetic mineral content results in high levels of magnetization (Fig. 9.8c). Crystalline basement rocks, which are commonly more mafic than overlying sedimentary deposits, are thus the main source of magnetic anomalies in a region. Amplitudes and gradients for magnetic anomalies decrease as the sources get farther from the surface observation points, because magnetic force is a potential field (see examples for gravity, Figs. 8.28 and 8.31). The depth to the basement in a region can be estimated, therefore, by studying the pattern of magnetic anomalies. Regions with high magnetic anomaly amplitudes, short wavelengths, and steep gradients suggest shallow basement (Fig. 9.14a); in areas where the basement is deep, magnetic anomalies are subdued (Fig. 9.14b).

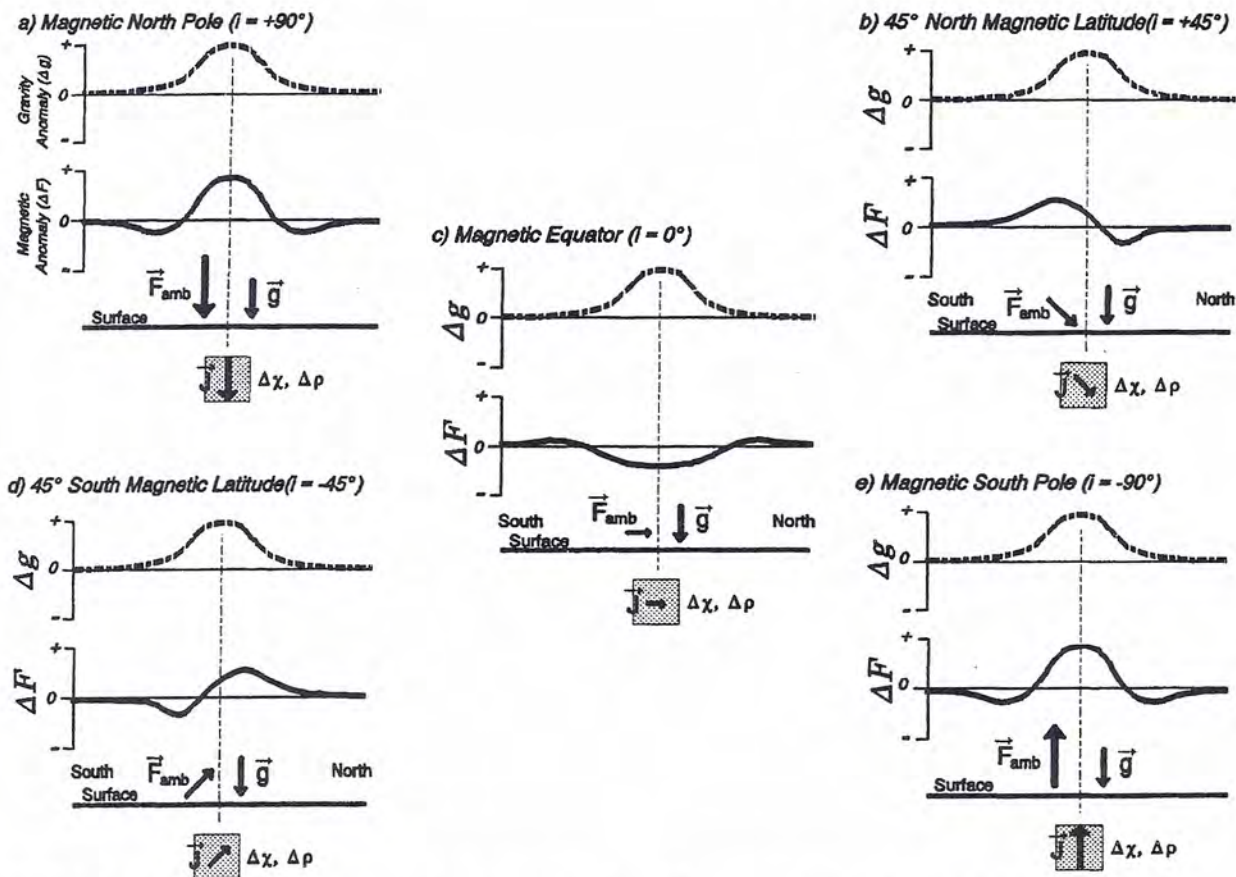


FIGURE 9.12 Gravity and magnetic anomalies from the same body, at different magnetic latitudes. At each latitude, the gravity anomaly (Δg) resulting from the body of density contrast ($\Delta \rho$) is the same. For the same body, with magnetic susceptibility contrast ($\Delta \chi$), the magnetic anomaly (ΔF) varies. At the magnetic north and south poles (a and e), the anomaly is a central high with flanking lows (Fig. 9.11a); a high magnitude ambient field ($F_{\text{amb}} \approx 60,000$ nT) induces high magnitude magnetization (J), resulting in high amplitude magnetic anomalies (ΔF). At the magnetic equator (c), the induced field opposes the ambient field at the surface directly over the body, leading to negative magnetic anomalies (Fig. 9.11b); $F_{\text{amb}} \approx 30,000$ nT leads to low amplitude ΔF . At mid-latitudes (b and d) the anomaly is asymmetric, with intermediate amplitude ΔF .

Curie Depth Minerals that exhibit strong (ferromagnetic) behavior at low temperatures have weaker (paramagnetic) properties when hotter than the *Curie temperature*. With increasing depth, temperature increases according to a geothermal gradient. Deeper than the *Curie depth*, rocks lose their strong magnetization as they heat up beyond the Curie temperature ($\approx 600^\circ\text{C}$ for most rocks). Areas with high geothermal gradient thus have a shallow **bottom** to magnetic basement, compared to colder areas (Fig. 9.15). The form of magnetic anomalies can thus be used to map the approximate depth where rocks reach about 600°C .

PALEOMAGNETIC STUDIES

The remanent magnetization in a rock records information about the direction to the north magnetic pole, at the time the rock lithified. Paleomagnetic studies may thus indicate the age of the rock, and perhaps suggest the latitude of the region at the time the rock formed.

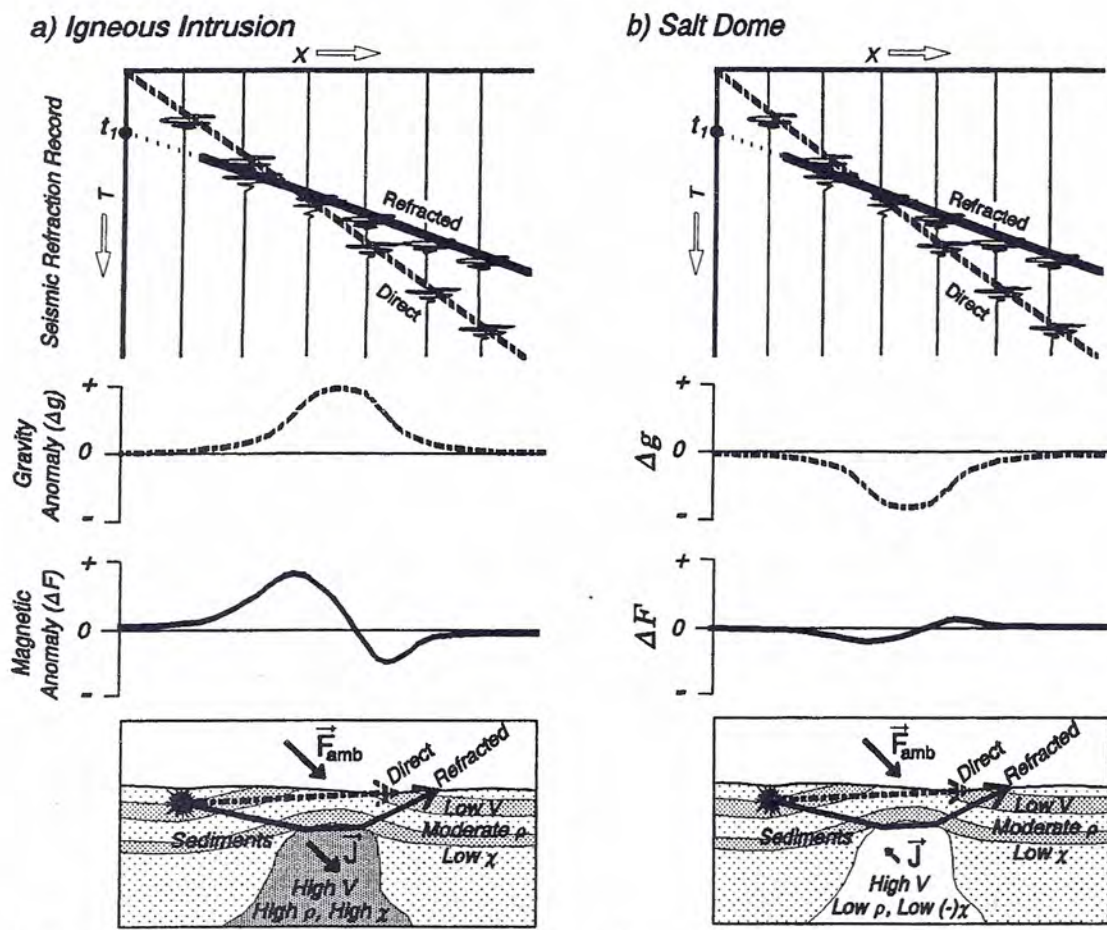


FIGURE 9.13 An igneous intrusion and salt dome might both be recognized as high-velocity material (V), leading to a critical refraction. a) An igneous intrusion generally has high density (ρ) and high magnetic susceptibility (χ), relative to surrounding sedimentary strata. A pronounced gravity maximum and high-amplitude magnetic anomaly result. b) A salt dome has low density, resulting in a gravity minimum. The small, negative susceptibility leads to a subdued magnetic anomaly.

The total magnetization of a material is the vector sum of the induced and remanent magnetizations:

$$\vec{J} = \vec{J}_{ind} + \vec{J}_{rem}$$

where:

- \vec{J} = total magnetization of the material
- \vec{J}_{ind} = induced magnetization of the material
- \vec{J}_{rem} = remanent magnetization of the material.

The total field at a given location is thus the local fields due to the induced and remanent magnetizations, added to the ambient field:

$$\vec{F} = \vec{F}_{amb} + \vec{F}_{ind} + \vec{F}_{rem}$$

where:

- \vec{F} = magnitude and direction of the total magnetic field
- \vec{F}_{amb} = Earth's ambient magnetic field in region

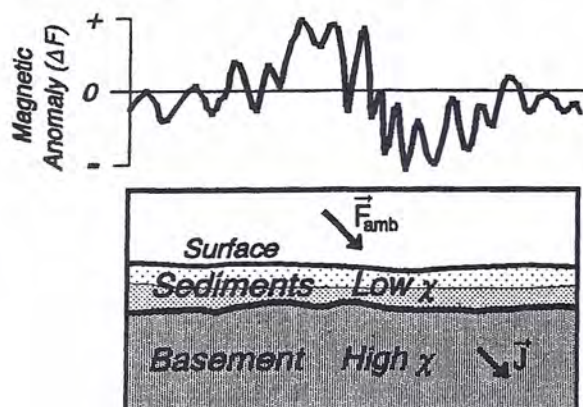
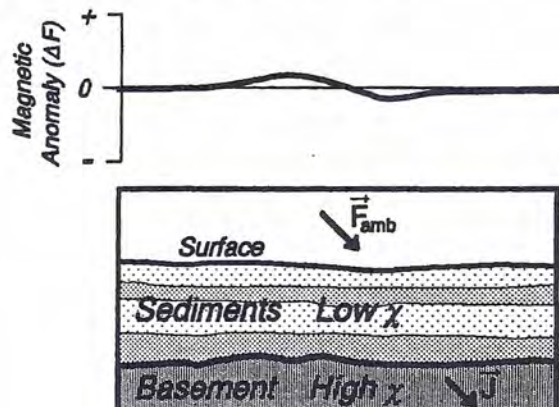
a) Shallow Magnetic Basement*b) Deep Magnetic Basement*

FIGURE 9.14 Depth to magnetic basement. Magnetic anomalies measured at Earth's surface depend on the depth of the magnetic sources, commonly located within crystalline basement. a) Where basement rocks are shallow, short-wavelength anomalies, with high amplitudes and steep gradients, occur. b) Basement buried deeply beneath sedimentary cover results in longer wavelength anomalies with smaller amplitudes and gradients.

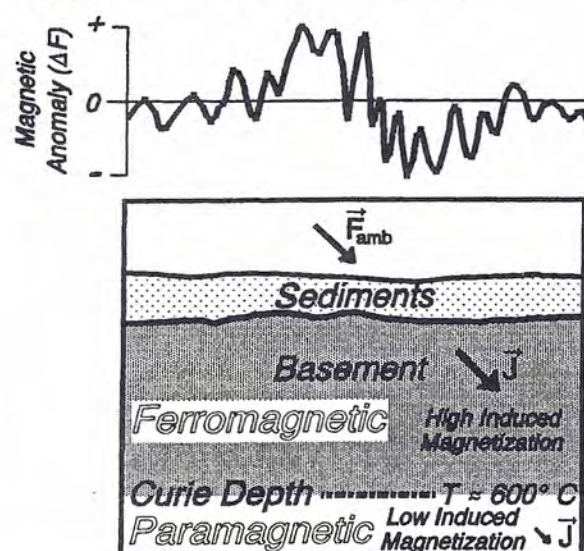
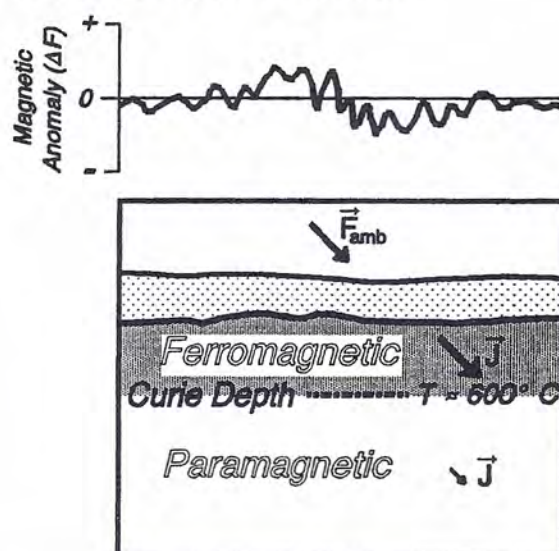
a) Normal Geothermal Gradient*b) High Geothermal Gradient*

FIGURE 9.15 Curie depth. a) Regions with a normal geothermal gradient reach 600°C at depths of about 20 to 30 km. Their magnetic anomalies may exhibit high amplitudes because of the great thickness of basement rocks capable of ferromagnetic behavior. b) The Curie depth for hot regions (high geothermal gradient) may be considerably less than 20 km, resulting in a thinner layer with ferromagnetic behavior. Magnetic anomalies are potentially lower in amplitude compared to those in colder regions.

\vec{F}_{ind} = magnetic field due to induced magnetization

\vec{F}_{rem} = magnetic field due to remanent magnetization.

After the magnitude of the ambient field (F_{amb}) is subtracted from the magnitude of the total field (F), the total field anomaly (ΔF) is a function of the magnitudes of the induced (F_{ind}) and remanent (F_{rem}) fields. In many instances the remanent mag-

netization is several times stronger than the induced magnetization, so that the total field anomaly reflects the paleomagnetism component.

Types of Remanent Magnetization

Rocks are collections of diamagnetic, paramagnetic, and ferromagnetic minerals. Diamagnetic and paramagnetic materials acquire a magnetization when exposed to an external magnetic field (Fig. 9.8). At a given temperature, they have a constant susceptibility, acquiring a magnetization which is linearly proportional to the external magnetic field. The magnetization goes away when the external field is removed. Ferromagnetic materials, however, retain a permanent (or remanent) magnetization, even when the external field is removed. There are three ways by which materials can acquire remanent magnetization (see also chapter 3 of Butler, 1992).

1. Thermoremanent Magnetization (\bar{J}_{TRM}) At high temperature a ferromagnetic material exhibits paramagnetic behavior. As rocks cool below the Curie temperature, some minerals (particularly magnetite) change from the paramagnetic to the much stronger, ferromagnetic behavior. The rocks acquire a large, *thermoremanent magnetization* as magnetic domains orient themselves to Earth's ambient field (Fig. 9.16a).

A common misconception about thermoremanent magnetization is that mineral crystals orient themselves to Earth's field as a lava flow cools and hardens. Actually, the flow, though still hot, is quite hard (crystals randomly locked in place) before the remanent magnetization is acquired; the crystals cannot rotate to align with the ambient magnetic field. Instead, the magnetic moments of the collection of mineral grains acquires a bias in the direction of Earth's ambient field during cooling. Thermoremanent magnetization is thus a statistical, thermodynamic phenomenon; it results from the fact that a magnetite grain is in a slightly lower energy configuration when its magnetic moment is aligned with Earth's ambient field.

2. Detrital Remanent Magnetization (\bar{J}_{DRM}) When sediments settle in water, ferromagnetic mineral grains (particularly magnetite and hematite) tend to orient themselves along the ambient magnetic field of the Earth (Fig. 9.16b). The rock thus acquires a *detrital remanent magnetization*.

3. Chemical Remanent Magnetization (\bar{J}_{CRM}) As ions are precipitated from solution, forming ferromagnetic minerals, the magnetic domains in the mineral crystals preferentially orient themselves with Earth's ambient field (Fig. 9.16c). The rock thus acquires a *chemical remanent magnetization*. The paleomagnetism in iron-rich, continental sediments is generally formed in this manner. These "redbeds" account for the bulk of paleomagnetic observations on land, facilitating paleomagnetic stratigraphy and paleo-latitude studies (discussed below); the red color is derived from the ferromagnetic mineral hematite.

Paleomagnetic Interpretation

The paleomagnetism in rocks can lead to interpretations of the ages of the rocks (geochronology; paleomagnetic stratigraphy), and to the positions of crustal blocks when the rocks formed (paleolatitude).

Dating of rocks based on magnetic measurements revolves around the observation that Earth's magnetic field periodically reverses (Fig. 9.17). Magnetic domains in minerals, like compass needles, point toward the north magnetic pole in

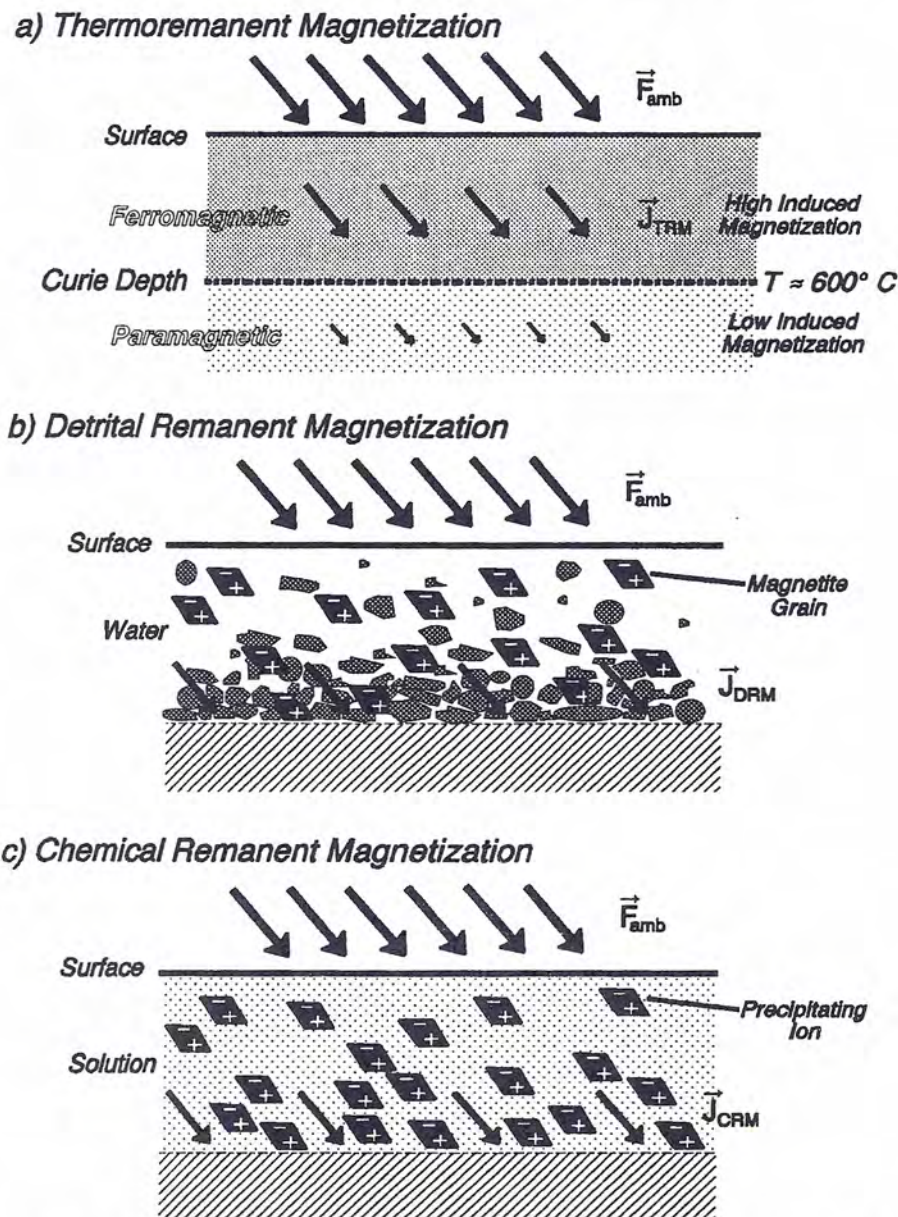


FIGURE 9.16 *Types of remanent magnetization.* For each type, the strength and direction of the magnetization remains, even after the ambient field is removed or changes orientation.
 a) *Thermoremanent magnetization (\vec{J}_{TRM}).* When the material (for example, a lava flow) cools below the Curie temperature, a strong ferromagnetization occurs, parallel to Earth's ambient field.
 b) *Detrital remanent magnetization (\vec{J}_{DRM}).* As sediments settle out in water, mineral grains rotate so that their magnetic domains preferentially orient with the ambient field.
 c) *Chemical remanent magnetization (\vec{J}_{CRM}).* As ions are precipitated from solution, their magnetic domains align with the ambient field.

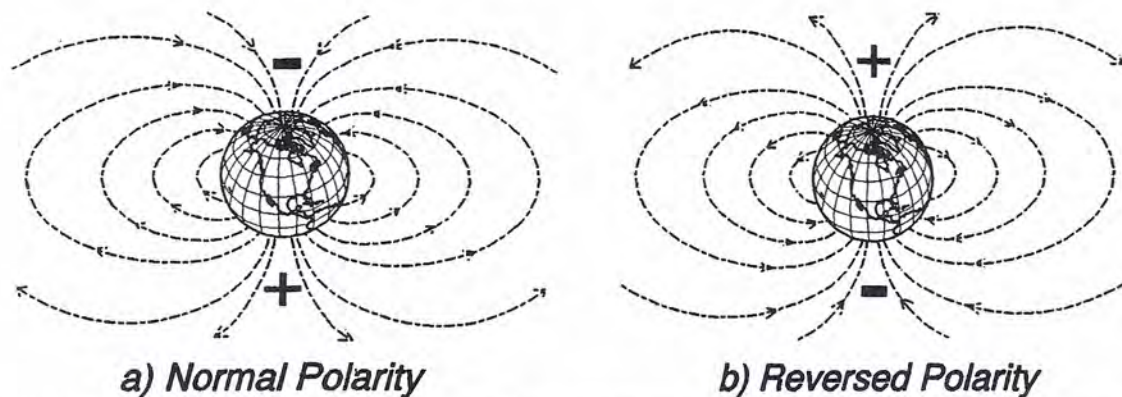


FIGURE 9.17 *Reversal of Earth's magnetic field.* a) "Normal" field, with lines of force pointing from a positive south pole to a negative north pole. b) "Reversed" field, with opposite polarities; a compass needle would point southerly.

the "normal" configuration that exists today. At times in the past, however, the magnetic field was reversed, so that mineral domains were magnetized in the opposite direction.

Utilizing observations of polarity reversals, a Geomagnetic Polarity Time Scale has been developed (Fig. 9.18). The scale is based on various methods, including: a) remanent magnetization studies of isotopically dated, young (< 5 million year old) igneous rocks; b) observations of marine magnetic anomalies, accompanied by paleontological dating of sediments and potassium/argon (K/Ar) dating of basalt recovered through the Deep Sea Drilling Project (DSDP); c) magnetic stratigraphy studies of sedimentary sections with unusually complete fossil records.

Geochronology Based on Paired Magnetic Anomalies across Mid-Ocean Ridges The ocean floors illustrate the utility of magnetic data to record the ages of certain Earth materials. As basaltic rocks at a mid-ocean ridge cool, they acquire a strong thermoremanent magnetization (Fig. 9.16a). A record of normal and reversed polarities is thus frozen into the basalt of oceanic layer 2 (Fig. 9.19b). The remanent magnetization of oceanic basalt results in additions and subtractions to Earth's ambient field. Profiles of total field anomalies recorded across mid-ocean ridges thus show alternating maxima and minima, representing times when oceanic layer 2 was normally or reversely polarized (Fig. 9.19c).

Magnetic polarity reversals observed across mid-ocean ridges agree with DSDP data showing that oceanic sediments and underlying basalts get progressively older away from mid-ocean ridge axes. The ages of oceanic rocks can thus be inferred from the pattern of observed magnetic anomalies, tied to the Geomagnetic Polarity Time Scale (Fig. 9.20).

The alternating bands of positive and negative magnetic anomalies show remarkable symmetry on opposite sides of mid-ocean ridges. This symmetry is testimony to the idea of creation of new lithosphere at divergent plate boundaries (Fig. 9.21). Anomaly widths indicate the rate at which plates diverge at mid-ocean ridges: narrow anomalies indicate slow spreading rates (Fig. 9.22a), wider anomalies faster rates (Fig. 9.22b).

Paleomagnetic Stratigraphy Sedimentary layers can acquire remanent magnetization through detrital and chemical mechanisms (Fig. 9.16). The ages of layers in a sequence of sedimentary strata may thus be determined by comparing the

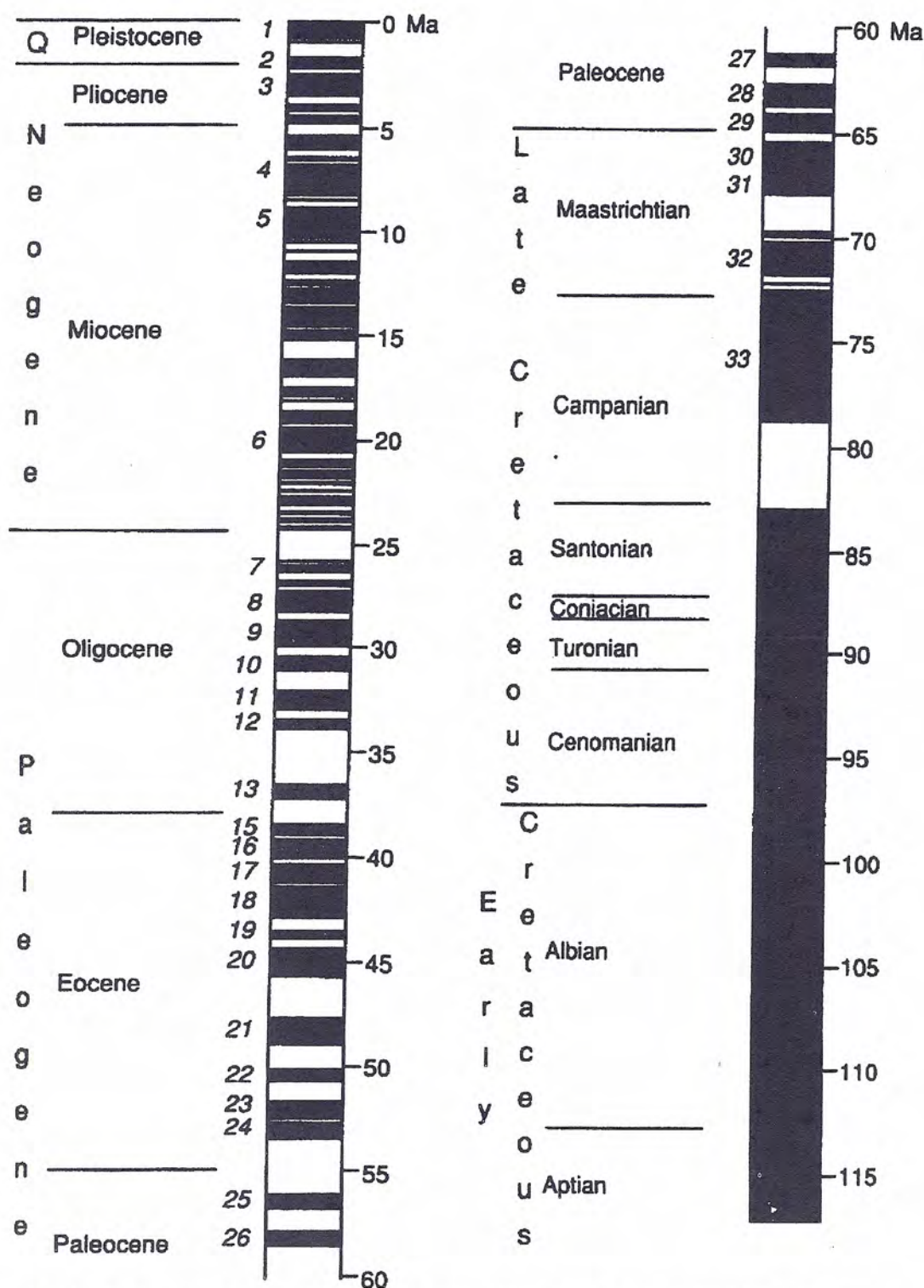


FIGURE 9.18 Geomagnetic polarity time scale for the past 117 million years. Times of normal polarity shown in black, reversed polarity in white. Magnetic anomaly numbers appear on the left sides of columns; corresponding ages in millions of years (Ma) are on the right. From "Magnetostratigraphic time scale," by A. Cox, in: *A Geologic Time Scale*, © 1982 Cambridge University Press. Reprinted with permission of Cambridge University Press, New York. Figure redrawn as in Butler (1992).

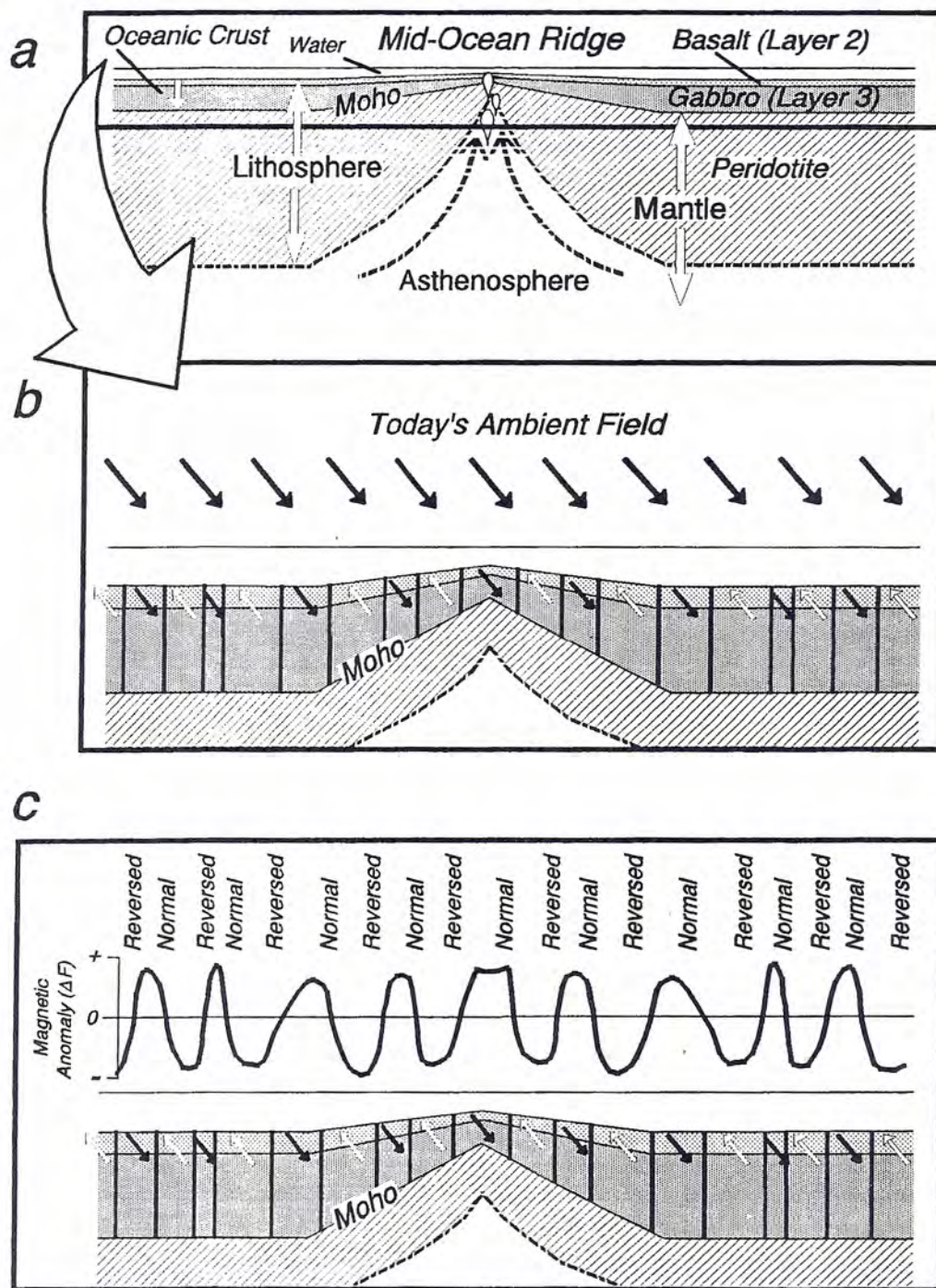


FIGURE 9.19 Paleomagnetic alignment at a mid-ocean ridge. a) Cross section of the lithosphere, showing formation of basalt (layer 2) and gabbro (layer 3). b) Closeup of the crust. Black arrow at the ridge axis illustrates magnetization aligned with a normal polarity, parallel to today's ambient field. Away from the axis, alternating bands of reversed (white arrows) and normal polarity reflect periodic reversals of the magnetic field. c) Magnetic anomaly pattern across a mid-ocean ridge. Alternating bands of oceanic crust with normal (black arrows) and reversed (white arrows) magnetization result in corresponding positive and negative total field magnetic anomalies (ΔF).

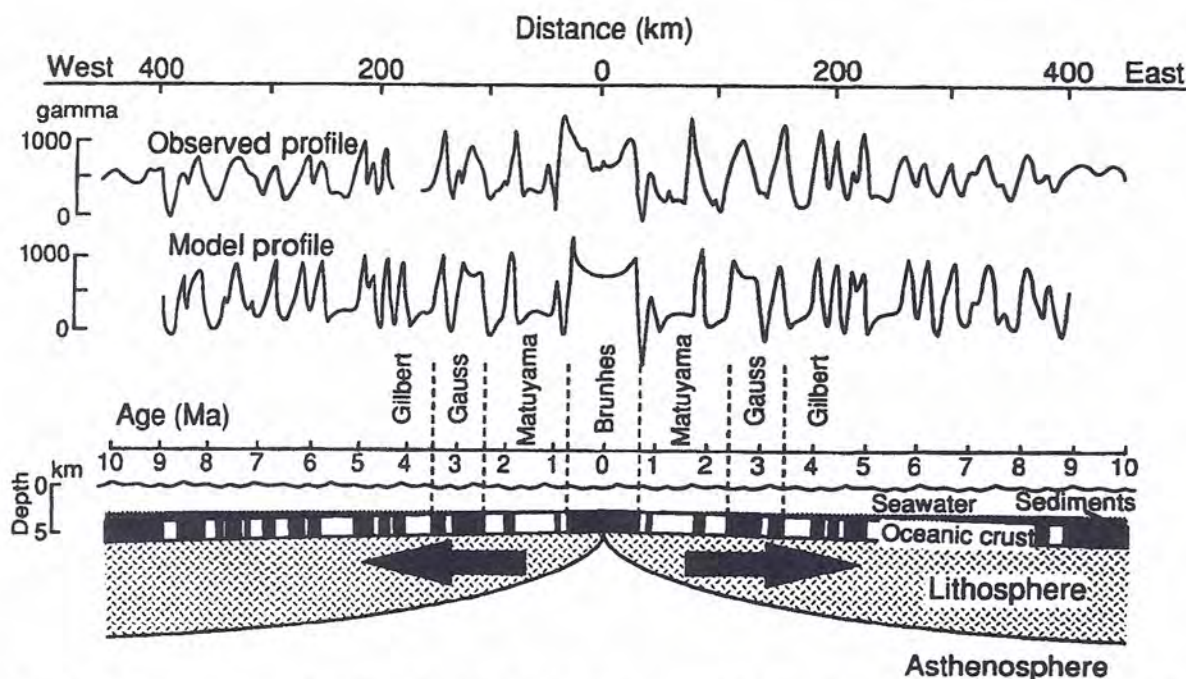


FIGURE 9.20 Magnetic anomaly profile and model of the Pacific-Antarctic Ridge. The observed total field magnetic anomaly profile (top) correlates well with a calculated profile (center) from the model of polarity reversals (bottom). The model incorporates times of normal (black) and reversed (white) paleomagnetism, according to the Geomagnetic Polarity Time Scale. Names refer to magnetic epochs in the time scale; numbers are ages in millions of years (Ma). Magnetic anomalies in gammas (1 gamma = 1 nT). From "Magnetic anomalies over the Pacific-Antarctic ridge," by W. Pitman, III, and J. Heirtzler, *Science*, vol. 154, pp. 1164–1171, © 1966. Figure redrawn as in Butler (1992).

observed polarity reversals with the Geomagnetic Polarity Time Scale. The technique is especially useful if parts of the section can be tied to isotopic dating of interbedded volcanic ash.

Fig. 9.23 shows an example from the Himalayan foreland basin deposits in Pakistan. Samples were taken from 10 stratigraphic sections, with results plotted in cross-sectional form on the diagram. According to *lithostratigraphy*, the sections are part of the Nagri Formation on the southwest, the Dhok Pathan Formation on the northeast. Samples analyzed for magnetic polarity show that there are correlations with positive and negative epochs of the Geomagnetic Polarity Time Scale. This *chronostratigraphy* thus reveals that parts of the Nagri and Dhok Pathan formations were deposited at the same time.

Paleolatitude Studies The remanent magnetization of a sedimentary or volcanic rock records the magnetic inclinations (i) at the time the rock formed. The inclination, in turn, can be related to the magnetic latitude (ϕ) of the rock at the time it formed, according to:

$$\tan i = 2 \tan \phi$$

The equation assumes that the rock's magnetization records the original magnetic direction at the time of formation, that the field acts as a geocentric dipole, and that secular variation has been averaged out. Rocks formed near the magnetic equator

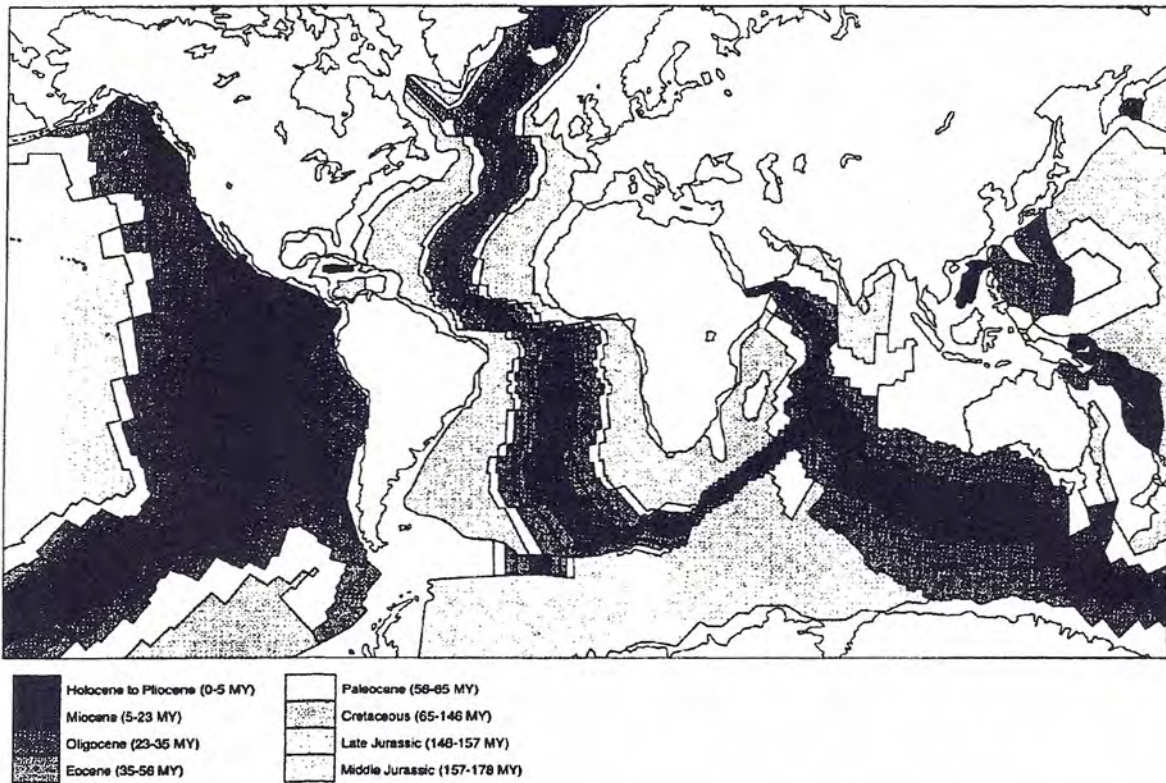


FIGURE 9.21 World map showing the age of oceanic lithosphere determined from magnetic anomalies. MY = Million years. From *Earth's Dynamic Systems*, 7th ed. by Hamblin/Christiansen, © 1995. Reprinted by permission of Prentice-Hall, Inc., Upper Saddle River, NJ.

would have remanent magnetizations oriented horizontally; magnetizations closer to the magnetic poles would be steeper (Fig. 9.4a). The magnetic inclination observed for a sedimentary layer thus indicates the magnetic latitude of the region at the time the layer was deposited (Fig. 9.24a). If the crustal block (terrane) on which the layer formed drifts to a different latitude, the inclination of remanent magnetization would differ from that of Earth's present magnetic field (Fig. 9.24b).

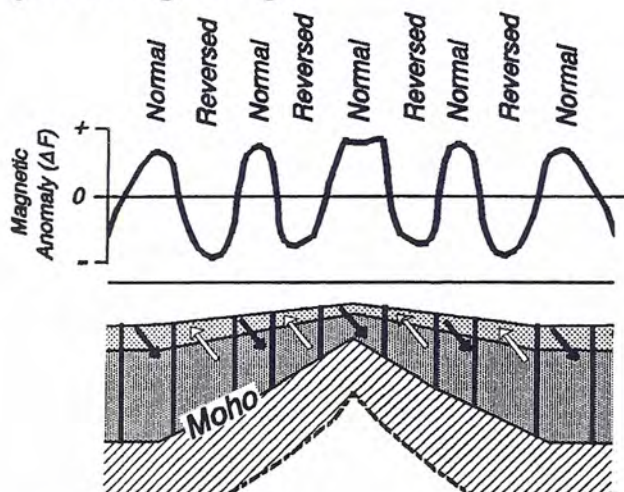
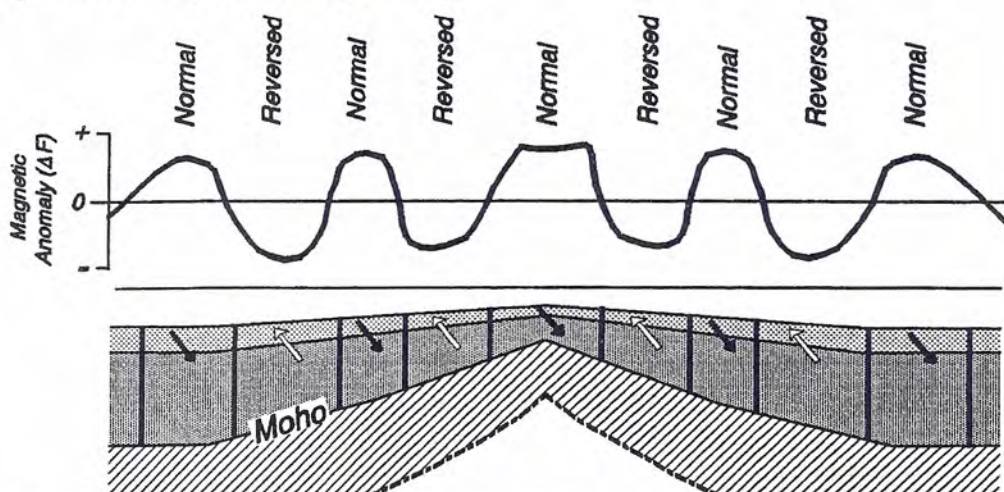
a) Slow - Spreading Ridge*b) Fast - Spreading Ridge*

FIGURE 9.22 The widths of magnetic anomalies can be used to infer the spreading rate of mid-ocean ridges. a) *Mid-Atlantic Ridge*. Slow-spreading rate of 2–3 cm/a (20–30 km/Ma) results in narrow anomalies. b) *East Pacific Rise*. Broader anomalies result from spreading of 5–15 cm/a (50–150 km/Ma), creating a broader region of new lithosphere over the same time span as in (a).

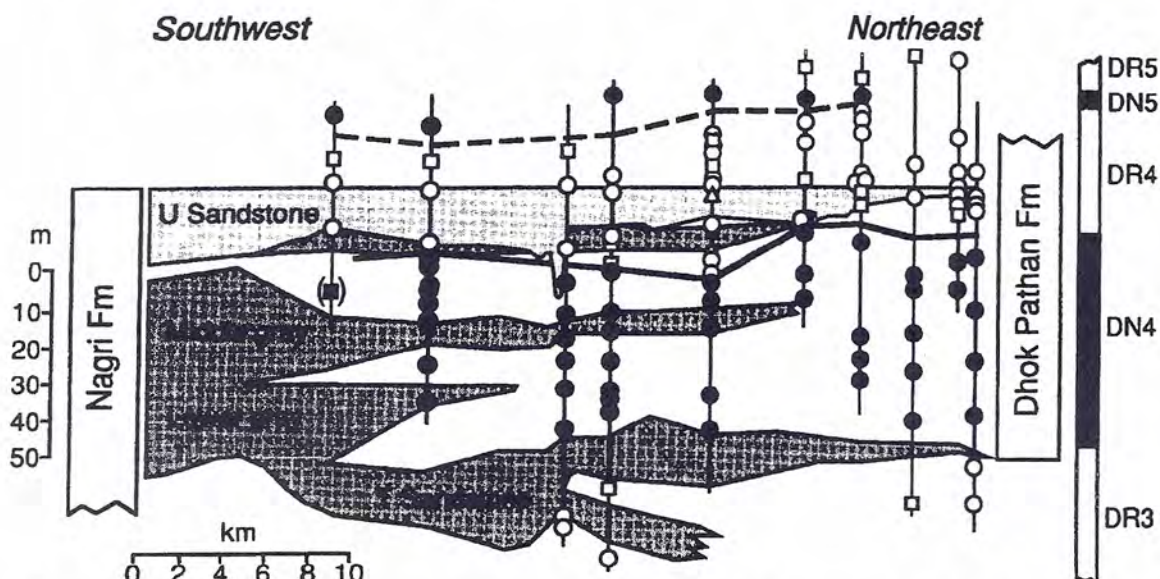


FIGURE 9.23 Example of paleomagnetic stratigraphy. Samples were taken from ten stratigraphic sections of Himalayan foreland basin deposits in Pakistan. Paleomagnetic normal polarities (filled circles and squares) and reversed polarities (open circles, squares, and triangles) were determined for each locality. The boundary between normal-polarity zone DN4 and reversed-polarity zone DR4 represents an 8.1 million-year-old time line, allowing age comparison of the various sedimentary deposits. From "Isochronous fluvial systems in Miocene deposits of northern Pakistan," by A. Behrensmeyer and L. Tauxe, *Sedimentology*, vol. 29, pp. 331–352, © 1982. Figure redrawn as in Butler (1992).

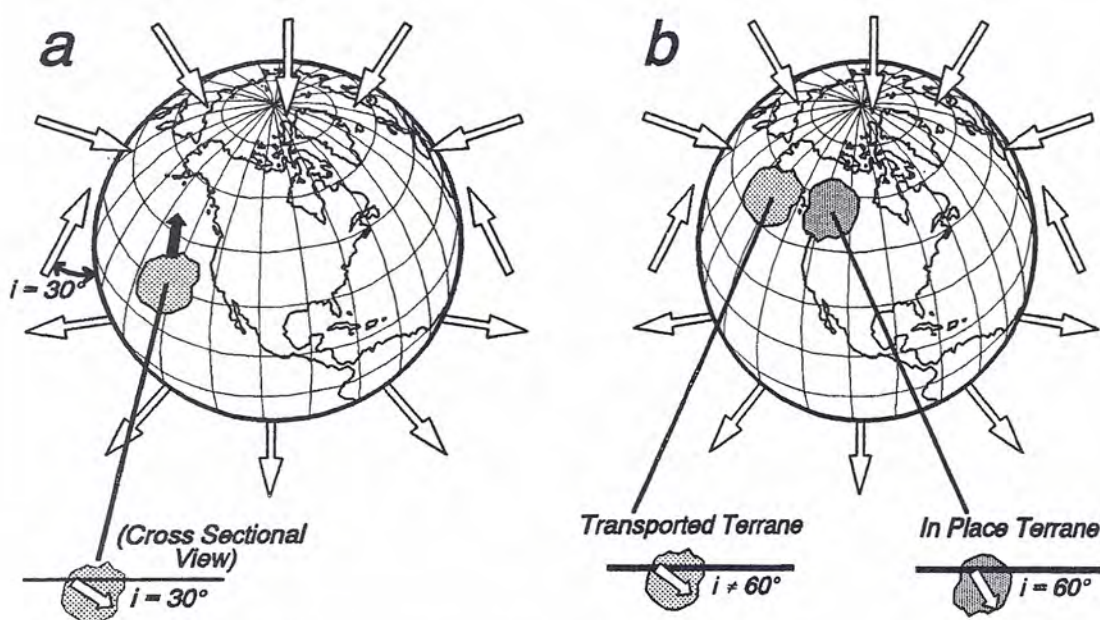


FIGURE 9.24 a) Direction of inclination of magnetization within a rock formed in the past at 30° magnetic latitude. b) The magnetic inclination (i) is retained when the rock drifts to a higher magnetic latitude, differing from the inclination of Earth's present field. The paleomagnetic inclination is thus a clue to the latitude at which the rock formed.